Design Trade Studies and Assessment for Advanced Quiet Aircraft Concepts

by

David York Luen Tan

Submitted to the Department of Aeronautics and Astronautics
in partial fulfillment of the requirements for the degree of

Master of Science in Aeronautics and Astronautics

at the

MASSACHUSETTS INSTITUTE OF TECHNOLOGY

February 2005

Author .....
Department of Aeronautics and Astronautics
January 14, 2005

Certified by .....
Professor Karen E. Willcox
Assistant Professor of Aeronautics and Astronautics
Thesis Supervisor

Accepted by .....
Professor Jaime Peraire
Professor of Aeronautics and Astronautics
Chairman, Committee on Graduate Students

Design Trade Studies and Assessment for Advanced Quiet Aircraft Concepts

by

David York Luen Tan

Submitted to the Department of Aeronautics and Astronautics
on January 14, 2005, in partial fulfillment of the
requirements for the degree of
Master of Science in Aeronautics and Astronautics

Abstract

This thesis describes the creation and use of tools to assess the noise impacts of conventional and blended-wing-body aircraft designs. These tools were used to set up trade studies to explore the effects of varying high level design parameters on noise. A framework was also created to conduct a detailed noise audit of various noise sources.

The trade studies explored four baseline high-level design parameters: range, cruise altitude and Mach number, and takeoff field length. The results of the trade study were assessed in terms of the change in size of noise contours on the ground predicted using the noise propagation model. The main conclusion from the study on conventional tube-and-wing designs was that the two main drivers for noise are range, followed by takeoff field length, with results showing a trend of noise footprint reduction for an aircraft designed for shorter range and longer takeoff field length. The trends observed in change of footprint areas show correlation to the weight of the aircraft, with a lower weight resulting in less noise. It was also found that as the design moved towards one with higher bypass ratio engines, the savings from design range reduction and takeoff length increase became less significant.

From a baseline silent aircraft configuration that consists of a blended-wing-body airframe and embedded engine technology, a similar trade study was conducted. The results from the study indicated that compared to a conventional tube-and-wing design, the jet noise footprint area of a blended-wing-body design that incorporates embedded engine technology is much less sensitive to changes in high level design parameters. To minimize the jet noise impacts given the baseline blended-wing-body design, the aircraft should be designed for 4,000nm range, 25,000 to 35,000ft cruise altitude, Mach 0.8 at cruise, and 10,000 to 14,000ft takeoff field length.

By identifying the main high-level design drivers of an aircraft design, the mission for a baseline silent aircraft planform and engine was determined. A silent aircraft was designed for a range of 4,000nm and 250 passengers. A noise assessment was conducted on the engine and airframe noise sources of the resulting design. The noise impacts of five engine (jet, fan forward, fan rearward, core, and turbine) and airframe (airfoil, elevator, slat, drag rudder, and undercarriage) noise sources were investigated in terms of their noise footprints and, more specifically, the loudest noise caused outside the airport boundary. The greatest noise source was the drag rudder, which was required to offset the idle thrust of the engine during approach. Because of the variable cycle and shielding effects on the embedded engines, engine noise at takeoff was greatly reduced. The main contribution of engine noise

was the fan rearward noise. Overall, airframe and engine noise during approach was found to be 12dBA and 9dBA louder than during takeoff respectively. The loudest airframe noise occurred during a 3-degree approach, and was about 6dBA louder than engine noise.

Thesis Supervisor: Professor Karen E. Willcox
Title: Assistant Professor of Aeronautics and Astronautics

Acknowledgments

I would like to thank my advisor, Prof. Willcox, for her guidance and help with my thesis. I am especially grateful for her help in connecting me with the right people to pull things together. I would also like to express my gratitude for my advisor's encouragement to take 16.888J, the multi-disciplinary optimization course (MSDO) at MIT. This course and its project provided much insight and many tools for design space exploration, which were used for the bulk of my research. Through her guidance in this project, I have learnt more than just how to be a researcher but how to deal with people as well.

I would also like to thank my lab mate, Adam Diedrich, who has provided essential insight and help in the aircraft design work. Out partnership through our research and the MSDO project has been fun and interesting.

My thanks for Jim Hileman, or James, as our Cambridge University colleagues would like to call him. Our conversations about research were always thought provoking and provided some spark to my thoughts. His help with the propagation model was key to the completion of this thesis.

I would like to thank Kiril Sakaliyski for starting up the jet noise codes and patience in sharing insights about jet noise and engine design.

My thanks also to Ryan Tam and Tom Reynolds, often our only contacts with the economics and operations teams. Their ideas and thoughts always provided a different and helpful perspective.

I would like to thank Professors Greitzer, Spakovsky, Clarke for giving critical and essential insight into the project tasks and their feasibility.

My thanks extend to my project-mates across the Atlantic. Chez, Dan, and the rest of the engine team have provided invaluable information and insight into the aspects of engine design and noise to help me along with my work.

Finally, much thanks to CMI for providing an opportunity to participate in this project and to travel in the UK!

Contents

1 Introduction **14**

1.1 Motivation for a Silent Aircraft 14

1.2 Background and Related Work 15

1.3 The Silent Aircraft Initiative 17

1.4 Scope of Thesis and Research Objectives 19

1.5 Methodology 19

1.6 Outline of Thesis 20

2 Creation and Validation of a Noise Prediction Framework **21**

2.1 Introduction 21

2.1.1 A-weighted sound pressure levels 23

2.2 Conventional Aircraft Sizing and Performance Model 23

2.3 Engine Noise Prediction Model and Engine Cycle Deck 25

2.3.1 Jet Noise Prediction Module 26

2.4 Airframe Noise Prediction Model 30

2.5 Noise Propagation And Visualization Model 31

2.5.1 NOISIM Inputs 31

2.5.2 NOISIM Noise Propagation Module 32

2.5.3 Visualization of NOISIM Outputs 32

2.6 Validation Of Noise Prediction Model 32

2.7 Summary 38

3 Trade Space Study for Conventional Tube-and-Wing Aircraft **40**

3.1 Introduction 40

3.2 Model Setup 40

3.2.1 Engine Noise Prediction Model Setup . . . 41
3.2.2 Noise Propagation and Visualization Model Setup . . . 42
3.3 Preliminary Trade Study Results . . . 42
3.3.1 250-Passenger, 2-Engine Conventional Aircraft . . . 42
3.3.2 450-Passenger, 2/3/4-Engine Aircraft . . . 45
3.3.3 Jet Noise Directivity and Spectra Variation . . . 46
3.4 Summary . . . 51

4 Trade Study for Silent Aircraft Designs 52
4.1 Introduction . . . 52
4.2 Framework modifications . . . 52
4.3 Trade Study Results . . . 57
4.4 Summary . . . 62

5 Noise Audit for Silent Aircraft Design 64
5.1 Introduction . . . 64
5.2 SAX Design Overview . . . 65
5.2.1 SAX Mission . . . 65
5.2.2 SAX Planform and Airframe . . . 66
5.2.3 SAX Engine Design . . . 67
5.3 Source Noise Assessment . . . 68
5.3.1 SAX Engine Source Noise . . . 68
5.3.2 SAX Airframe Source Noise . . . 70
5.4 Shielding . . . 71
5.5 Ground Noise Assessment . . . 72
5.5.1 Flight effects . . . 72
5.5.2 Noise Propagation Model . . . 72
5.5.3 Engine Noise Footprints and Results . . . 78
5.5.4 Airframe Noise Footprints and Results . . . 84
5.6 Summary . . . 92

6 Conclusion and Future Work 94
6.1 Summary and Conclusions . . . 94

6.2 Recommendations for Future Work 95

A Engine Cycle Parameters **97**

List of Figures

1-1 Silent Aircraft Initiative Research Components [41] 18

2-1 DIF Framework 22
2-2 ASPM Layout [12] 23
2-3 Aircraft Noise Component Contributions during Approach and Takeoff [34] 26
2-4 Aircraft Component Noise Prediction (30-degree polar angle) 27
2-5 Aircraft Component Noise Prediction (150-degree polar angle) 27
2-6 Sensitivity of Jet Noise to Core Jet Velocity (Directivity) 28
2-7 Comparison of Spectra for Jet Noise Produced between Jet Noise Model and ANOPP [25] 29
2-8 Sensitivity of Jet Noise SPL to Jet Velocities, Temperatures, and Pressures 30
2-9 Total Aircraft Noise Directivity Comparison between NPM Prediction and Wallops Flight Data (50, 63, 80, 100 Hz) for 767-400 at Takeoff with CF6-80C2B8F Engines 33
2-10 Total Aircraft Noise Directivity Comparison between NPM Prediction and Wallops Flight Data (5000, 6300, 8000, 10000 Hz) for 767-400 at Takeoff with CF6-80C2B8F Engines 34
2-11 Forward Angles (0,10,20,30) of Wallops Data and NPM Noise Prediction Spectra 35
2-12 Aft Angles (120,130,140,150) of Wallops Data and NPM Noise Prediction Spectra 35
2-13 Contour plot of difference in SPL between Wallops Data and NPM 36
2-14 Noise Footprint (in dBA) of 767 Take-off Procedure from Logan International Airport from Wallops Data 37

2-15 Noise Footprint (in dBA) of 767 Take-off Procedure from Logan International Airport from NPM Noise Prediction (CF6-80C2B8F Engines at T/O, 20 degree flaps) 37
2-16 Comparison of Area Affected Using Flight Test Data Against NPM Data . 38

3-1 NOISIM framework and Integration with NPM [24] 42
3-2 Cumulative curve of footprint areas (all regions); varying design range (250PAX, 2-Engine, tube-and-wing design) 43
3-3 Cumulative curve of footprint areas (>50dBA regions); varying design range (250PAX, 2-Engine, tube-and-wing design) 44
3-4 Cumulative curve of footprint areas (>50dBA regions); varying design takeoff field length (250PAX, 2-Engine, tube-and-wing design) 45
3-5 Noise footprint area comparison for all four tube-and-wing design configurations for design range of 5,000km 47
3-6 Jet Noise Spectra and Directivity with Range Variation 47
3-7 Jet noise spectra and directivity with take-off field length variation for tube-and-wing design 48
3-8 Jet noise spectra and directivity with cruise altitude variation for tube-and-wing design 49
3-9 Jet noise spectra and directivity with cruise Mach variation for tube-and-wing design 49
3-10 Cumulative curve of footprint areas (all regions); varying design range (250PAX, 2 Hi-BPR Engine, tube-and-wing design) 50

4-1 DIF for silent aircraft designs 53
4-2 Maximum takeoff weights of IDT-produced and optimized silent aircraft designs for different ranges 54
4-3 Maximum takeoff weights of IDT-produced and optimized silent aircraft designs for different cruise Mach numbers 55
4-4 Mission profile mapped onto contour plot of thrust (normalized by sea-level conditions) variation with altitude and Mach number 56
4-5 Mission profile mapped onto contour plot of SFC (normalized by sea-level conditions) variation with altitude and Mach number 56

4-6 Variation of MTOW with design parameters (250PAX, 4-Engine, silent aircraft design), circle symbol denotes the baseline design 58
4-7 Variation of thrust required per engine with design parameters (250PAX, 4-Engine, silent aircraft design), circle symbol denotes the baseline design . 58
4-8 Silent aircraft full trajectory footprint 59
4-9 Conventional full trajectory footprint 59
4-10 Silent aircraft cumulative curves for varying range 60
4-11 Conventional cumulative curves for varying range 60
4-12 Silent aircraft cumulative curves for varying cruise altitude 61
4-13 Conventional cumulative curves for varying cruise altitude 61
4-14 Silent aircraft cumulative curves for varying cruise Mach 61
4-15 Conventional cumulative curves for varying cruise Mach 61
4-16 Silent aircraft cumulative curves for varying takeoff field length 62
4-17 Conventional cumulative curves for varying takeoff field length 62

5-1 Airport boundary used for SAX noise audit 64
5-2 Ground distance and altitude for optimized SAX jet noise reduction takeoff trajectory [11] 66
5-3 SAX10 planform 67
5-4 Points along trajectory used for noise audit 69
5-5 Grid for propagation model validation 73
5-6 Grid for propagation model validation 74
5-7 Variation of geometrically attenuated OASPL with height at all receiver locations 75
5-8 Variation of laterally attenuated OASPL with height at all receiver locations 76
5-9 Variation of OASPL directly underneath source with height (all attenuation components) 77
5-10 Fan forward noise (dBA) at start of climb condition 78
5-11 Fan rearward noise (dBA) at start of climb condition 79
5-12 Core noise (dBA) at start of climb condition 79
5-13 Jet noise (dBA) at start of climb condition 79
5-14 Turbine noise (dBA) at start of climb condition 80

5-15 Estimated upper bound engine noise (dBA) at start of climb condition . . . 80
5-16 Estimated lower bound engine noise (dBA) at start of climb condition . . . 81
5-17 All engine noise components along airport sideline boundary at start of climb condition . . . 81
5-18 Estimated upper bound engine noise (dBA) at flyover condition . . . 82
5-19 All engine noise components underneath aircraft at flyover condition . . . 83
5-20 Estimated upper bound approach engine noise directly underneath aircraft 83
5-21 All engine noise components underneath aircraft at flyover condition . . . 84
5-22 Airfoil noise (dBA) at start of climb condition . . . 85
5-23 Elevator noise (dBA) at start of climb condition . . . 85
5-24 Slat noise (dBA) at start of climb condition . . . 85
5-25 Estimated upper bound airframe noise (dBA) at start of climb condition . . 86
5-26 Estimated lower bound airframe noise (dBA) at start of climb condition . . 86
5-27 All airframe noise components along airport sideline boundary at start of climb condition . . . 87
5-28 All airframe noise components underneath aircraft at flyover condition . . . 88
5-29 Undercarriage noise (dBA) at 3-degree approach condition . . . 89
5-30 Drag rudder noise (dBA) at 3-degree approach condition . . . 89
5-31 All airframe noise components underneath aircraft at 3-degree approach location (dashed line indicates total airframe noise when the drag rudder is not deployed) . . . 90
5-32 Airframe noise (including drag rudder) footprint for aircraft at 3-degree approach location . . . 90
5-33 Airframe noise (without drag rudder) footprint for aircraft at 3-degree approach location . . . 91
5-34 All airframe noise components underneath aircraft at 3-degree approach location (dashed lines indicate upper and lower bounds of total airframe noise) 91
5-35 All airframe noise components underneath aircraft at 6-degree approach location . . . 92
5-36 Maximum noise heard outside the airport boundary for all aircraft locations 93

List of Tables

2.1 Inputs into ASPM for 767-300ER and 747-400ER validation 25
2.2 Validation Results from APSM 25
2.3 Comparison of Area Affected Using Flight Test Data Against NPM Data . 39
2.4 FAA Estimated Noise Levels (in dBA) of 767-300 [16] 39

3.1 Range of values for parameters in trade study 41
3.2 Parameters for baseline aircraft 41
3.3 Summary of change in areas due to an increase in design range of tube-and-wing designs from 5,000 to 15,000km 46
3.4 Change in area due to increasing range from 5,000 to 15,000km for different BPR designs 50
3.5 Change in area due to decreasing takeoff field lengths from for designs with Hi-BPR engines 51
3.6 Summary of change in areas due to an increase in design range 51

4.1 Mission characteristics for the SAX 57
4.2 Design parameters used for trade studies 57

5.1 Mission characteristics for the SAX 65
5.2 Engine and airframe design parameters for the SAX 67
5.3 Noise source components 68
5.4 Noise audit location conditions 69
5.5 Engine Noise source prediction accuracy [20] 70
5.6 Takeoff and landing conditions used for SAX10 noise assessment 71
5.7 Airframe noise source prediction accuracy 71

A.1 CF6-80C2B8F Engine Cycle Values at Takeoff 97
A.2 Fan Noise Prediction Module Input Values from Cycle Analysis of CF6-80C2B8F at Takeoff 98
A.3 Comparison of Engine Noise Prediction Module Input Values from Cycle Analysis of CF6-80C2B8F and PW4056 98
A.4 GE90-90B Engine Cycle Values at Takeoff 99

Chapter 1

Introduction

1.1 Motivation for a Silent Aircraft

Over the past 40 years, aircraft noise has increasingly become an inhibitor of commercial airport growth. Noise pollution around airport communities continues to be a critical environmental issue. Airports with high-volume traffic in Europe and the United States have sought to relieve capacity constraints and ease delays via expansion, but have met with much resistance from local communities. The reasons cited are disruptive intrusions and economic dislocations caused by aircraft noise.

With worldwide air traffic expected to increase by as much as 40% in the next 20 years, a step-change in noise reduction would greatly ease the constraints faced by airports and carriers alike. The design and form of civil transport aircraft has remained essentially unchanged over the past four decades. The civil aviation industry has been introducing small, incremental decreases in aircraft noise but can only achieve steps of 3-5 dB for noise reduction. However to attain a radical change in noise levels - so that the noise of aircraft flying would be imperceptible to the public beyond the airport perimeter, much larger noise reductions (20-30 dB) are required. Attaining this goal would allow for the expansion of airport capacity without the penalties resulting from increased noise levels to the community.

Using noise as a prime design variable inevitably requires unconventional airframe and engine designs. Integration of these concepts is necessary for a qualitative assessment of the performance and noise characteristics at the aircraft system level. A framework needs to be designed to enable aircraft conceptual design with noise as the primary objective. This

thesis presents the integration and validation of such a framework, and its use to study the system level metrics that drive a low-noise aircraft design.

1.2 Background and Related Work

Previous attempts have been made to answer the question of how using noise as a prime design variable drives the design of an aircraft. A multidisciplinary approach was used by Antoine and Kroo [3] to identify aircraft conceptual designs with reduced environmental impacts at minimal cost. This study, along with another study by Liebeck et al. [28] identified the blended-wing-body design to have considerable promise in noise reduction because of potential shielding of engine noise by the airframe.

The blended-wing-body concept was introduced by Liebeck et al. [29] as a large subsonic transport that had the potential for significant improvements in performance compared to a conventional tube-and-wing design. Pilczer [36] performed a preliminary assessment on the potential noise reductions that could be achieved using quiet lift and silent drag concepts applied to a blended-wing-body type aircraft, estimating possible noise reduction on approach and takeoff EPNL of 30dB and 22.5dB respectively. Preliminary noise estimates of multiple embedded high aspect ratio engines yielded a potential noise reduction of 22.5dB in takeoff EPNL. The feasibility and the benefits from these quiet concepts associated with non-conventional aircraft were assessed using semi-empirical noise prediction methods. Among the noise prediction methods considered, the Stone [42] jet and ANOPP [48] airframe methods were considered to be most suited for jet and airframe noise prediction because they were based on experimental data and scaling laws which could be applied to non-conventional geometries.

Using similar noise prediction methods, Manneville [31] conducted an assessment of low-noise propulsion system concepts applied to a silent aircraft. The study of embedded propulsion system concepts suggested that ultra-high bypass ratio turbofan engine cycles could achieve a 30dB in jet noise reduction. However, to achieve this reduction in noise, engines with bypass ratios of order 70 are required for separate flow exhaust nozzles and of order 40 for a mixed flow exhaust nozzle. Performance-related penalties resulting from an ultra-high bypass ratio engine include an increase in engine weight and installation drag because of the significantly larger engine diameters.

One of the main issues identified by Pilczer [36] in the application of silent lift concepts was the requirement for increased airframe drag. To reduce the drag requirement, it was suggested that the blended-wing-body could be scaled down. Though a half-scale blended-wing-body planform yields only a 2dB EPNL reduction in trailing edge noise, the silent drag requirements were reduced by more than 50%, a significant consideration when deciding on the mission requirements of a silent aircraft.

Manneville [31] suggested the use of an engine air-brake system with variable geometry turbomachinery to achieve a quiet approach without high-drag devices. It was also found that there is potential for a jet noise reduction of 34dB in takeoff EPNL when implementing a distributed propulsion system with engine air-brake capability. On approach, it was suggested that a blended-wing-body aircraft implementing boundary layer ingestion and silent engine air-brakes could see as much as 32dB in noise reduction.

A framework was created by Antoine et al. [5] to conduct trade studies on the effects on aircraft design on noise, emissions, and cost. The results suggested that large reductions in aircraft environmental impacts are possible even without dramatic changes to propulsion systems, but at significant cost. It was suggested that a 250-seat, 6,000nm conventional tube-and-wing aircraft optimized for minimum noise would fly at a cruise altitude between 31,700 and 35,500ft, and at Mach 0.664. The study also established a trade-off between operating cost, emissions and noise. Furthermore, it is suggested that aircraft primarily optimized for low environmental impact are able to satisfy stringent environmental constraints than aircraft optimized for cost and operated to reduce environmental impacts.

A similar study was conducted Greener by Design [10] on the potential impact of subsonic air travel over the next 50 years. The study compared a set of aircraft design concepts and their potential contribution that technology can make to alleviating environmental impacts, especially for emissions and noise. The analysis indicated that the greenhouse effect of a medium range aircraft at 32,000ft is less than half that of the long-range aircraft at 40,000ft and its fuel burn is 15% lower. The study also suggested that a short-range aircraft (no longer than 7,500km) is more fuel-efficient, and thus incur lower operating cost, than a long-range aircraft.

Results from Antoine and Kroo[4] also show that there is minimal gain from takeoff thrust cutbacks (about 2-3dB), where the greatest noise reduction comes from cutting thrust as much as allowable to maintain the minimum climb gradient carried out close to the

measurement location. This was found to merely shift the noise from one location to another, doing very little in actual significant noise abatement.

Operational considerations for approach done by Pilczer [36] suggested a relationship between glide slope angle, approach speed and noise. The assessment estimated a noise reduction of 8dB EPNL could be achieved using a constant 10-degree glide slope at a corresponding $75m/s$ approach speed. Significant noise reduction from a continuous descent approach, an approach profile that applies a constant glide slope, was also determined through simulations conducted by Elmer et al. [13] and analysis by Clarke [9]. All the results were in agreement that an constant glide slope approach profile would result in significant noise reduction.

Current research includes the work done by the Cambridge-MIT Institute (CMI) to design a 'silent' aircraft. The project, known as the Silent Aircraft Initiative [41], aims to discover ways to reduce aircraft noise dramatically. Hopes to achieve this dramatic step change in noise involve the integration of many of the potential silent aircraft concepts mentioned above.

1.3 The Silent Aircraft Initiative

The Silent Aircraft Initiative (SAI) is a multi-disciplinary program that aims to enable competitive differentiation through innovative low-noise strategies in aircraft and engine system design and operation. The primary goals of the SAI are to enhance the competitiveness, productivity and entrepreneurship of the United Kingdom economy [41], with a focus on the areas of manufacturing and operations. This is to be achieved by developing technology and operation procedures that enable a dramatic reduction in aircraft noise.

The estimated time to achieve these goals is three years, beginning in the second half of 2003. The near term milestone of this project is for operational procedures which decrease community noise to be established and demonstrated for current aircraft, thereby permitting increased air operations at existing airports. The mid term milestone is the generation of noise reduction technology which may be applied to aircraft wings and engines of current design, extending the life of current UK products. The use of this technology is also expected to generate airport expansion guidelines which minimize the impact of noise on the community, increasing the likelihood of new runways and airports. In the long term, the

SAI will provide the economic and engineering framework for a revolutionary commercial transport whose noise is below that of the urban environment and thus almost imperceptible to the surrounding community.

The program is made up of five tightly coupled research components, as shown in Figure 1-1.

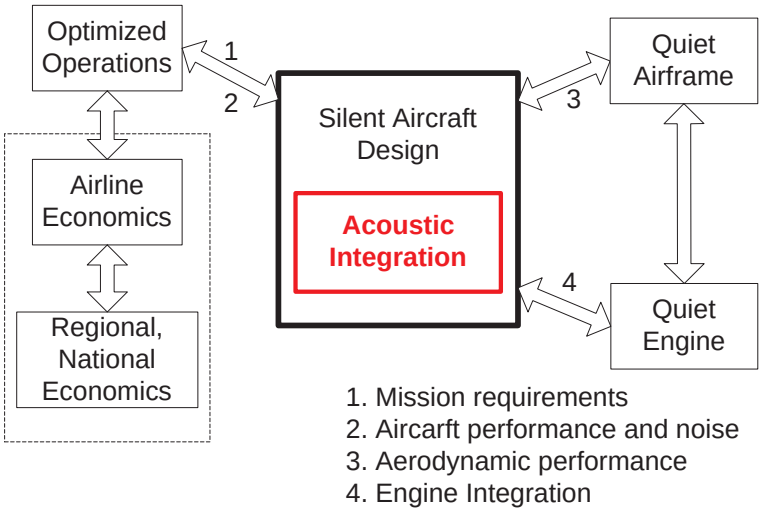

Figure 1-1: Silent Aircraft Initiative Research Components [41]

The silent aircraft design and acoustic integration research component, to which this thesis contributes, provides the integrative capability required by creating a framework for aircraft conceptual design with noise as the primary objective [41]. The framework is used to provide quantitative assessment of performance and noise characteristics at the aircraft system level. The deliverables for the research [41] are listed below.

1. Establish a framework for integrating airframe, engine and operational requirements with noise reduction as a prime goal

2. Produce aircraft system-level acoustic design

3. Assess unconventional configurations with engine shielding

This thesis addresses the first item on this list.

1.4 Scope of Thesis and Research Objectives

This thesis focuses on the prediction and analysis of engine and airframe noise sources. Most of the analysis will be done for takeoff and a greater emphasis will be given the former noise source. These prediction tools are combined with noise propagation models to produce the noise footprint and quantify the area on the ground affected by the noise from a given configuration. The studies conducted focus on trends of changes in noise levels based on varying high level design metrics like range, takeoff field length and cruise altitude. In the thesis, the following questions are addressed:

- What high level design parameters are the main drivers for noise and how does their relative noise impact on the ground compare?
- What is the potential reduction in noise impact experienced in the surrounding airport area when implementing revolutionary technologies like variable nozzle engines and blended-wing-body designs?
- After implementing these noise reduction technologies, what other noise sources become more significant?

1.5 Methodology

The methodology for the analysis involved the integration and modification of aircraft design, noise prediction, and noise propagation tools to conduct trade studies. Designs from each of the specific components were put together and the noise impact evaluated on a system level.

A trade study was done for tube-and-wing aircraft designs: 2-, 3-, and 4-engine 450-seater, and a 2-engine 250-seater. The results identified the high-level design parameters that are the main drivers for noise in conventional tube-and-wing designs. These results were then used to help set mission characteristics of a blended-wing-body type planform. Using the 250-seater blended-wing-body design as a baseline silent aircraft, a second trade study was conducted for the same high-level design parameters. The noise footprints were then compared with those of the conventional design.

Each trade study assumed the same takeoff trajectory while varying the design parameters. Within each trade study the engine cycle was also assumed to remain the same

as the design parameters varied. Because of the complexity in blended-wing-body design significant computation intensity was required to produce optimized planforms. As such, a simplified model was used for the trade study to scale the baseline weight and thrust requirements.

The trends observed in the trade studies served as guidelines for future aircraft designs to meet certain noise targets on the ground. Finally, a detailed noise audit is conducted on a silent aircraft design from which some design recommendations were made based on the results and these recommendations were compared with those made by the Greener by Design [10] report.

1.6 Outline of Thesis

The thesis is organized in the following manner: Chapter Two describes the setup and validation of the initial noise prediction and propagation framework for conventional tube-and-wing-designs, explains the reason for use of certain methods, and presents a sensitivity analysis of the jet noise prediction method.

Chapter Three presents the approach taken for the trade space study for conventional tube-and-wing designs, and discusses the results and design implications of the study. A similar trade space study done on a silent aircraft design is presented in Chapter Four. These results are then compared with those of a conventional design. Chapter Five describes the design of a silent aircraft and an audit of its noise source components. Finally, Chapter Six lists the conclusions from the noise audit and trade study results and recommendations for future work.

Chapter 2

Creation and Validation of a Noise Prediction Framework

2.1 Introduction

In order to assess how the size of the silent aircraft design will affect noise levels on the ground, a framework needs to be created using the most accurate noise prediction methods available. Traditional methods try to take into account tone and duration corrections for certain areas on the ground during take-off and approach procedures. Usually this involves the weighted summation of sound pressure levels (SPL) across tones, weighting tones that are more annoying to the human ear. Duration corrections are taken into account, for example, with the Effective Perceived Noise Level (EPNL), computing time-averaged indexes of noise exposure.

For example, the Federal Aviation Administration (FAA) in the US uses 3 locations on the ground as certification points. However, this does not take into consideration the community around the airport, which is the main driver for reduction of aircraft noise in the first place. To this end, the FAA created the Integrated Noise Model (INM), which predicts the noise footprint of an aircraft based on past empirical data at various recording stations around the airport. This method is limited as a design tool because the INM does not allow for much, if any, deviation from conventional design. Hence, a more involved framework that takes into account non-conventional designs and can implement noise reduction technologies is more useful for design purposes.

This tool is made out of an integrated framework of codes and is called the Silent Aircraft Design Integration Framework (DIF). The DIF consists of five main models: first, a code that predicts the aircraft size given high level design parameters; second, an engine cycle deck to predict the engine cycle of a given aircraft; third, a semi-empirical noise prediction model for the engine and airframe, which are the main components of noise at take-off and approach; fourth, a noise propagation model to predict the noise levels on the ground; finally, a visualization model to quantify the effects of the noise at ground level. This chapter begins by presenting the methodology employed and validation of individual components of this framework, and ends with the validation of the complete framework.

The DIF for conventional tube-and-wing designs consists of an Aircraft Performance and Sizing Model (APSM) [12], an engine cycle deck (GasTurb 9.0) [27], a Noise Prediction Model (NPM), a propagation model (MIT NOISIM) [24], and a visualization model. Figure 2-1 shows the framework used and the interactions between each model. The high-level design parameters are entered into the ASPM and the outputs are produced in terms of noise footprints of a takeoff profile from Logan International Airport. A more detailed description of each model is given in the next sections.

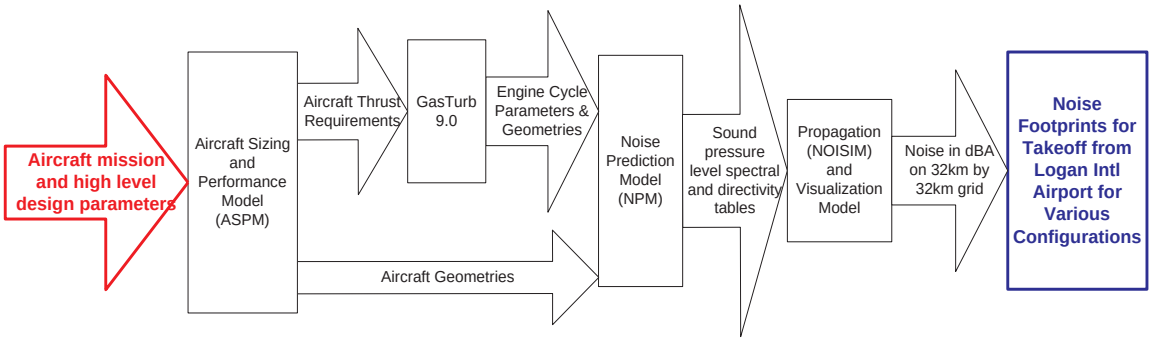

Figure 2-1: DIF Framework

This framework has been used to conduct trade studies for four high-level aircraft design parameters: range, cruise altitude, cruise Mach, takeoff field length. These four inputs were varied across a range of values and processed by the DIF. The results were assessed in terms of the change the size of noise contours on the ground.

2.1.1 A-weighted sound pressure levels

The noise footprints are output in terms of A-weighted SPL (dBA). The A-weighted SPL is commonly used to assess noise levels on the ground. According to Williams and Dowling [47] the human ear responds more strongly to some frequencies than others, and the A-weighting factors takes into account the ear's sensitivity to a given frequency range. The A-weighting is internationally accepted and easy to record with a sound meter. It does not, however, take into account the duration effects of an event.

2.2 Conventional Aircraft Sizing and Performance Model

This section presents a brief outline of the the aircraft sizing process within the ASPM created by Diedrich [12]. The ASPM layout can be seen in Figure 2-2.

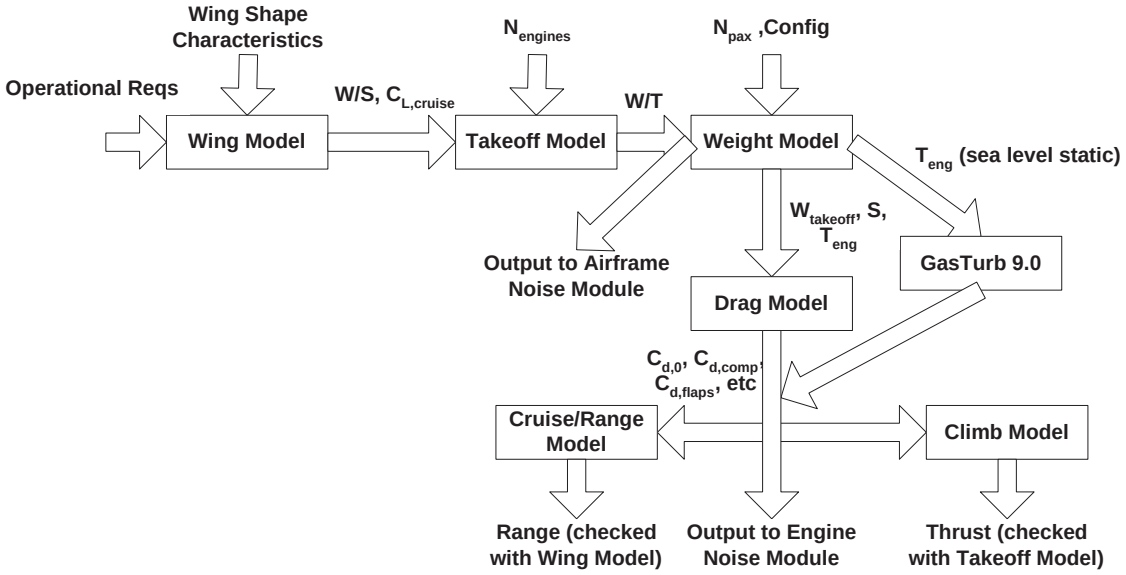

Figure 2-2: ASPM Layout [12]

The ASPM first sets the design range and the number of passengers to specify the mission. Next, an initial fuel fraction estimate is computed by solving for the fraction of total weight that is needed for cruise and reserves. This done using the Breguet Range equation, which is as follows:

$$R = \frac{V}{g}\frac{1}{TSFC}\frac{L}{D}\ln\frac{W_0}{W_1}, \tag{2.1}$$

where V is cruise velocity, g is the acceleration due to gravity, $TSFC$ is the thrust specific fuel consumption, L is the lift, D is the drag, W_0 is the initial aircraft weight, and W_1 is the final aircraft weight. For the purposes of the initial fuel fraction calculation, a typical airliner lift-to-drag ratio of 16 and a typical cruise SFC value of 0.48lbf/lb-hr are used.

Next, an empirical wing module sets various wing parameters such as thickness, lift coefficient at cruise, and wing loading. These are set by empirically predicting the thickness allowable by the sweep angle and the cruise Mach number before significant transonic drag rise begins. This thickness in turn determines the maximum lift coefficient value for the aircraft, which determines the maximum wing loading. These are all non-dimensional parameters, since the weight module sets the actual size of the aircraft. The thrust loading is set according to the wing loading and Federal Aviation Regulations (FAR) for balanced field takeoff length.

All of the non-dimensional calculations done thus far are dimensionalized when the weight module sizes the aircraft. This method uses empirically derived formulas to calculate component weight fractions. A Newtonian solver is then used to find the gross takeoff weight that satisfies all of the component weight equations.

Next, a skin friction build-up is done to compute the parasitic drag coefficient. This will be used for the climb and cruise performance estimates. The climb performance estimator calculates the thrust required and available during climb, as well as the distance covered and the fuel burned during climb to cruise altitude. The cruise performance estimator calculates the thrust available and required for cruise. It uses the same drag data as the climb module, plus a compressibility correction from Shevell [39]. The range module then checks that the airplane as configured will be able to make the design range with the design payload (the number of passengers specified for the mission).

All of the thrust availability calculations rely on data from a jet engine cycle deck. The cycle deck in this case is GasTurb 9.0, as described by Kurzke [27]. The engine cycle parameters are entered into GasTurb, and tables of thrust and SFC as functions of Mach number and altitude are produced. The thrust table is then non-dimensionalized so that the

data can be used in the model as the engine size varies. The assumption made in this thesis is that changes in engine size will not cause a significant change in component efficiencies or the specific thrust value.

The engine size is iterated to meet any shortfall in thrust available in the cruise or climb modules. Likewise, the fuel fraction estimate is iterated to meet any range shortfall.

The ASPM was validated against published Boeing data for the maximum takeoff weight (MTOW), thrust per engine, and wing span of a 767-300ER [6] and a 747-400ER [7]. The inputs are listed in Table 2.1 and the results are summarized in Table 2.2.

	767-300ER	747-400ER
Number of Passengers	218 (typical 3-class)	416 (typical 3-class)
Number of Engines	2	4
Cruise Altitude (ft)	33,000	33,000
Cruise Mach Number	0.80	0.855
Wing Sweep	40	40
Aspect Ratio	7.7	7.7
Takeoff Field Length	9,950	9,950
Approach Speed (kts)	157	157
Range (mi)	6,000	7,670
Sea Level Static Engine SFC	0.33	0.33
Taper	0.28	0.28
Allowed Weight Fraction at Landing	0.75	0.75

Table 2.1: Inputs into ASPM for 767-300ER and 747-400ER validation

	767-300ER			747-400ER		
	ASPM	Boeing Data [6]	Percent Error	ASPM	Boeing Data [7]	Percent Error
MTOW (lbs)	419,500	412,000	1.82	932,200	910,000	2.4
Thrust per Engine (lbs)	66,800	63,300	5.5	63,600	63,700	-0.2
Wing Span (ft)	144	156	-7.7	213	211	0.9

Table 2.2: Validation Results from APSM

2.3 Engine Noise Prediction Model and Engine Cycle Deck

The engine component of the NPM is a semi-empirical model based on NASA ANOPP [48]. The model consists of four modules: Heidmann Fan Module [21], Stone Jet Module [42], General Electric (GE) Turbine Module [32], and the Matta Combustion Module [14].

The typical main contributors to aircraft noise are listed in Figure 2-3. It can be seen that jet and fan noise make significant contributions to overall aircraft noise.

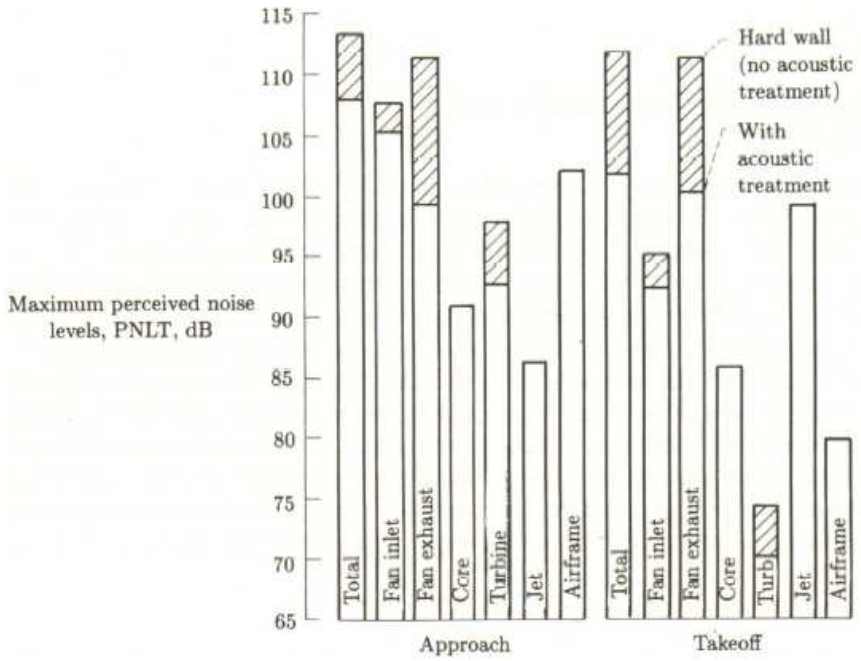

Figure 2-3: Aircraft Noise Component Contributions during Approach and Takeoff [34]

With regards to engine noise at takeoff, Kontos et al. [25] show that jet noise dominates at low- to mid-frequencies and fan noise dominates at high frequencies. The outputs from the engine noise prediction model, shown in Figures 2-4 and 2-5, demonstrate similar trends.

2.3.1 Jet Noise Prediction Module

In the comparison of noise models done by Pilczer [36], the Stone jet noise model was compared with the SAE method [2], and the method by Tam et al. [44], and Tam and Zaman [45], it was concluded that the Stone jet model was the most suitable for a jet takeoff parametric study. This is because it captures the large and fine scale turbulence structures, was fitted to experimental data over a wide range of test conditions, and also includes a detailed prediction of flight effects.

The original jet noise prediction code was thus based on the Stone [42] jet noise prediction method, and improved based on changes listed in Stone et al. [43]. This semi-empirical prediction models the effect of nozzle size, jet velocity, jet temperature and flight effects.

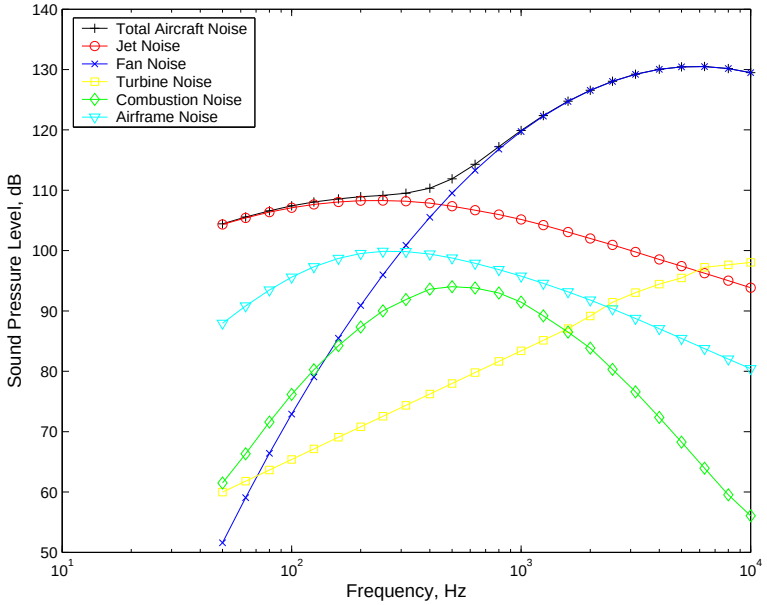

Figure 2-4: Aircraft Component Noise Prediction (30-degree polar angle)

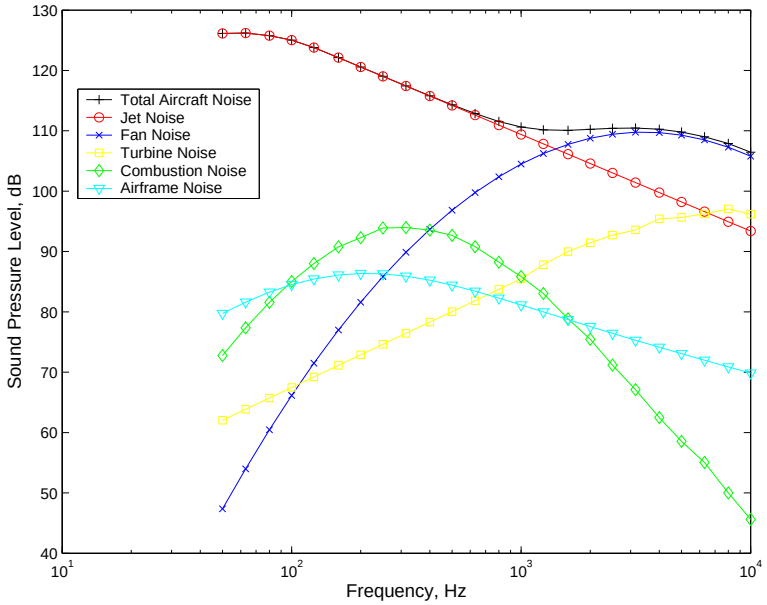

Figure 2-5: Aircraft Component Noise Prediction (150-degree polar angle)

According to Stone et al. [43], the mean-square acoustic pressure, $\langle p^2 \rangle$, of jet noise can be expressed in non-dimensional form as

$$\langle p^2 \rangle^* = \frac{\Pi^* A_j}{4\pi(r)^2} \cdot D \cdot F \cdot H, \tag{2.2}$$

where $*$ denotes non-dimensional parameters. Π^* depends on the jet velocity U_j, with a dependence close to the power 7.5 for low jet velocities. Π^* is also dependent on the jet density and the polar directivity angle. $D(\theta, U_j)$ and $F(S_t, \theta, U_j)$ are the directivity and spectral functions respectively, where θ is the polar directivity angle and S_t is the Strouhal number. The forward flight effect factor H is a function of the flight Mach number, θ, the jet velocity, temperature and density.

Jet noise is highly sensitive to jet velocities, with jet acoustic power proportional to jet velocity close to the power of eight. Figure 2-6 shows how the jet noise SPL prediction varies with varying core jet velocities.

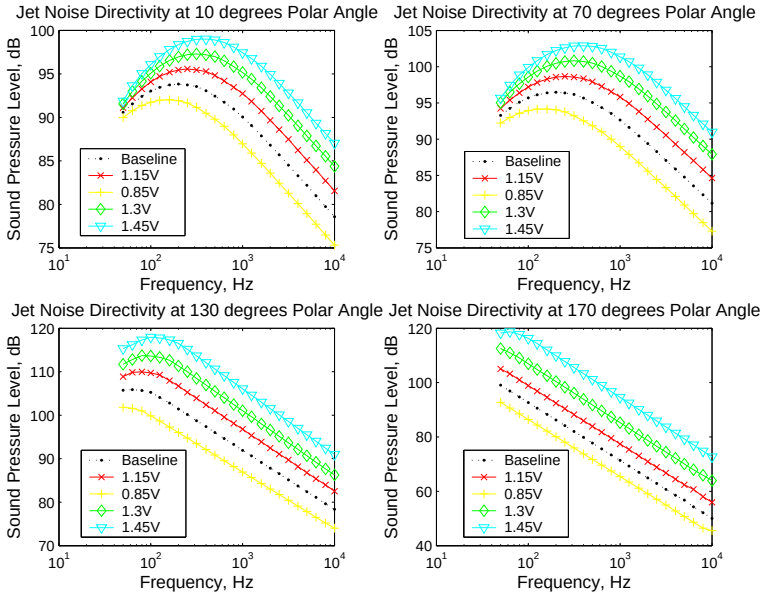

Figure 2-6: Sensitivity of Jet Noise to Core Jet Velocity (Directivity)

This prediction method is used for jets exhausting from coaxial nozzles with conventional velocity profiles. The predictions formulated cover the full angular range from 0 to 180 degrees. According to Stone et al. [43], there are no inherent limitations on the directivity and spectral range of the prediction methods, and comparisons with static model data

indicate that overall SPL is predicted within a standard deviation of 1.8dB.

A comparison between the published outputs from ANOPP and the NPM was done because the ANOPP computer program has gone through a number of versions over the years, not all of which were recorded in reports. The only published results available were by Kontos et al. [25] for jet noise at a single directivity angle. The SPL predicted by the jet noise model was found to be within a margin of 2dB of the ANOPP output. This comparison is illustrated in Figure 2-7.

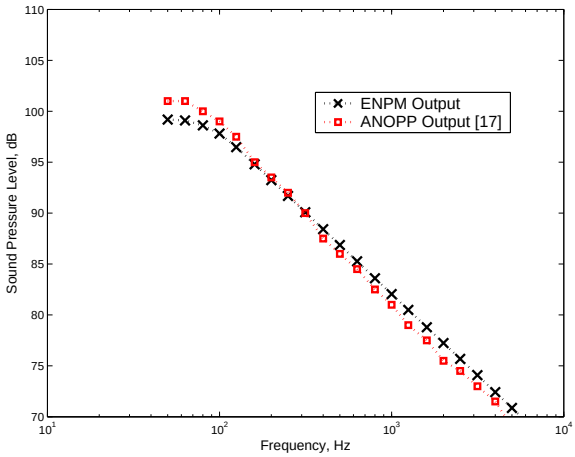

Figure 2-7: Comparison of Spectra for Jet Noise Produced between Jet Noise Model and ANOPP [25]

We can use the governing equations used in the jet noise module to quantify the sensitivity of the jet noise. From equation 2.2 we know that the mean-square acoustic pressure has the following relation to jet noise

$$\langle p^2 \rangle^* \propto U_j^{7.5}, \tag{2.3}$$

at peak frequencies and directivities. Also, note that the SPL is calculated as

$$SPL = 10 \lg \langle p^2 \rangle^* + 10 \lg \frac{\rho_\infty^2 c_\infty^4}{p_{ref}^2}, \tag{2.4}$$

where ρ_∞ and c_∞ denote the ambient density and speed of sound, and denotes the reference pressure, taken to be $2 \times 10^{-5} Pa$. With the 2 equations above, we can calculate ΔSPL_{max},

the maximum change in SPL due to change in jet velocity from U_1 to U_2 as

$$\Delta SPL_{max} = 10 \lg(\frac{U_2}{U_1})^{7.5}. \tag{2.5}$$

Using equation 2.5, we can approximate the change in SPL due to a change in the jet total temperature (T_t) and pressure (p_t) inputs from the engine cycle deck. The quantification of the sensitivities is summarized in Figure 2-8, which agrees with the observation in the bottom 2 graphs in Figure 2-6, where a 45% increase in the jet velocity resulted in a maximum increase of about 12dB in the SPL (at 120 to 130 degrees polar angle.).

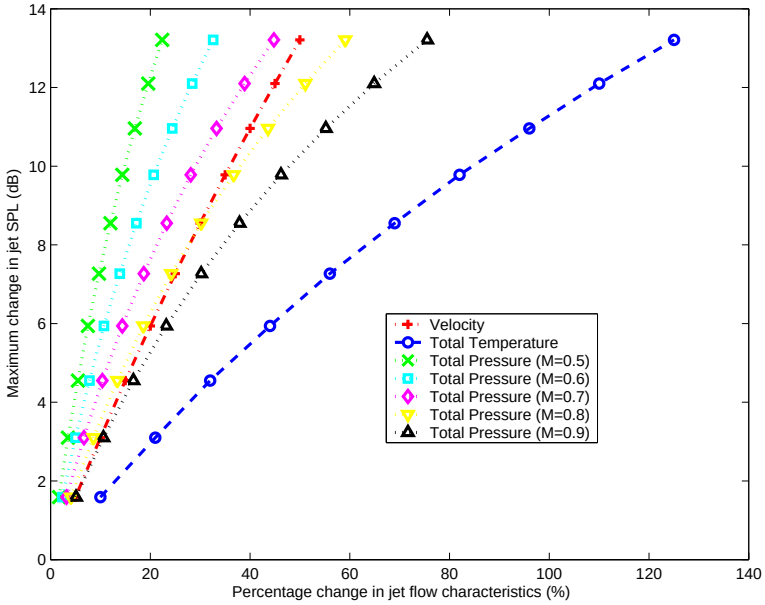

Figure 2-8: Sensitivity of Jet Noise SPL to Jet Velocities, Temperatures, and Pressures

2.4 Airframe Noise Prediction Model

In the previously mentioned comparison of noise models done by Pilczer [36], the Fink [18] method outlined in the NASA ANOPP manual [48], and the self-noise model by Brooks et al. [8] were investigated for trailing edge noise estimation. It was found that both methods are in good agreement regarding the peak frequency and their slope at low and high frequencies. The Brooks method was found to be superior in terms of non-conventional airframe evaluation.

However the Fink method used in ANOPP does account for noise radiation due to flaps,

slats, landing gear, horizontal and vertical tail, and wing trailing edge. The prediction methods are based on trailing edge noise theory and fitted to flyover noise data. The airframe noise makes significant contributions on approach but will not be a major factor in the validation of takeoff noise.

The Fink method characterizes the mean-square acoustic pressure of airframe noise as

$$\langle p^2 \rangle^* = \frac{\Pi^*}{4\pi(r)^2} \frac{D(\theta, \phi)F}{(1 - M\cos\theta)^4}, \tag{2.6}$$

where the directivity function $D(\theta, \phi)$, is a function of both polar (θ) and azimuth (ϕ) angles, and F is the spectral distribution function. The overall power is

$$\Pi^* = K \cdot (M_\infty)^a \cdot G, \tag{2.7}$$

where K and a are constants determined from empirical data and vary depending on which airframe component is being considered, and G is the geometry function. Each of the components has its own directivity function and spectrum function.

2.5 Noise Propagation And Visualization Model

The noise propagation model used for conventional tube-and-wing designs is called NOISIM and is described in detail by Huber [24]. NOISIM is made of several modules that require inputs of standard weather profiles, aircraft trajectories (or procedures) and noise source characteristics. These inputs are processed in the Noise Propagation Module in NOISIM and output in the form of a 32-by-32 km grid with 40,000 square cells.

2.5.1 NOISIM Inputs

The inputs from the weather profile to NOISIM include atmospheric conditions such as altitude, pressure, temperature, absolute humidity, components of wind in the east and north directions, and air density.

Aircraft procedures are specified in terms of throttle settings as a function of altitude. The aircraft performance module then determines the position, speed, attitude and thrust of the aircraft as a function of time that make up the trajectory. The aircraft trajectory can also be input directly into the NPM.

The noise source characteristics required are the SPL on a 100ft hemisphere as a function of both frequency and direction. Direction is defined by the polar and azimuth angles relative to the body-fixed axis of the aircraft. The NPM output provides the required data for input into the Noise Propagation Module. This is in the form of SPL as a function of azimuth and polar angles and one-third octave frequency bands for two distinct operating conditions.

2.5.2 NOISIM Noise Propagation Module

The Noise Propagation Module models the propagation of sound using far-field acoustics, assuming that the sound wave is spread spherically. The module uses a ray-tracing algorithm that computes the path taken by the sound waves by integrating the effects of wind and temperature gradients. The algorithm also takes into account the effects of multiple bouncing. The receiver is assumed to be at a height of four feet above the ground and the ground is assumed to be flat and described by its specific flow resistance.

The module accounts for amplitude variation along the rays and calculates transmission loss for each ray, which is then mapped on the output grid. Atmospheric absorption is also taken into account as attenuation occurs due to the internal friction in the air. Sounds directly from the source and reflected sounds can be of different phases and thus cause excess ground attenuation. Creeping waves into the shadow zone, where no ray can penetrate, are also accounted for.

2.5.3 Visualization of NOISIM Outputs

The output from NOISIM is in terms of peak dBA (A-weighted decibels) in each of the 40,000 square cells in a 32-by-32 km region. Noise contours are mapped onto the ground area (noise footprints) to provide a graphical representation of the noise impact.

2.6 Validation Of Noise Prediction Model

Noise data from a flight test [24] of a Boeing 767-400 at the Wallops Flight Test Facility in Virginia were used to compare with the NPM. The validation was done against a General Electric CF6-80C2B8F two-spool unmixed flow turbofan engine. The engine cycle values for the CF6-80C2B8F engine at takeoff conditions are listed in Table A.1.

The low-frequency directivity plots from the validation are shown in Figure 2-9.

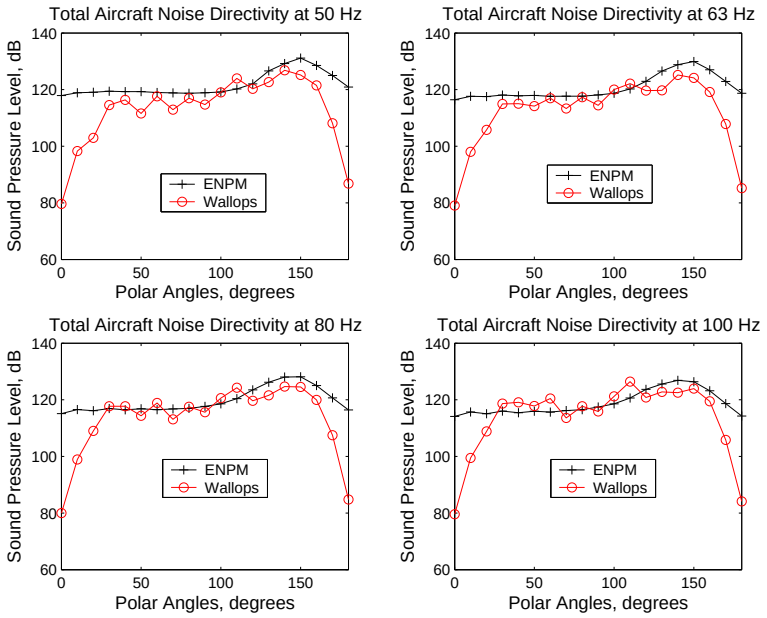

Figure 2-9: Total Aircraft Noise Directivity Comparison between NPM Prediction and Wallops Flight Data (50, 63, 80, 100 Hz) for 767-400 at Takeoff with CF6-80C2B8F Engines

From Figure 2-9 it is observed that for low frequency noise, at angles between 20 to 160 degrees, there is a relatively good correlation of trends, with a varying amount under-prediction between 0.5 to 5dB and a maximum over-prediction of about 5dB at the aft angles. The low frequency noise at takeoff mostly corresponds to the jet noise and similar effects were observed during the validation of ANOPP with actual flight data. In a validation study Shivashankara [40] found ANOPP to under-predict by between 2 to 15dB for all directivity angles at low frequencies.

For the ANOPP validation study, noise levels were recorded at angles between 20 to 160 degrees. It was noted that for data collection at shallow angles to the horizontal, the propagation path is large and when corrections are made to change the polar angle to zero, the propagation distance corrections become appreciable. This effect is believed to account for the discrepancies between predicted noise and recorded data during the flight tests. From the information gathered about the flight test data, the propagation distance corrections could have been significant enough to account for the difference observed.

During the validation study mentioned above, ANOPP was also found to over-predict the SPL at high frequencies. This is due to erroneous buzzsaw (fan) noise component predic-

tions, which occurs at the forward arc and at high frequencies, where fan noise dominates.

When taking noise measurements, two corrections usually need to be made: spherical divergence correction, and standard day atmospheric conditions correction. The former correction is only about 1dB for a pitch angle correction of 3 degrees at 160-degree directivity. The latter correction is substantial at frequencies greater than 5000 Hz (see Figure 2-10). Hence, the over-prediction at shallow angles at high frequencies is attributed to large atmospheric attenuation corrections made to high frequency data to correct from test day to standard day conditions.

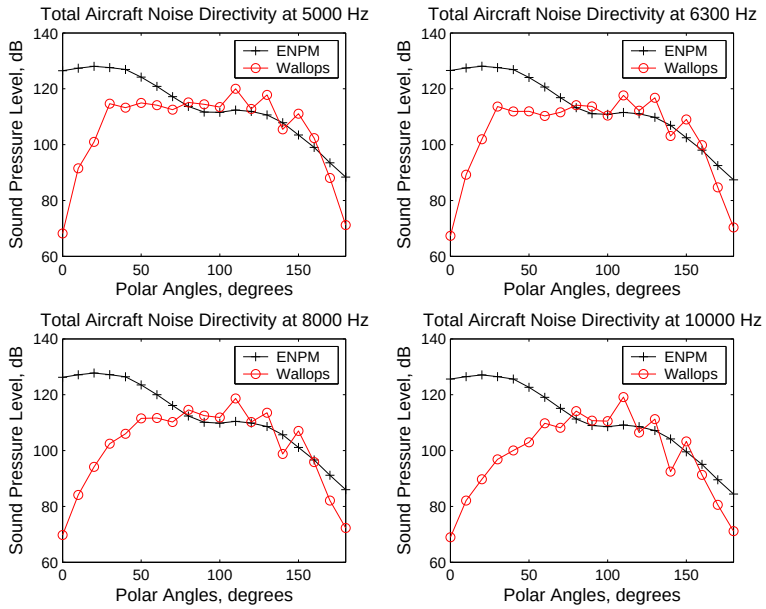

Figure 2-10: Total Aircraft Noise Directivity Comparison between NPM Prediction and Wallops Flight Data (5000, 6300, 8000, 10000 Hz) for 767-400 at Takeoff with CF6-80C2B8F Engines

The aforementioned discrepancies can also be observed from plots of the spectra as in Figure 2-11 and Figure 2-12.

From these plots, it is observed that there is a greater discrepancy in predicted SPL at the shallow angles; but at intermediate angles, like 120 and 140 degrees, the prediction is fairly accurate. Figure 2-13 gives an overall view of the difference in data and prediction.

Further validation was done at the ground level. The Wallops data and NPM predictions were run through a propagation model, NOISIM, and visualized as a noise footprint. Figure 2-14 shows the noise footprint of a 767 take-off procedure from Logan International Airport

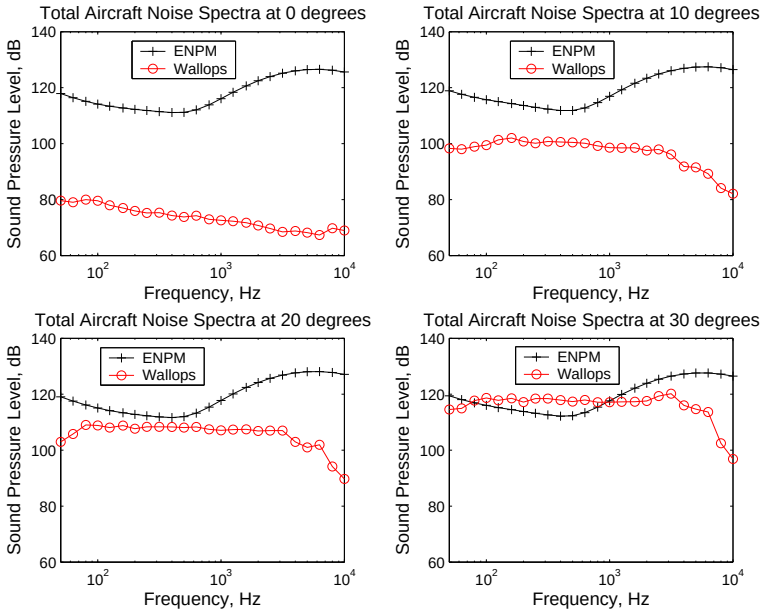

Figure 2-11: Forward Angles (0,10,20,30) of Wallops Data and NPM Noise Prediction Spectra

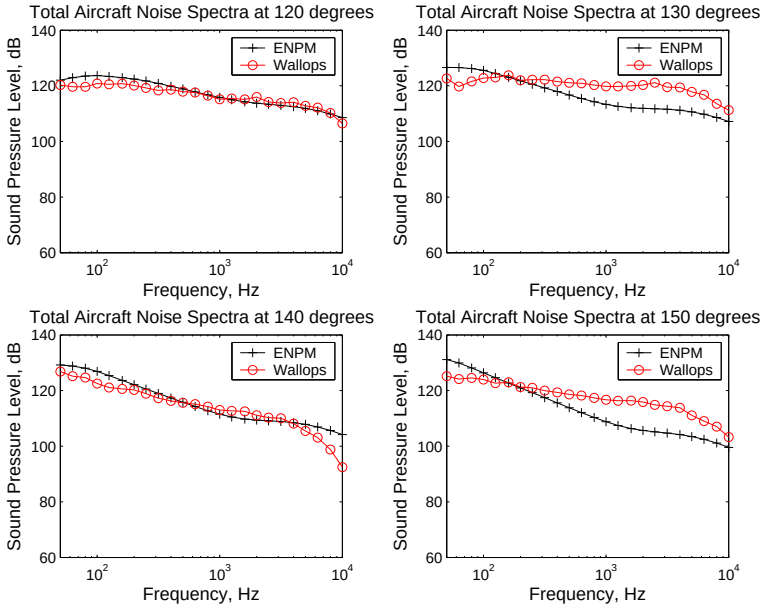

Figure 2-12: Aft Angles (120,130,140,150) of Wallops Data and NPM Noise Prediction Spectra

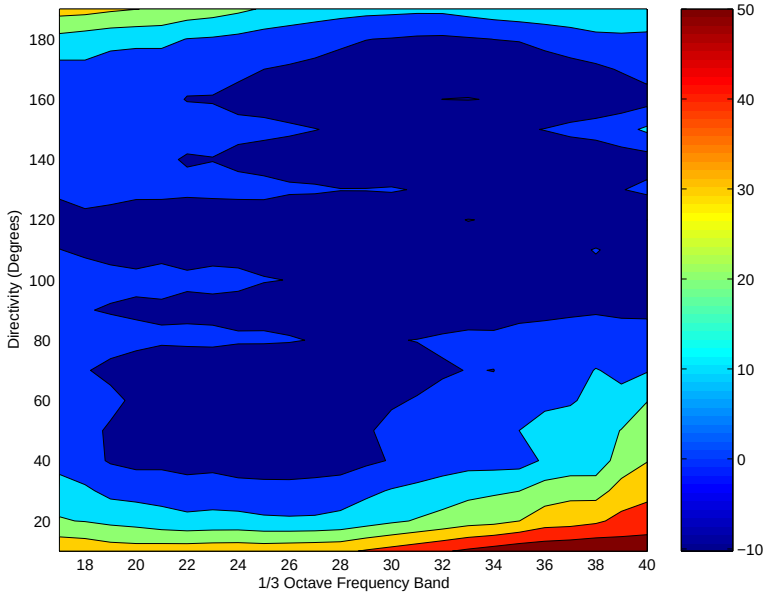

Figure 2-13: Contour plot of difference in SPL between Wallops Data and NPM

in units of A-Weighted Decibels (dBA). The predicted noise levels were validated by Huber [24] against four noise-monitoring stations around the airport and were highly correlated.

Figure 2-15 shows the noise footprint with NPM noise prediction data using the CF6-80C2B8F engine cycle at takeoff with 20-degree flaps.

Details of the footprint results are summarized in Figure 2-16 and Table 2.3. The DIF over-predicted for all regions above 55dBA by a total of 6.58% of the total area, with a maximum over-prediction of 2.58% for each 5dBA interval. The region between 55dBA and 50dBA are under-predicted by 0.66%, regions below 50dBA by 5.91%. The validation was also done for takeoff conditions without flaps deployed, which resulted the same areas.

To illustrate the sensitivity of the framework to the engine cycle, this validation was re-done for a PW4056 engine cycle. This showed a general trend of under-prediction of about 10dBA on the ground. This main difference in engine cycles was that the PW4056 engine had a lower exit jet Mach number by about 0.2 (see Table A.3). As opposed to the initial validation done for the CF6-80C2B8F, where the exit jet was considered fully mixed, the exit jet areas were considered separately for the validation with PW4056.

Comparing the noise footprints for the two different engines indicated that a 767-400 fitted with CF6-80C2B8F engines has greater noise impact than when fitted with PW4056 engines. This observation was found to be consistent with data from the FAA.

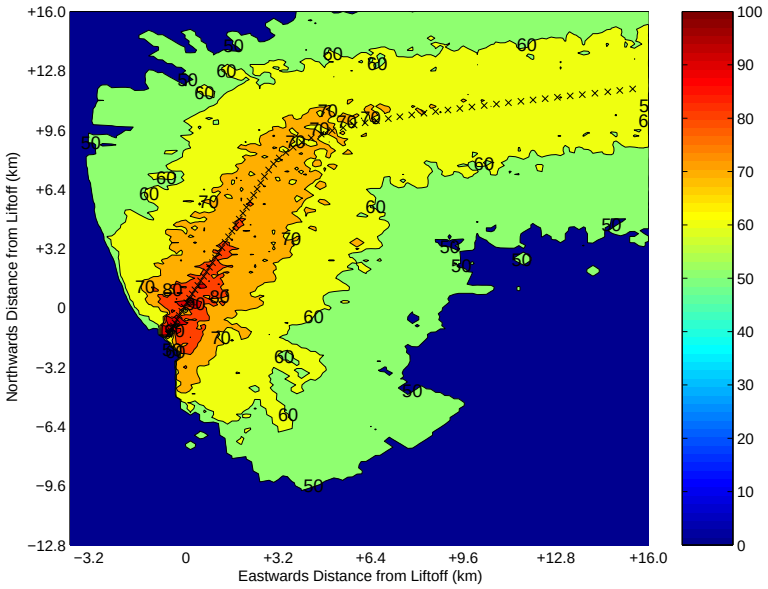

Figure 2-14: Noise Footprint (in dBA) of 767 Take-off Procedure from Logan International Airport from Wallops Data

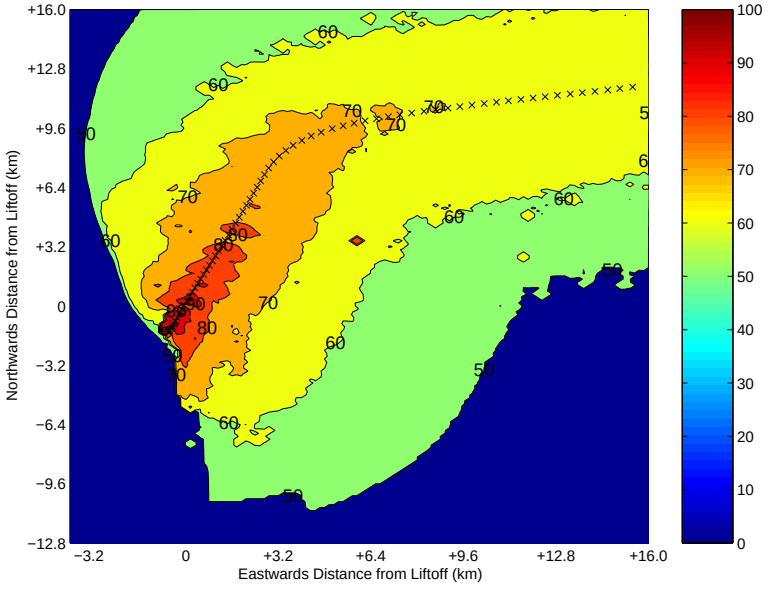

Figure 2-15: Noise Footprint (in dBA) of 767 Take-off Procedure from Logan International Airport from NPM Noise Prediction (CF6-80C2B8F Engines at T/O, 20 degree flaps)

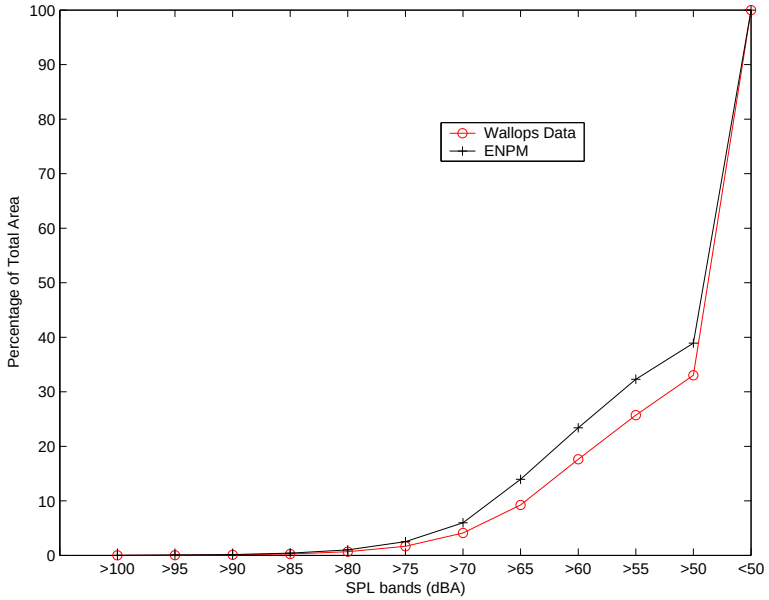

Figure 2-16: Comparison of Area Affected Using Flight Test Data Against NPM Data

The FAA estimated the A-weighted noise levels for a number of commercial aircraft as they might occur during type certification tests conducted under CFR part 36. From this data, the aircraft noise measurements for two 767-300's with similar takeoff weight were compared, shown in Table 2.4.

The difference in takeoff noise, corrected for the difference in takeoff gross weight, is about 5dBA. This result supports the observation that the CF6-80A engines have larger noise impact in terms of noise footprints. However, the difference in A-weighted noise estimation from the FAA is less than the observed trend of a 10dBA difference between the CF6-80A and the PW4056. This might be attributed to inaccuracies in the engine cycle prediction. Also, it must be noted that the FAA Advisory Circular [16] mentions that the data is not intended for establishing the absolute noise levels of individual aircraft.

2.7 Summary

This chapter has presented the creation and validation of the DIF for conventional tube-and-wing designs. The description and rationale for the use of each component of the framework was also stated. A qualitative and quantitative analysis was done for the noise at the component level and the at the noise footprint level. The standard deviation between

Region (dBA)	Difference in Predicted Area (km^2)	Over-prediction (% of total area)
> 100	0.05	+0.005
$95 < 100$	0.36	+0.035
$90 < 95$	0.18	+0.017
$85 < 90$	1.05	+0.103
$80 < 85$	1.87	+0.182
$75 < 80$	5.22	+0.523
$70 < 75$	10.37	+1.013
$65 < 70$	28.98	+2.830
$60 < 65$	11.19	+1.093
$55 < 60$	7.99	+0.780
$50 < 55$	-6.78	-0.663
< 50	-60.47	-5.905

Table 2.3: Comparison of Area Affected Using Flight Test Data Against NPM Data

Engine	Gross Take-off Weight ('000 lbs)	Take-off Noise (dBA)
CF6-80C2B8F	300	74.5
PW4056	295	68.9

Table 2.4: FAA Estimated Noise Levels (in dBA) of 767-300 [16]

the footprint areas produced by the DIF prediction and the Wallops flight test data is taken into consideration in the subsequent use of the DIF. In the following chapter, a trade space study will be conducted using this framework to analyze the trends in noise footprint area changes as high level design parameters are varied.

Chapter 3

Trade Space Study for Conventional Tube-and-Wing Aircraft

3.1 Introduction

With the DIF in place, we can explore the design space for conventional tube-and-wing aircraft. The trade study is conducted for four high-level design parameters that have significant effect on aircraft sizing: range, cruise altitude and Mach number, and takeoff field length.

Another significant design parameter that will be used for this trade study is the number of passengers. The validation of the ASPM was done for 250 and 450 passenger aircraft and showed good agreement between the prediction and real data, and thus these two aircraft types were chosen for the study.

This chapter begins by describing the setup of the DIF for the trade study. The results from the studies are then presented for each of the design parameters. Finally the conclusions and design implications of the study will be discussed.

3.2 Model Setup

For the trade study, we looked at 4 distinct cases: a 250 passenger tube-and-wing aircraft with 4 engines, and a 450 passenger aircraft with 2, 3 and 4 engines. The design parameters

were varied to match the analysis done in Greener by Design [10], which included preliminary analysis on the performance and potential emissions and noise impacts of aircraft design range and cruise altitude. The range of values, listed in Table 3.1, was also determined by constraints on aircraft operations. For example, the takeoff field length was varied between 9,000 to 15,000ft, which encompasses most of the airports in the US and UK. The parameters of the baseline aircraft (7260nm range, 33,000ft cruise altitude, 0.85 cruise Mach, 9950ft takeoff field length) for each of the 4 cases are listed in Table 3.2.

	Lower Bound	Upper Bound
Range (km/nm)	5,000/2,700	15,000/8,100
Cruise Altitude (ft)	25,000	33,000
Cruise Mach Number	0.8	0.9
Takeoff Field Length	9,000	15,000

Table 3.1: Range of values for parameters in trade study

Capacity (Number of Engines)	250 (2)	450(4)	450(3)	450 (2)
MTOW (lbs)	669,000	938,300	963,500	1,091,300
Thrust required per engine (lbs)	112,400	64,100	93,300	180,700
Wing Area (ft^2)	4,291	6,157	6,323	7,089
Wing Span (ft)	181.8	217.8	220.7	233.6

Table 3.2: Parameters for baseline aircraft

3.2.1 Engine Noise Prediction Model Setup

The engine cycles used for this trade study were scaled from two engines of different bypass ratios (BPR), General Electric CF6-80C2B8F (BPR 5.05) and GE-90B (BPR 8.7) two-spool unmixed flow turbofan engines. It is important to note that for the trade study it was assumed that as the thrust required per engine varies for each design, the engine cycles were kept essentially the same, maintaining a constant bypass ratio. The bypass ratio of the engine has significant effect on the noise generated by the engine, especially jet noise, as is observed from the trade studies.

It is also important to note that the jet temperatures, pressures, and velocities were kept constant for the trade studies. To provide a higher net thrust while keeping these variables constant, the mass flow through the engine basically has to scale directly with the thrust. This assumes that the jet area will also scale directly with thrust. Based on the thrust

requirement scaling, the jet, fan, turbine, and combustor areas, mass flows, and engine area are assumed to scale linearly with thrust.

3.2.2 Noise Propagation and Visualization Model Setup

The framework of NOISIM and how it interacts with NPM is illustrated in Figure 3-1, which was adapted from Huber [24]. In the trade study, the weather and trajectory inputs were assumed to remain the same. Though it would have been more realistic to have the trajectory vary with the high-level design parameters, the relationship between the parameters and noise would be more difficult to identify.

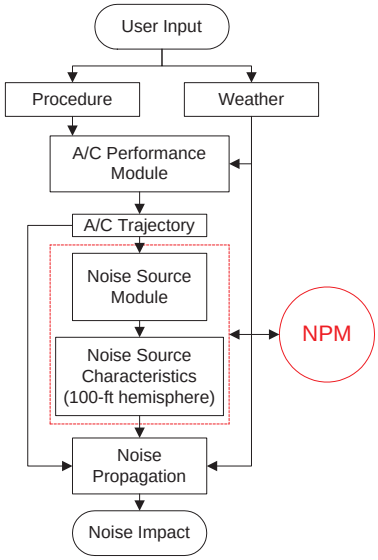

Figure 3-1: NOISIM framework and Integration with NPM [24]

3.3 Preliminary Trade Study Results

The results from the preliminary sizing study and figures that help quantify the implications of these results are presented in this section.

3.3.1 250-Passenger, 2-Engine Conventional Aircraft

The first trade study done was for a 250-passenger, 2-engine conventional design aircraft. As range was increased from 5,000 to 15,000km (about 2,700 to 8,000nm), the size of the aircraft and the thrust requirements for each engine increased with the design range.

The thrust requirement and aircraft geometries were passed to the noise prediction and propagation modes and the results were quantified in terms of the size of ground area affected by a given level of noise.

The noise footprint areas were first divided into three regions: 55dBA and above, between 50 to 55dBA, and less than 50dBA. 55dBA represents typical conversational noise levels and is a good gauge of how the design range affects this noise band. A cumulative graph of the size of each area is shown in Figure 3-2. From this analysis we observe the trend of the increasing noise footprint area above 55dBA as we increase the design range. As we look at the next bands of noise, we observe that most of the designs have the same cumulative noise footprint area. This indicates the the regions of noise below 50dBA remain essentially the same even as we change the design range, and that the region between 50-55dBA falls with design range, making up for the increased areas of the regions greater than 55dBA.

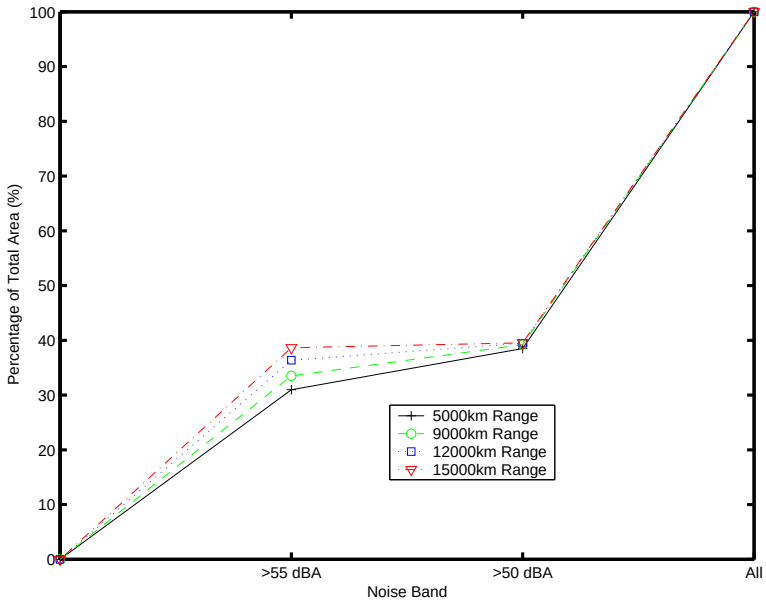

Figure 3-2: Cumulative curve of footprint areas (all regions); varying design range (250PAX, 2-Engine, tube-and-wing design)

For a more detailed analysis, the areas above 50dBA are broken down into 4 noise bands, as shown in Figure 3-3. There was the clear trend of increase in areas affected by more than 65dBA, and the decrease of areas affected by 50-65dBA as design range was increased. The increase in area affected by more than 75dBA was 3.05±0.87% (31.3±8km^2). This range is

determined based on the validation results, summarized in Table 2.3, that take into account the potential error of the framework.

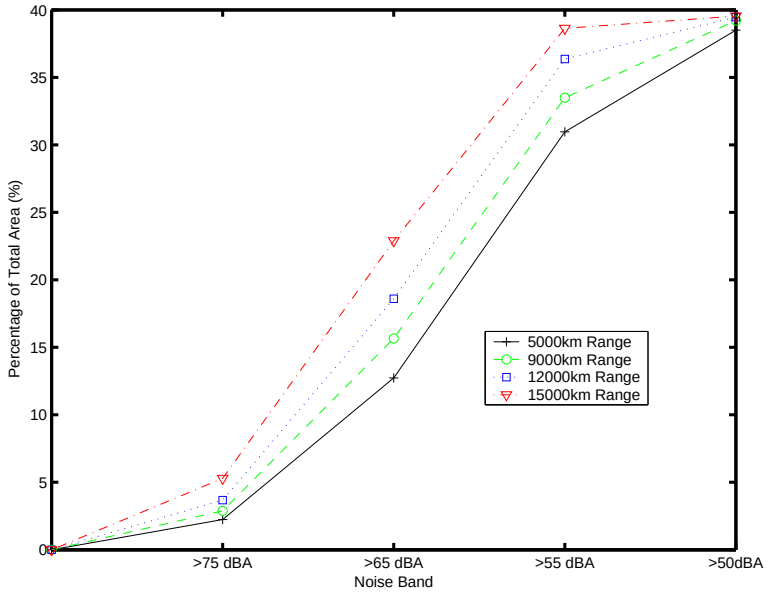

Figure 3-3: Cumulative curve of footprint areas (>50dBA regions); varying design range (250PAX, 2-Engine, tube-and-wing design)

There was also a significant trend as takeoff field length was increased, as shown in Figure 3-4. When the design takeoff field length was increased from 9,000 to 15,000ft, the area affected by more than 75dBA decreased by 1.34±0.87%, and the area affected by between 50-55dBA increased by 3.83±0.66%.

Results from varying design cruise altitude and Mach number showed no significant trend in noise footprint changes for aircraft designed for the given range of cruise altitudes and Mach numbers, given the level of accuracy in the DIF, as listed in Table 2.3.

One reason for the insensitivity to cruise Mach number is the result of using a fixed engine cycle and a low bypass ratio. For the design of a silent aircraft that tries to reduce jet noise, the engine will need to have a much higher bypass ratio than conventional engines at cruise and especially at takeoff. One possible way to do this is to use a variable engine cycle. Taking this into account, it is expected that as the design cruise Mach number increases; the amount of variable cycle required for the engine will increase, resulting in an increase in the size, weight and complexity of aircraft design. This will ultimately increase noise but was accounted for in this study because there was no way to accurately scale the

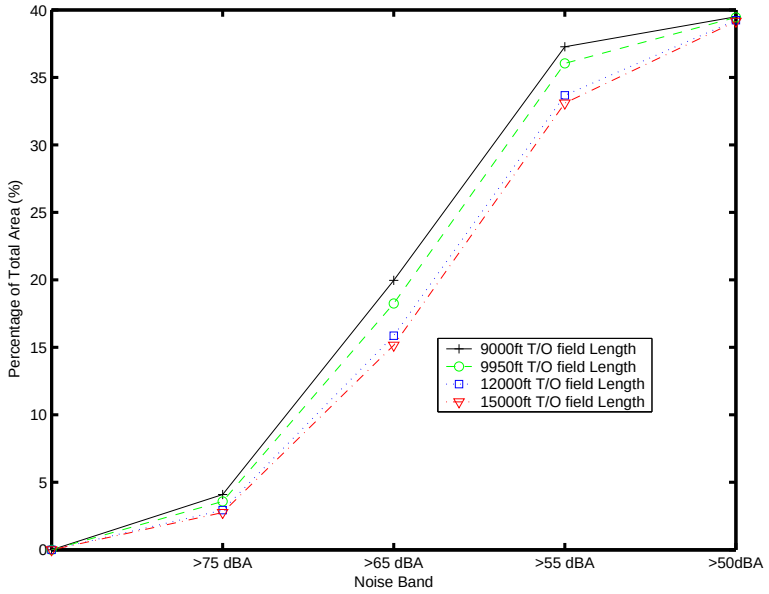

Figure 3-4: Cumulative curve of footprint areas (>50dBA regions); varying design takeoff field length (250PAX, 2-Engine, tube-and-wing design)

changes in size, weight and complexity with respect to variable cycle requirements.

3.3.2 450-Passenger, 2/3/4-Engine Aircraft

Similar trends were observed when the same high-level parameters were varied for the 450-passenger aircraft. When range was increased, there was an increase in the area with noise levels higher than 65dBA and a decrease in area affected by between 50-65dBA. And likewise, the area with less than 50dBA remained roughly the same at 60% of the total area within the $1024km^2$ grid. There was also no significant change in size of regions affected by the specified noise bands as cruise altitude and Mach number were varied.

Observing these similar trends and given the potential errors from the validation, we can summarize the first results of the trade study for range (an increase from 5,000 to 15,000km) in Table 3.3, where Regions A, B, C, and D correspond to the >75dBA, 65-75dBA, 55-65dBA, and 50-55dBA regions respectively. Comparing across aircraft configurations, the noise footprint of the 250-passenger aircraft was most sensitive to changes in range, followed by the 2-, 3-, and 4-engine 450-passenger aircraft respectively.

Because the 450-passenger, 2-engine aircraft has the most critical engine-out condition, it also had the largest area for Regions A and B, and smallest area for Regions C and D.

	Increase in area of footprint regions (%)			
	A	B	C	D
250PAX 2-Engine	3.06	7.11	-2.49	-6.64
450PAX 2-Engine	3.75	5.74	-3.79	-5.32
450PAX 3-Engine	2.19	5.99	-1.46	-5.74
450PAX 4-Engine	1.72	5.64	-0.51	-5.23

Table 3.3: Summary of change in areas due to an increase in design range of tube-and-wing designs from 5,000 to 15,000km

The engine-out condition refers to the one-engine-inoperative climb requirement stated in the Federal Aviation Regulation Part 25.121 [17]. This essentially requires that an aircraft, once at a certain point in the takeoff trajectory, to be able to continue to climb after one engine has failed. This effectively requires that a 2-engine aircraft to be able to climb with one engine; a 3-engine aircraft with 2, and so on. This results in similar-sized aircraft equipped with lesser number of engines requiring more total thrust.

The comparison between the four different configurations is shown in Figure 3-5. Reducing the number of engines on a 450-passenger plane designed for 5,000km range from four to two engines resulted in an increase in regions affected by more than 55dBA by 3.76% (38.5km^2). Note that the 450-passenger, 4-engine is quieter than the 250-passenger, 2-engine configuration. The reason is that the increase in thrust requirement, and thus noise, due to the reduction in number of engines more than offset the thrust increase due to a higher MTOW.

3.3.3 Jet Noise Directivity and Spectra Variation

After examining the footprints from the trade space study, a more detailed look was taken at the change in jet noise directivity and spectra. Though both jet and fan noise dominate during take-off, only jet noise is examined in detail because jet noise dominates at the low frequencies (seen in Figure 3-6), which is more critical when noise is propagated through the atmosphere. Figure 3-6 shows how the directivity and spectral map for jet noise changes as we increase the design range of the aircraft.

As the range, and hence size and thrust requirement, of the aircraft increases, the loudest noise remains in the low frequency bands but spreads from aft of the aircraft to almost slightly forward-propagating.

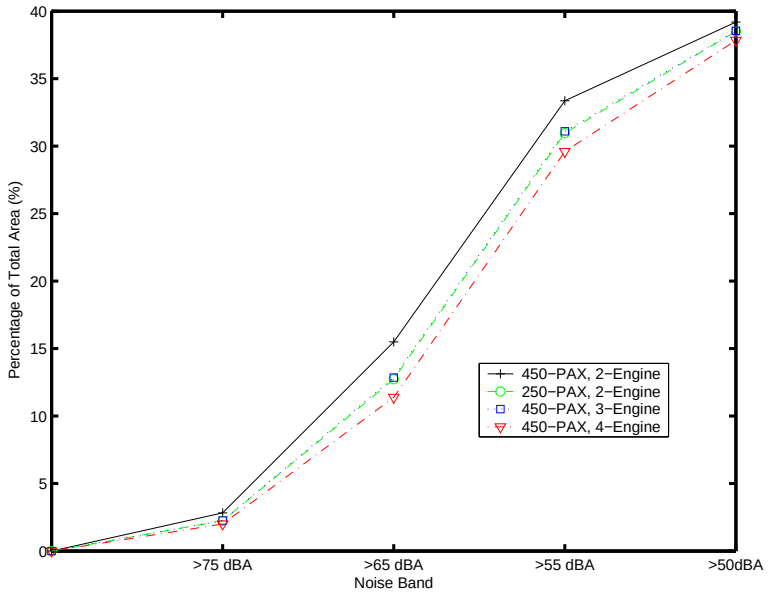

Figure 3-5: Noise footprint area comparison for all four tube-and-wing design configurations for design range of 5,000km

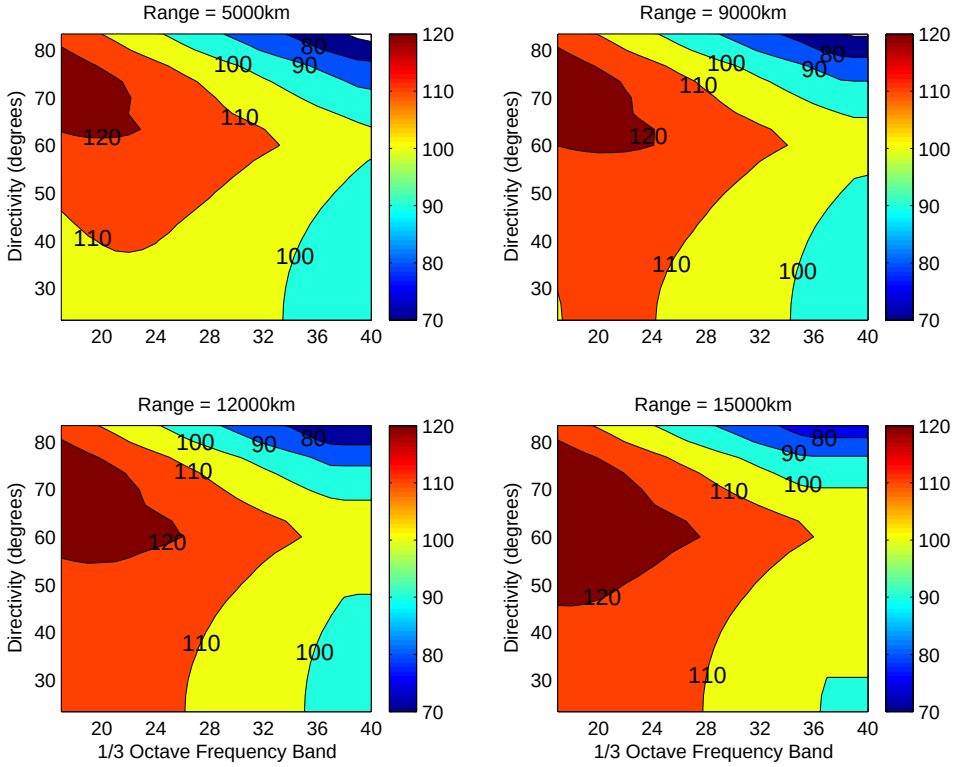

Figure 3-6: Jet Noise Spectra and Directivity with Range Variation

As the design take-off field length was decreased from 15,000ft to 9,000ft, the aircraft weight rose by 55%. The corresponding thrust requirement increase of 135% resulted from the balanced field length calculations done in the sizing model. The corresponding directivity and spectral map can be found in Figure 3-7.

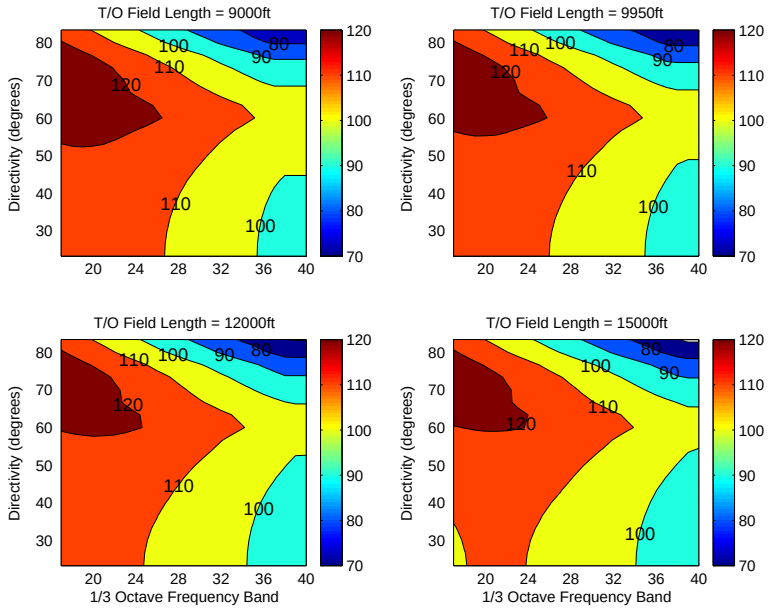

Figure 3-7: Jet noise spectra and directivity with take-off field length variation for tube-and-wing design

For design cruise altitude, the jet noise showed little variation (see Figure 3-8). There was only a maximum of 3.1% weight increase, and thus, thrust required, resulting from the trades done. This was to be expected because for the trade study done, the range of altitudes varied across would not result in a severe penalty in engine performance.

The trades for design cruise Mach number show almost as little variation as the cruise altitude trades (see Figure 3-9). This reflected the result of using a fixed engine cycle and a low bypass ratio.

The conventional aircraft design study was redone using an engine cycle with a bypass ratio of 8.4 (originally 5.05), with mass flow rates and geometries scaled accordingly. The engine cycle analysis results can be found in Table A.4. Figure 3-10 shows the areas of the noise bands 50dBA and above.

The first observation was that the noise contours were significantly smaller compared to the aircraft fitted with the lower bypass ratio engines (10% smaller footprint area for regions

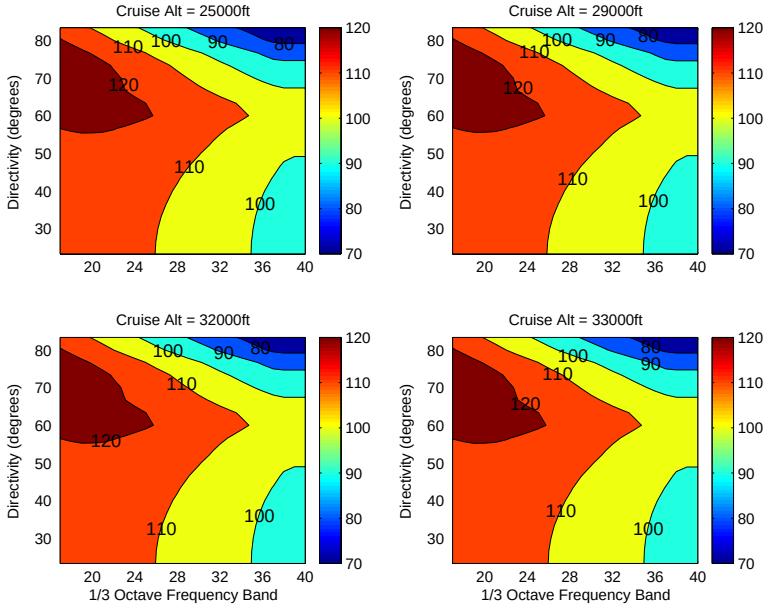

Figure 3-8: Jet noise spectra and directivity with cruise altitude variation for tube-and-wing design

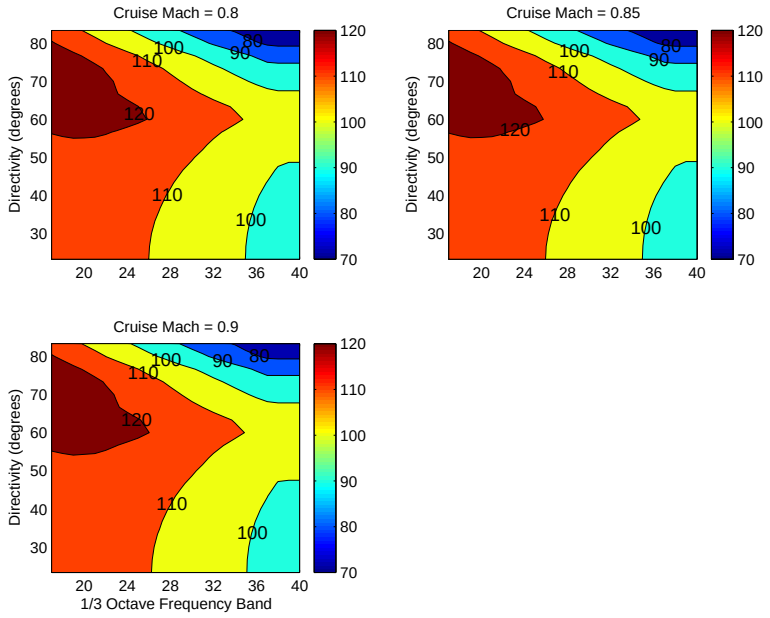

Figure 3-9: Jet noise spectra and directivity with cruise Mach variation for tube-and-wing design

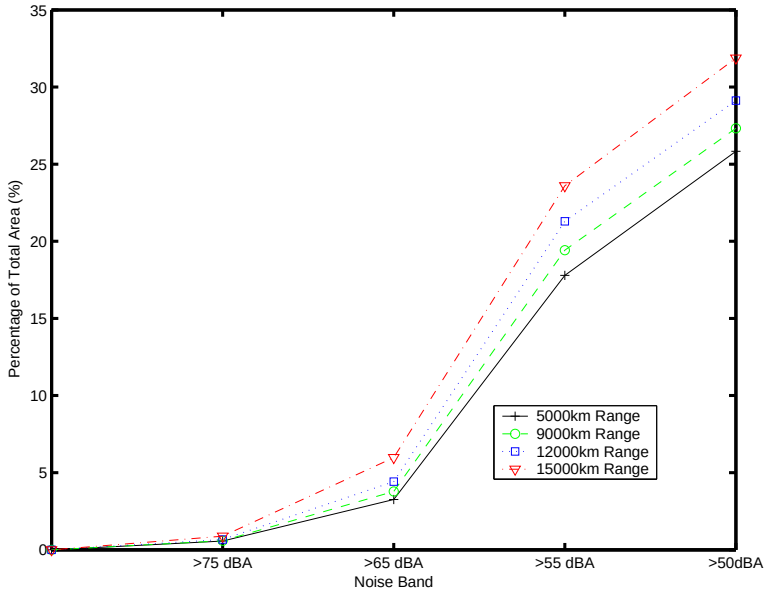

Figure 3-10: Cumulative curve of footprint areas (all regions); varying design range (250PAX, 2 Hi-BPR Engine, tube-and-wing design)

with 50dBA or more). This trend was expected because, as mentioned earlier, higher bypass ratio engines produce lower jet noise.

The observation that was more significant was that the change in areas of regions when varying design parameters had also become less significant. For example, when varying design range from 5,000km to 15,000km, the increase in Region A is at most 1.18%. A summary of the findings is presented in Table 3.4 and Table 3.5.

	Increase in area of footprint regions (%)			
	A	B	C	D
250PAX 2-Engine (BPR 8.4)	0.32	2.42	-2.95	-0.22
250PAX 2-Engine (BPR 5.05)	3.06	7.11	-2.49	-6.64

Table 3.4: Change in area due to increasing range from 5,000 to 15,000km for different BPR designs

Comparing across the 250-passenger aircraft with different number of engines, as shown in Table 3.6, we see a trend of reducing sensitivity of areas to design range, especially for the regions with higher noise levels (Regions A and B).

	Increase in area of footprint regions (%)			
	A	B	C	D
250PAX 2-Engine (BPR 8.4)	0.14	1.04	1.83	-0.17
250PAX 2-Engine (BPR 5.05)	1.34	3.47	-1.88	-3.83

Table 3.5: Change in area due to decreasing takeoff field lengths from for designs with Hi-BPR engines

	Increase in area of footprint regions (%)			
	A	B	C	D
250PAX 2-Engine	3.06	7.11	2.49	6.64
250PAX 3-Engine	7.45	5.74	3.79	5.32
250PAX 4-Engine	1.73	5.65	0.51	5.23

Table 3.6: Summary of change in areas due to an increase in design range

3.4 Summary

Based on the results from this preliminary trade study, some drivers of noise were identified. The trends observed in change of footprint areas show correlation to the MTOW of the aircraft. Minimizing design range and maximizing takeoff field length can potentially reduce the noise levels on the ground. However, it was also found that as the design moved towards one with higher bypass ratio engines, the savings from design range reduction and takeoff length increase became less significant.

The effects of varying the cruise altitude and Mach number on the noise footprint areas were minimal, although several important factors were not modelled. The results for cruise Mach number were far less conclusive for a silent aircraft design with alternative engine designs like a variable cycle engine because of the related complexities.

In the next chapter we will discuss the extension and use of the DIF for trade studies on blended-wing-body designs. There will be some description on how the framework was modified for use on an unconventional framework and thus its subsequent limitations. The trade study results were compared with conventional planform studies to show the difference in sensitivity of noise footprint areas to high level design parameters.

Chapter 4

Trade Study for Silent Aircraft Designs

4.1 Introduction

This section presents the results of a trade study on a silent aircraft design (based on a blended-wing-body planform) and compares the jet noise footprints to conventional tube-and-wing designs. Only jet noise footprints were used for this trade study because we were yet unable to predict the parameters of the other engine components throughout the entire takeoff procedure. Airframe noise was not used because it is a function of the planform geometry, which was held constant for this trade study. The parameters used for this trade study parallel those done in the pervious section: range, cruise altitude, cruise Mach number, and takeoff field length. For each parameter sweep, thrust requirement was used as the scaling factor.

In this chapter, we first describe the modifications made to the original DIF to accommodate the new planform and list their subsequent limitations. Second, the results from the trade study are presented and discussed. Third, these results are compared with those of a conventional aircraft and the design implications are discussed.

4.2 Framework modifications

To accommodate a silent aircraft design that implements noise reduction concepts, some changes were made to the design framework. The conventional aircraft sizing model was

no longer appropriate or adequate to define the size, weight, and thrust requirements for a blended-wing-body planform. Hence a new tool was created to adequately capture the sizing and performance of these designs. This tool, termed the Independent Design Tool (IDT), was created by Diedrich [12] and replaces the ASPM in estimating the gross take-off weight and thrust requirement of the silent aircraft. The IDT uses a similar algorithm to that of the ASPM. Because the engines are embedded, the engine design also becomes more involved and is a more iterative process than before. An overview of the new design framework is shown in Figure 4-1. Instead of just having high-level design parameters as inputs, the noise targets were also input to help guide the engine and trajectory design. The rest of the engine was designed to meet the mission requirements given by the designed trajectory and thrust requirements. The boxes in Figure 4-1 within the dashed lines were also de-automated from the trade study process. As the design parameters were varied, simple scaling laws were used to vary the jet areas of the engine with respect to the thrust requirements.

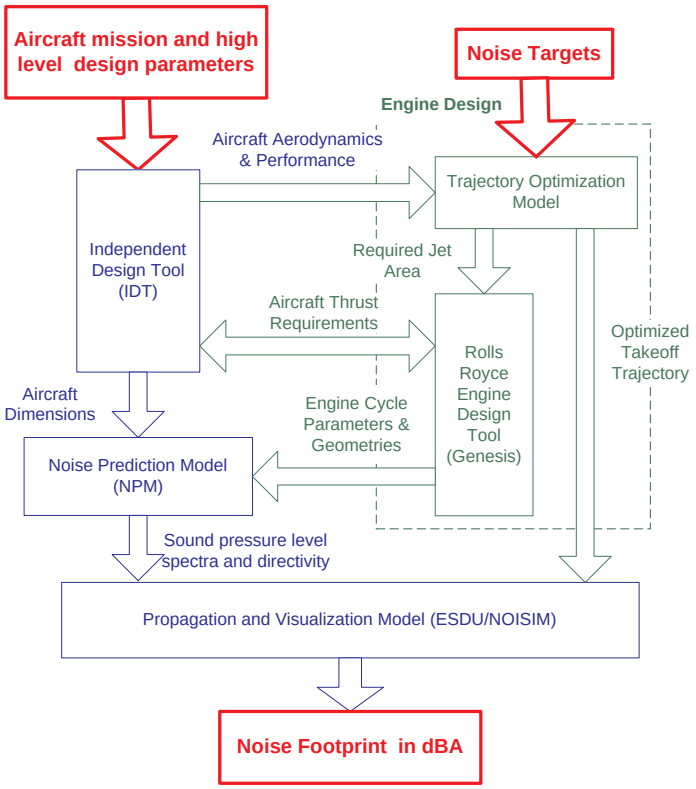

Figure 4-1: DIF for silent aircraft designs

Because of the lack of empirical data for scaling silent aircraft designs, there is considerable computational intensity required to generate an optimized silent aircraft planform for a given mission requirement. For this study, a less computationally intensive method was used to generate the aircraft weights and thrust requirements. It is important to note that because the IDT uses the planform of an optimized 250-passenger, 4000nm design range aircraft as a baseline, the further we deviated from this configuration, the less confidence there was that the predicted aircraft weight was optimized and satisfied all the design constraints set on the baseline design. For example, as the design range was increased from 4,000 to 8,000nm, there was an increasing difference in gross takeoff weight of the IDT-produced aircraft and an aircraft with an optimized planform, as shown in Figure 4-2.

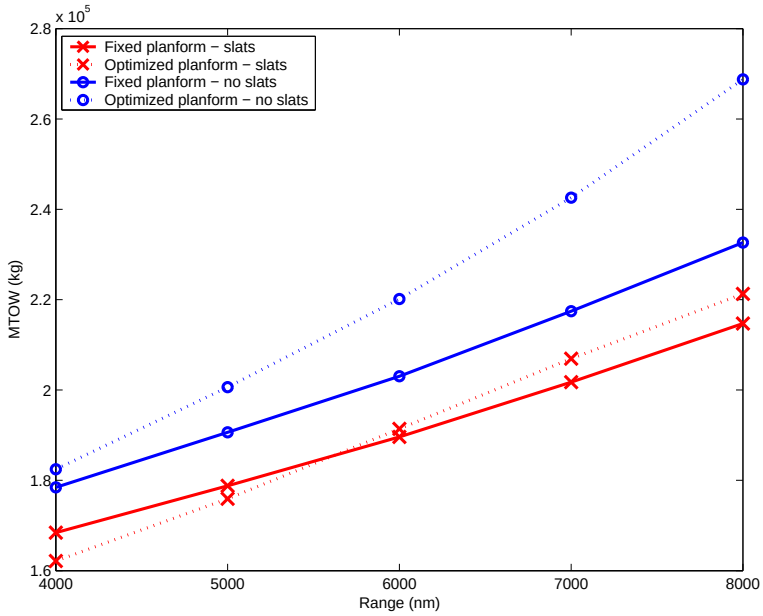

Figure 4-2: Maximum takeoff weights of IDT-produced and optimized silent aircraft designs for different ranges

The planform with slats had a lesser maximum deviation from the takeoff weight of the optimized design and was thus be used as the baseline planform. A similar trend was observed for a sweep of cruise Mach numbers in Figure 4-3.

The IDT, like the ASPM, sized the engine according to the mission requirements and engine-out condition. Since the engine was also designed for a 250-passenger, 4000nm design range aircraft it was also less accurate as the thrust requirement deviated from the baseline. The engine design was based on an embedded propulsion system which Hall et al.

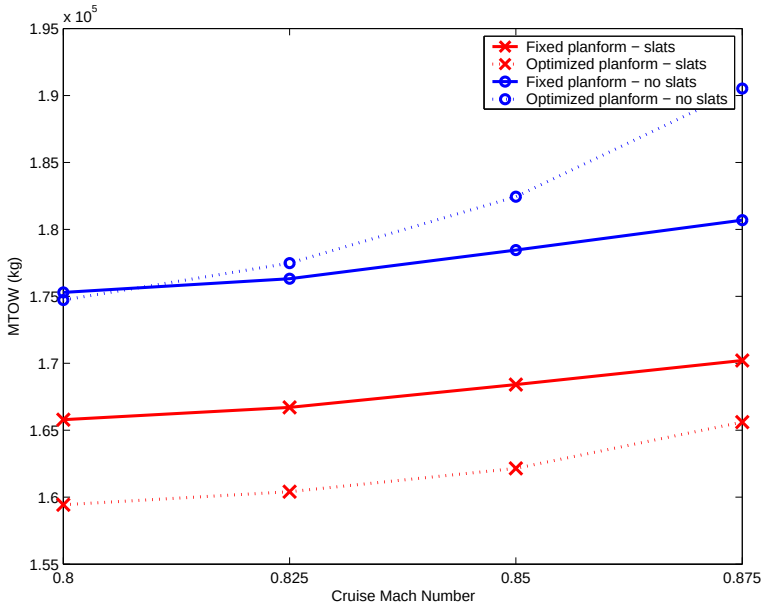

Figure 4-3: Maximum takeoff weights of IDT-produced and optimized silent aircraft designs for different cruise Mach numbers

[19] discuss in detail. A parametric study on the engine design yielded the variation of the thrust and specific fuel consumption (SFC) with cruise altitude and Mach number at both cruise and climb conditions. These values were normalized by sea-level conditions such that when the aircraft was scaled from the baseline, the thrust and SFC were scaled according to the size of the engine.

Figures 4-4 and 4-5 separate the portions of the takeoff profile where the engine is assumed to operate at climb and cruise conditions. As with the baseline design in the previous chapter, the takeoff trajectory was optimized for 2 different airport conditions: sea level, and hot and high. The climb portion of the mission profile can be approximately separated into 2 main portions: brakes off to cutback (at Mach 0.23, 200m above runway), and climb to cruise altitude (at 12,192m). It was assumed that the transition of the engine cycle takes place somewhere in the second portion of the climb profile, defined by the point where the trajectory crosses the dashed line representing the climb conditions. The discontinuity observed in both plots was a result of superimposing the climb and cruise performance of the engine, which took into account the variable cycle engine.

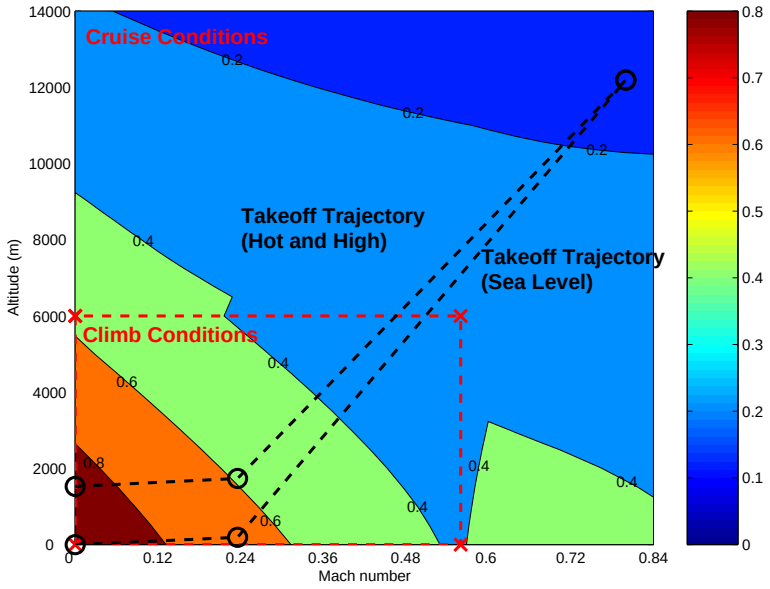

Figure 4-4: Mission profile mapped onto contour plot of thrust (normalized by sea-level conditions) variation with altitude and Mach number

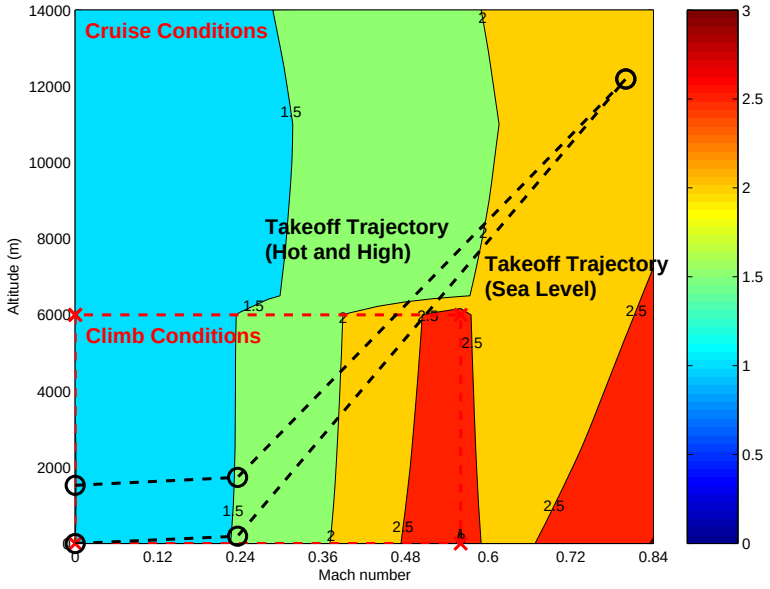

Figure 4-5: Mission profile mapped onto contour plot of SFC (normalized by sea-level conditions) variation with altitude and Mach number

4.3 Trade Study Results

For the trade study, we first analyzed how the predicted MTOW and thrust requirement of each design varied with the design parameters. The baseline design parameters, listed in Table 4.1, were kept constant unless that particular parameter was being varied for the trade study. This baseline was chosen because it most closely resembled that of the originally optimized planform.

Baseline Parameters	
Range (nm)	4,000
Cruise Altitude (ft)	35,000
Cruise Mach Number	0.8
Takeoff Field Length (ft)	10,000
Number of Passengers	250
Number of Engines	4
Wing Area (m^2)	790

Table 4.1: Mission characteristics for the SAX

For ease of comparison each design parameter was varied across five values with a constant interval. For ease of reference, each of those values will be referred to according to the parameter index assigned in Table 4.2. For example, Figure 4-6 shows the MTOW of the aircraft rise linearly as we increase the cruise Mach number from 0.8 to 0.9, with indices 1 and 5 representing cruise Mach numbers of 0.8 and 0.9 respectively. Note that the baseline design corresponds to the first design parameter index for range and cruise Mach number, and the third design parameter index for cruise altitude and takeoff field length. These four designs are identical have a corresponding MTOW of 164,000kg. This is also true for the thrust requirement outputs from the IDT, as shown in Figure 4-7.

Parameter Index	1	2	3	4	5
Range (nm)	4,000	5,000	6,000	7,000	8,000
Cruise Altitude (ft)	25,000	30,000	35,000	40,000	45,000
Cruise Mach Number	0.8	0.825	0.85	0.875	0.9
Takeoff Field Length (ft)	14,000	12,000	10,000	8,000	6,000

Table 4.2: Design parameters used for trade studies

As range was increased, the required fuel weight also increased, resulting in a rising MTOW and thrust requirement. Because the engine was designed to operate at Mach

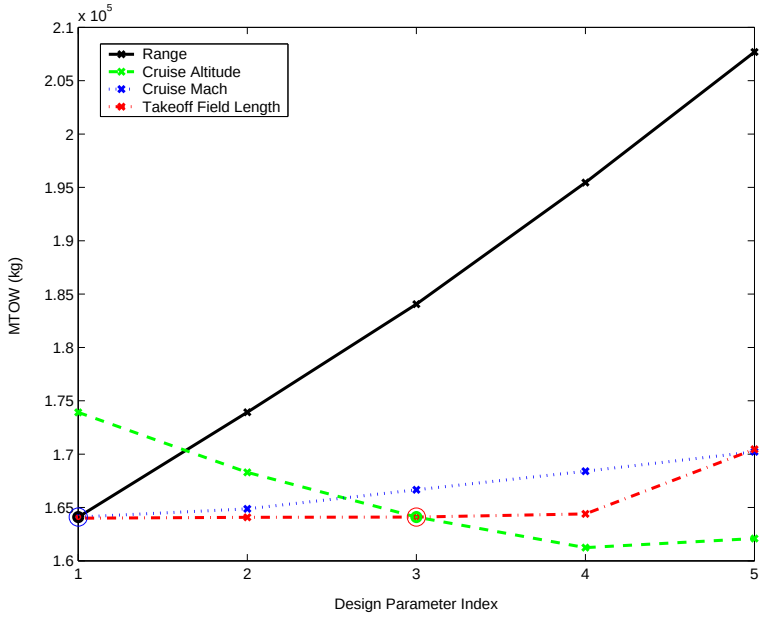

Figure 4-6: Variation of MTOW with design parameters (250PAX, 4-Engine, silent aircraft design), circle symbol denotes the baseline design

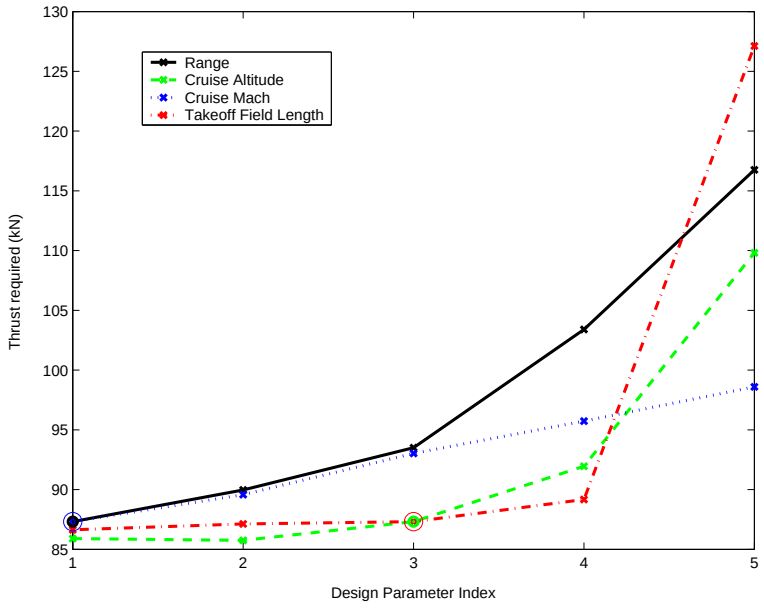

Figure 4-7: Variation of thrust required per engine with design parameters (250PAX, 4-Engine, silent aircraft design), circle symbol denotes the baseline design

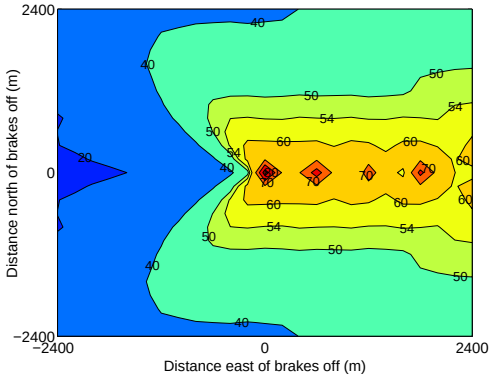

Figure 4-8: Silent aircraft full trajectory footprint

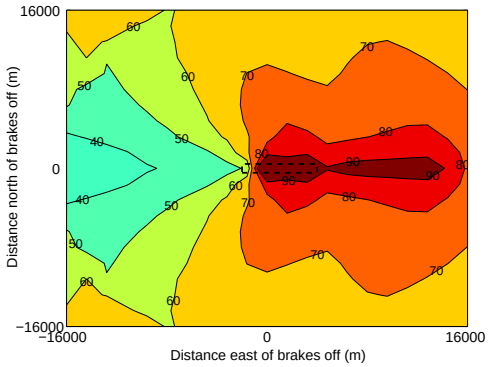

Figure 4-9: Conventional full trajectory footprint

0.8, flying faster would result in a poorer engine performance and a subsequent increase in thrust requirement to perform a given mission. The relationship between MTOW and thrust to takeoff field length was a result of the engine-out conditions. Between a takeoff field length of 10,000 to 14,000ft, the engine-out condition was satisfied, but a shorter field length required the engine to be scaled up to produce significantly more thrust. The cruise altitude was the only parameter that displayed an opposing relationship between MTOW and thrust required. The MTOW was minimized at around 40,000 to 45,000ft cruise altitude because the planform was optimized for that design point. However, for the engine, cruising at a higher altitude would mean a reduction in mass flow rate and thus net thrust. As a result, the thrust requirement increases.

For consistency in comparison, the same trajectory, designed for jet noise reduction, was used for this trade study. The typical shape of a full-trajectory jet noise footprint over a 32-by-32km area centered around the brakes off location is shown in Figure 4-8. The results showed that the footprint areas remain the same for all the design variations. This was due to the fact that the resolution of the footprint was not fine enough to capture the changes in footprint area. For more meaningful results, it was better to compare the footprints at a higher resolution. The footprints were thus compared within a 4.8-by-4.8km area with a grid resolution of 200-by-200m.

As a comparison, a trade study was conducted on a conventional tube-and-wing design equipped with four CF6-80C2F8 engines using the same conditions. A jet noise footprint for the conventional design is shown in Figure 4-9. Comparing the noise footprints show that the SAX design produces 30-35dBA less jet noise than conventional designs.

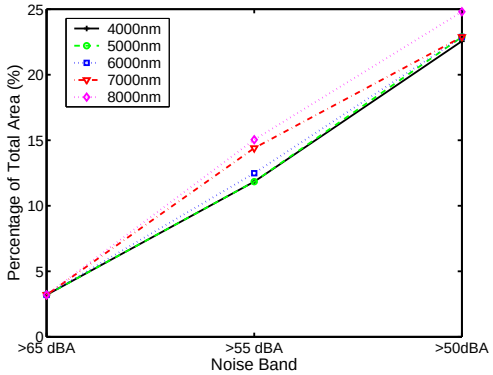

Figure 4-10: Silent aircraft cumulative curves for varying range

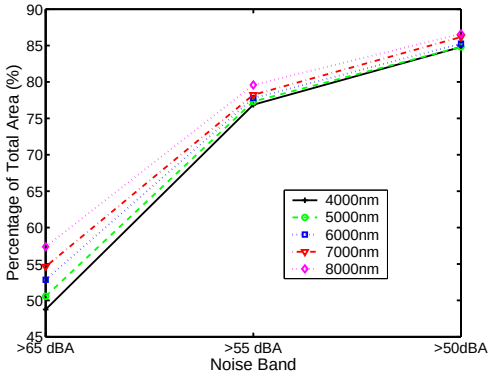

Figure 4-11: Conventional cumulative curves for varying range

The footprints were separated into 3 noise bands as the design parameters were varied: greater than 65dBA, between 55 and 65dBA and less than 55dBA. The footprint regions receiving more than 65dBA of noise were much more sensitive to range changes for the conventional design (see Figure 4-10), increasing by 9% ($92km^2$) when varying range from 4,000 to 8,000nm. For the silent aircraft (see Figure 4-11), there were no observed changes in the region greater than 65dBA. For the same increase in range, there were similar changes in both silent aircraft and conventional footprints in the 50-65dBA region, with a 4% increase in the regions receiving greater than 55dBA of noise. However, due to the difference in resolution, the absolute increase in area was more significant for the conventional aircraft ($41km^2$) than silent aircraft ($0.92km^2$). It was also observed that for a 4,000nm range conventional aircraft, $768km^2$ of the area received noise louder than 55dBA, whereas the grid for the silent aircraft only had $2.53km^2$. Even for the 8,000nm silent aircraft, the region receiving more than 55dBA is minimal ($3.46km^2$) compared to that of a conventional aircraft.

The increase in footprint area for cruise altitude variation occurred when the cruise altitude deviated from the condition at which the engine would perform most efficiently. From Figure 4-12, we found that the most favorable cruise altitude for the silent aircraft was 35,000ft, with a 3% ($0.69km^2$) increase in the 55-65dBA region when the cruise altitude is set at 45,000ft. This trend was similar for the conventional aircraft (see Figure 4-13 except that the best cruise altitude is 30,000ft. Similar to the results for range variation, the regions greater than 65dBA were more sensitive for the conventional than the silent aircraft designs when varying cruise altitude.

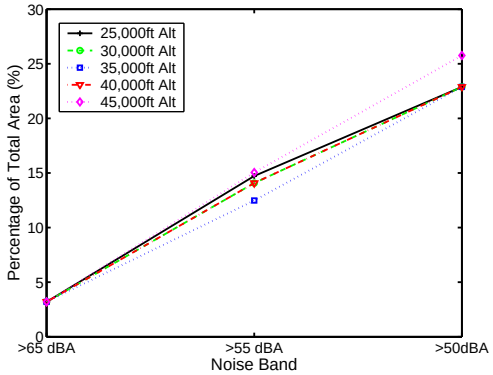

Figure 4-12: Silent aircraft cumulative curves for varying cruise altitude

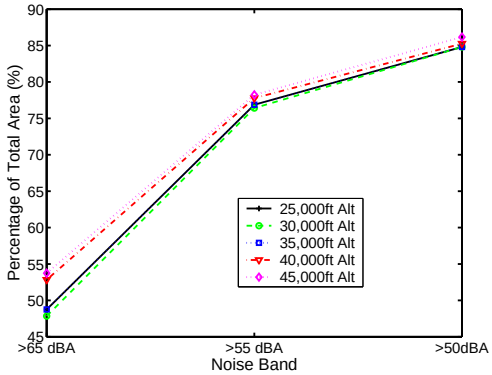

Figure 4-13: Conventional cumulative curves for varying cruise altitude

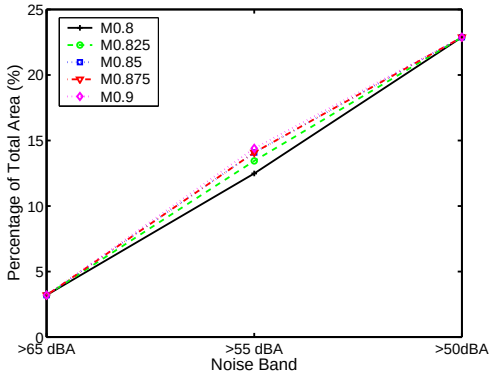

Figure 4-14: Silent aircraft cumulative curves for varying cruise Mach

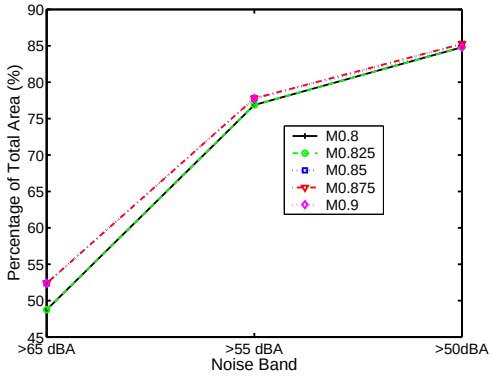

Figure 4-15: Conventional cumulative curves for varying cruise Mach

The results for cruise Mach number variation from 0.8 to 0.9 indicated that there was a 2% ($0.46km^2$) increase footprint area in the 55-65dBA region for the silent aircraft (see Figure 4-14). This result however, like in the previous trade study, did not take into account the increase in the size, weight and complexity of an aircraft designed to fly faster during cruise, which most likely will result in a noisier aircraft at Mach 0.9. Figure 4-15 shows that the conventional designs were again more sensitive to changes in cruise Mach number, especially in the regions receiving greater than 65dBA of noise.

Figure 4-16 shows the takeoff field length variation, where the most significant changes for the silent aircraft design were observed. When takeoff field length was reduced from 10,000 to 6,000ft, there was a significant increase of about 5% ($1.15km^2$) in the 55-65dBA region. Contrary to the observations in the other design parameters, the conventional design showed less sensitivity to takeoff field length variation. The thrust requirement, and thus

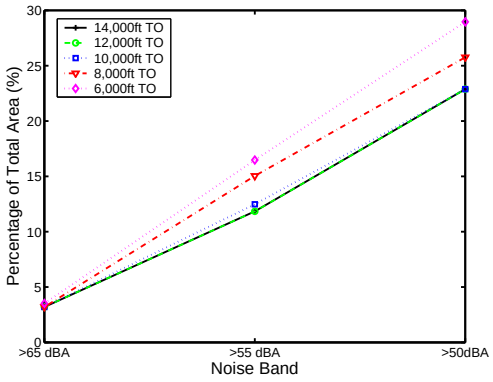

Figure 4-16: Silent aircraft cumulative curves for varying takeoff field length

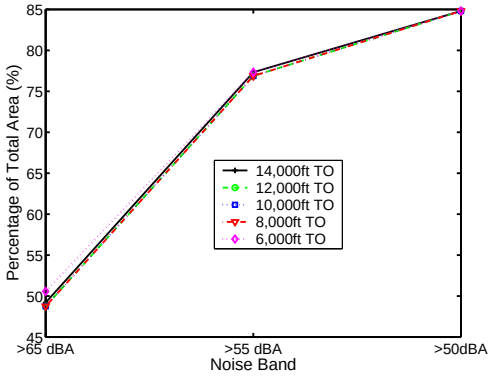

Figure 4-17: Conventional cumulative curves for varying takeoff field length

the noise footprints, did not change significantly at the different field length settings. This was because the baseline engine for the conventional design was able to meet the engine-out condition without being scaled up significantly.

The trends observed in the trade study show that the footprint areas are generally more sensitive to corresponding design parameter changes. For all designs, there was most significant increase in the 55-65dBA footprint area as the range was increased from 4,000 to 8,000nm. The cruise altitude that yielded the best engine performance for the silent aircraft, and thus least noise impact was at 35,000ft. Likewise, the engine performed best at a cruise Mach number of 0.8. The takeoff field length had significant effect on the noise footprint because the baseline engines needed to be scaled up to meet the thrust requirements for the engine-out condition for runway lengths greater than 8,000ft.

4.4 Summary

This trade study presented results of how the noise footprint area was affected by varying high level design parameters. The results indicated that, compared to a conventional tube-and-wing design, the jet noise footprint area of a silent aircraft was less sensitive to changes in all high level design parameters investigated in this trade study. The only exception is takeoff field length. To minimize the jet noise impacts given the current embedded engine design, the 250 passenger SAX aircraft should be designed for 4,000nm range, 35,000ft cruise altitude, Mach 0.8 at cruise, and 10,000 to 14,000ft takeoff field length.

Comparing these design recommendation with a preliminary analysis done in the Greener

by Design [10] report, we find a similar suggestion for designing for short-range flights. A preliminary analysis was also done for the impact of flight altitude on greenhouse effects, taking into account the effect of NOx on ozone creation and the effect of water emissions. The analysis indicated that the greenhouse effect of a medium range aircraft at 32,000ft is less than half that of the long-range aircraft at 40,000ft and its fuel burn is 15% lower. This suggestion is also in agreement with the trade study results.

The next chapter will discuss the design and detailed noise audit of a silent aircraft that employs quiet engine and blended-wing-body airframe design concepts. Noise footprints will be used to identify the main noise contributions for this unconventional aircraft design.

Chapter 5

Noise Audit for Silent Aircraft Design

5.1 Introduction

The silent design concepts that can be applied to an aircraft are limited by the type of airframe used. The analysis by Pilczer [36] suggests a potential reduction of 27 dB in approach EPNL using quiet lift concepts, and 22.5 dB in takeoff EPNL for multiple high aspect ratio jets embedded into the blended-wing-body airframe. A more detailed analysis for this planform can be done by visualizing the noise impacts in terms of noise footprints.

One of the noise assessment goals of the SAI is to compare the noise caused by the aircraft outside a typical airport boundary to urban noise levels. The dimensions of the airport boundary used for this noise audit are shown in Figure 5-1. For the noise audit, we focused on how the implementation of various technologies affected the noise levels outside this airport boundary.

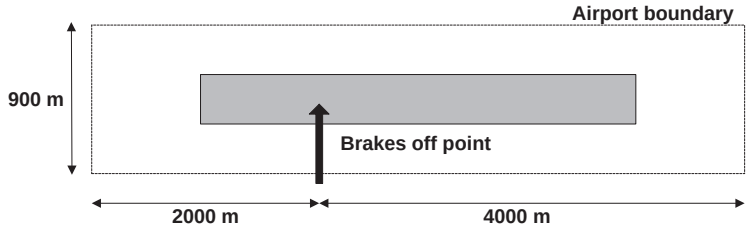

Figure 5-1: Airport boundary used for SAX noise audit

This chapter describes the investigation of the noise characteristics of an aircraft that integrates both silent engine and blended-wing-body airframe design concepts, henceforth termed the Silent Aircraft Experimental (SAX) design. First we discuss the design concepts that led to the creation of the SAX mission, planform, and engine. Next we present the methodology and fidelity of the noise prediction in this noise audit. Following that is a brief discussion about the methodology and application of shielding approximations by the airframe. Finally, we examine the single-event noise footprints for individual components at critical points along the mission profile. The noise source components can be broadly categorized into engine and airframe. Within these two categories are a number of sub-categories that will also be assessed for their contributions to noise.

5.2 SAX Design Overview

5.2.1 SAX Mission

The mission characteristics of the SAX are listed in Table 5.1. From the preliminary trade study in the previous chapter it was shown that range is a major driver for the size and thus noise of the aircraft. Two constraints were thus set on the range of the aircraft. It was beneficial for the SAX to be designed for a minimal range to reduce noise, but the range still needed to be practical for commercial use. The range was finally set at 4,000nm to satisfy the Trans-Atlantic route between New York and London.

The payload was set to 250 to match a Boeing 767. This was because one of the goals of the SAI [41] was that the SAX design be economically viable. By matching the SAX payload to a commercial design, this would at least ensure the market exists.

Mission Parameters	
Range (nm)	4,000
Number of Passengers	250
Cruise Altitude (ft)	40,000 - 45,000
Cruise Mach Number	0.8

Table 5.1: Mission characteristics for the SAX

The cruise altitude of the SAX design was set to be between 40,000 to 45,000ft because of improved lift coefficients at higher altitudes. This is a result of the chords of the SAX wing, which is significantly longer than conventional tube-and-wing aircraft of comparable

size.

The typical cruise Mach number of a commercial aircraft is between 0.8 to 0.9, depending on the engine design. Hall et al. [19] suggest that a lower cruise Mach number is better for the integration of a variable cycle engine design, which is what the SAX incorporates in attempts to significantly reduce noise levels. As such, a cruise Mach number for the SAX design was set to be 0.8.

For a comprehensive study of its noise profile, a takeoff trajectory was required and we used a takeoff trajectory designed by Crichton et al. [11] for jet noise reduction. The flight path of the aircraft is a simple eastwards climb without any bank or roll maneuvers, and the flight path is shown in Figure 5-2. This trajectory was designed for a 10,000ft long runway at sea level with International Standard Atmosphere(ISA)+12K conditions to satisfy the majority of takeoff conditions at Heathrow airport.

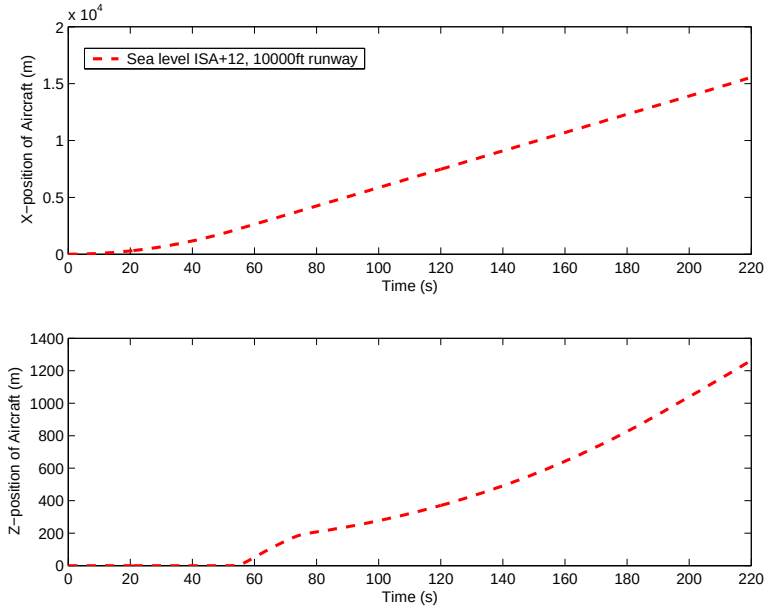

Figure 5-2: Ground distance and altitude for optimized SAX jet noise reduction takeoff trajectory [11]

5.2.2 SAX Planform and Airframe

The SAX planform was optimized to reduce the maximum gross takeoff weight (MTOW) and constrained to meet the mission and performance requirements. This planform optimization process is discussed in detail by Diedrich [12]. A design space sensitivity analysis

was also conducted for the mission parameters of the SAX planform to see their effects on MTOW. Table 5.2 is a summary of both the engine and airframe design parameters of the optimized SAX design. The SAX planform shown in Figure 5-3 has its coordinates non-dimensionalized with reference to the span.

Design Parameters	
Wing Span (m)	58.52
Planform Area (m^2)	753.68
Maximum takeoff weight (kg)	152,809
Operating Empty Weight (kg)	95,282
Landing Weight (kg)	120,360
Engine installed mass (lbs)	28,987
Takeoff bypass ratio	20.3 - 21.7
Cruise bypass ratio	17.8
Specific fuel consumption at cruise ($lb/lb-h$)	0.54
Cruise L/D	21.4 - 22.0

Table 5.2: Engine and airframe design parameters for the SAX

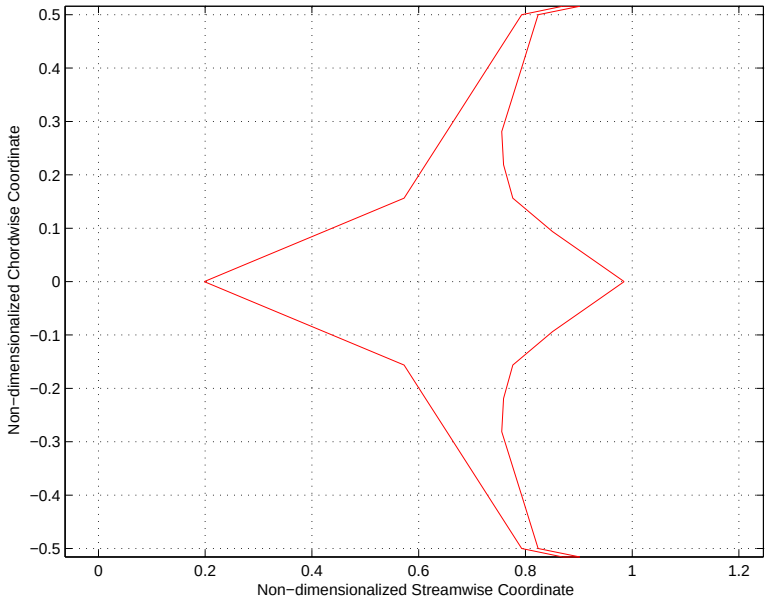

Figure 5-3: SAX10 planform

5.2.3 SAX Engine Design

The engine of the SAX design is called the Granta-251, and is a high bypass ratio 2-shaft turbofan with a geared fan, booster compressor, axial-radial HP compressor and variable

area exhaust nozzle. The gearbox has a 3:1 reduction ratio (i.e. the fan rotational speed is one-third of the low pressure turbine rotational speed). The component efficiencies and temperature limits are set appropriately for 2025 technology levels. Four of these engines are embedded into the SAX airframe. One of the reasons for using four engines was because of the trade study results for conventional tube-and-wing designs, where it was found that the thrust requirement, and thus noise footprint areas, were less for a 4-engine design than a 2-engine design. Having more engines could potentially further reduce the noise but we will only analyze the 4-engine design for now. The mechanical design of Granta-251 was completed using the engine cycle performance data at two critical conditions: top-of-climb and maximum continuous thrust. All other points along the mission were considered off-design points.

5.3 Source Noise Assessment

5.3.1 SAX Engine Source Noise

The engine noise was separated into five main categories: jet, fan forward, fan rearward, turbine, and core. Each of these categories have several contributing noise sources, as listed in Table 5.3.

Fan Forward	Broadband, Rotor locked buzz, Distortion buzz, Liner induced buzz, Steady distortion, Bypass wake interaction, Rotor alone, Supersonic distortion, Low engine orders, Engine section wake interaction
Fan Rearward	Broadband, Steady distortion, Bypass wake interaction
Jet	Jet exhaust
Turbine	Steady distortion, Upstream wake Interaction, Downstream wake interaction, Broadband, Haystack
Core	Broadband

Table 5.3: Noise source components

The noise from these five main components was examined at three low altitude locations of the mission during which the most noise was thought to be caused. These three locations are illustrated in Figure 5-4 and listed as start of climb, flyover, and approach.

The approach was separated into 2 conditions: a 3-degree and 6-degree continuous descent approach. The details about the aircraft and atmospheric conditions at these points are listed in Table 5.4. The ambient air considered for takeoff was ISA+12K to satisfy most

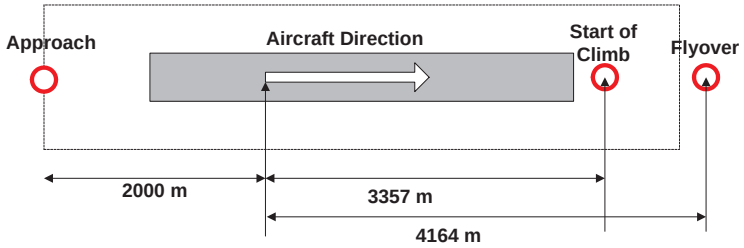

Figure 5-4: Points along trajectory used for noise audit

takeoff conditions from Heathrow [11] airport. For approach the differences between ISA and ISA+12K were insignificant so only ISA conditions were considered. The aircraft pitch is presented in the table as the angle of attack of the aircraft plus or minus the climb or glide slope angle for takeoff and approach respectively.

	Start of Climb	Flyover	3-degree approach	6-degree approach
Ambient air	ISA+12K	ISA+12K	ISA	ISA
Altitude (m)	180	200	105	210
Distance from brakes off point (m)	3,357	4,164	-2000	-2000
Aircraft pitch (degrees)	11.25+6.535	11.65+2.135	14.6−3	14.6−6
Flight speed (m/s)	80.1	82.2	75	75
Total net thrust (kN)	316.7	174.1	40.0	40.0

Table 5.4: Noise audit location conditions

The amount of error of each noise source OASPL, summarized in Table 5.5, is based on the limitations of the prediction methods used by SAI Engine Team[1]. It must be noted that the accuracy of noise prediction depends on both the engine parameters and the prediction methods themselves. For example, the errors associated with the jet noise prediction will depend greatly on the level of accuracy in predicting the jet velocity, area and other parameters. Additional errors can come from the prediction methods themselves. Because semi-empirical noise prediction methods were used, the accuracy of the noise levels depends on how far the design deviates from those used to validate the noise prediction method. For an unconventional design like the Granta-251, it is hard to determine the errors associated with the noise prediction. Thus for this analysis, a rough estimate of the expected upper

[1]For a preliminary noise audit of the SAX design, the SAI Engine Team predicted most of the engine noise using VN02, the noise prediction component of Genesis, a Rolls Royce engine design tool. The Stone [42] method was used to predict the jet noise because the exhaust nozzle area was not set correctly in VN02 and could not be changed easily within the input data file.

bound is provided.

Fan Forward	±5dB
Fan Rearward	±5dB
Jet	±5dB
Turbine	±10dB
Core	±5dB

Table 5.5: Engine Noise source prediction accuracy [20]

The reason that the turbine noise prediction has higher potential errors is because the turbine parameters were significantly more difficult to predict than the other parameters. The turbine noise was derived from correlations based on the turbine geometry and the flow conditions within each turbine stage. As a result of inaccuracies in the precise turbine shaft speed at off-design operating conditions, Hall et al. [20] expect significant error in these values. This error is in addition to inaccuracies in the liner attenuations and propagation effects, and could be as much as ±10dB.

Because of the definition of the A-weighted SPL, an OASPL increase of 5dB in all one-third octave center band frequencies corresponds to a 5dBA rise in A-weighted SPL, and likewise for a decrease. These potential errors were taken into account when interpreting the noise footprints.

5.3.2 SAX Airframe Source Noise

Most of the airframe noise prediction was based the Fink [18] method outlined in the NASA ANOPP manual [48]. The airfoil noise was based on Lockard and Lilley [30], using the the directionality from Howe [23] and the spectral shapes from ESDU airframe noise [22]. The drag rudder noise was based on extrapolations of wind tunnel data done at the MIT GTL [38]. Noise estimates were computed for both approach and landing conditions as listed in Table 5.6.

Like engine noise, the amount of error of each noise source OASPL, summarized in Table 5.7, is an estimate based on the limitations of the prediction methods used. The rationale behind the estimates was similar to those made for the engine noise prediction, with potential errors coming from the methods themselves and also the deviation from conventional designs. For the slats, elevators, and undercarriage, the noise prediction methods were found to to consistently have one-sided errors based on comparisons with Boeing data

	Approach	Takeoff
Ambient Air	ISA	ISA+12K
Flight Speed (m/s)	75.0	81.8
Angle of Attack (degrees)	14.6	11.7
Elevator Deflection (degrees)	-8.0	-9.2
Airframe Components	Airfoil, Slats, Elevators, Undercarriage, Silent Drag Rudder	Airfoil, Slats, Elevators

Table 5.6: Takeoff and landing conditions used for SAX10 noise assessment

[37] and FAA Regulation Part 36 Appendix A [35].

Airfoil	$\pm$3dB
Slats	$-0/+6$dB
Elevators	$-0/+5$dB
Undercarriage	$-0/+4$dB
Drag Rudder	$\pm$5dB

Table 5.7: Airframe noise source prediction accuracy

5.4 Shielding

Shielding was applied to engine noise based on the method developed by Agarwal and Dowling [1]. As mentioned previously, the engines are embedded near the rear of the planform. The intakes are on the upper surface, and as such, a large portion of the forward propagating noise is assumed to be shielded by the airframe.

The shielding calculations were done assuming a simple mononpole source at one location above the wing. Low frequency solutions were obtained using Boundary Element Method (BEM) calculations. Calculations on simple two-dimensional geometries by Agarwal and Dowling [1] revealed that ray-acoustics approach is valid even at the lowest frequencies of interest. High frequency shielding data was thus obtained by extrapolating BEM data using a ray-theory approach. To extrapolate to higher frequencies both leading and trailing edges of the wing were assumed to be sharp to provide a lower bound on shielding. The shielding calculations applied to the current SAX planform did not account for source directivity and mean flow effects.

5.5 Ground Noise Assessment

5.5.1 Flight effects

Before propagating the noise source, we have to take into account the effects of the aircraft in motion. Three effects have been included with the source noise prediction: Doppler refraction, Doppler amplification, and Doppler frequency shift. These modifications were performed in the order listed on all noise sources except the jet, for which flight effects were already included. Broadband and tonal sources are processed separately to minimize the introduction of further inaccuracies. It must be noted that this is only one of several possible methods of incorporating flight effects. A more complicated alternative is to perform the frequency shift on the narrowband that has been converted from a one-third octave spectra.

5.5.2 Noise Propagation Model

For the SAX design noise audit, the propagation model used was different from that in the first trade study. The previous model used two operating conditions to extrapolate the aircraft noise along the entire trajectory. For a variable cycle propulsion system, the engine performance at each point during takeoff could be significantly different. With the new propagation model, we were able to plot footprints for specific points on the trajectory. Four processes are captured in this model: Geometric attenuation due to spherical spreading, atmospheric attenuation, lateral attenuation, and ground reflections.

Assuming there are no barriers between the aircraft and the observer, Evans et al. [15] estimate the noise level on the ground, L_{om}, using the free-field aircraft noise level, L_a, to be as follows:

$$L_{om} = L_a + R - G - A - A_L, \tag{5.1}$$

where R is the ground-reflection correction, G is the attenuation due to spherical spreading, A is the attenuation due to atmospheric absorption, and A_L is the lateral attenuation. The following sections give a description of the processes being modelled. Figure 5-5 gives an overview of all the propagation effects modelled. The effects are applied in the numbered order in the figure. The amplitude and directivity of L_a is input as a hundred-foot hemi-

sphere. The attenuation due to spherical spreading is then applied followed by atmospheric attenuation. Then lateral attenuation is applied to all receiver locations not on the projected flight path on the ground. Finally corrections are made for ground reflections. The following sections give more detailed descriptions of the processes being modelled.

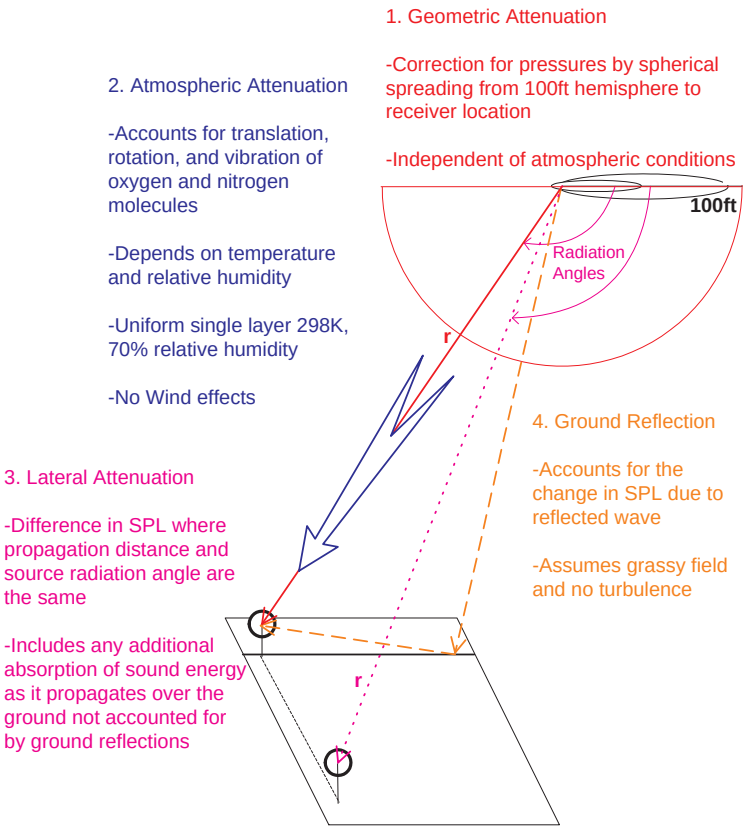

Figure 5-5: Grid for propagation model validation

Geometric attenuation

When noise is propagated, there is a loss of energy due to spherical spreading of the sound wave. This loss is inversely proportional to the square of the distance of propagation and is independent of atmospheric conditions. The relation between the mean-square acoustic pressure, $\langle p^2 \rangle$ (MSP) and the distance from the source to the observer, r, is as follows

$$\langle p^2 \rangle \propto \frac{1}{r^2}, \tag{5.2}$$

and since the MSP has a logarithmic relation with the SPL, the relation of the SPL with r, is as follows

$$SPL \propto k \cdot r, \tag{5.3}$$

where k is a constant. This qualitative relationship was validated by varying the height of a monopole source of SPL magnitude 100dB for all one-third octave frequency bands, and observing the changes in Overall Sound Pressure Level (OASPL), as defined by

$$OASPL = 10 \lg \sum_{i=1}^{n} \langle p^2 \rangle_i^* + 20 \lg \frac{\rho_\infty c_\infty^2}{P_{ref}}, \tag{5.4}$$

where n is the number of frequency terms in the spectra considered and $\langle p^2 \rangle_i^*$ is the dimensionless mean-square pressure for the $i-th$ frequency band.

A 3-by-3 grid was used for receiver locations on the ground, with noise predicted at the locations as specified in the Figure 5-6. Figure 5-7 shows that the OASPL varying linearly with the distance from observer, as theory predicts.

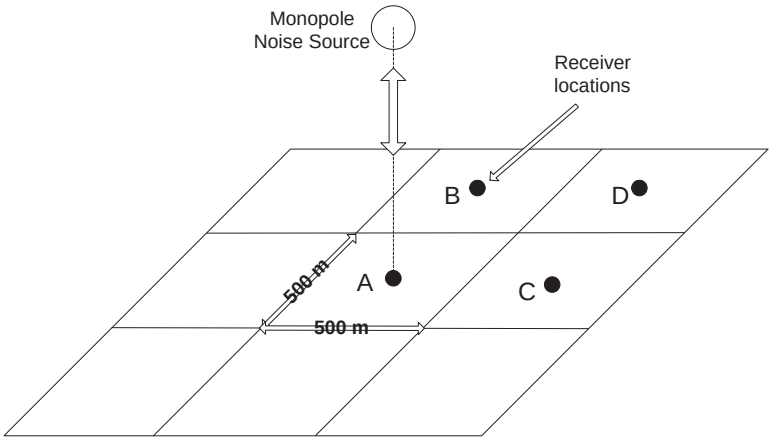

Figure 5-6: Grid for propagation model validation

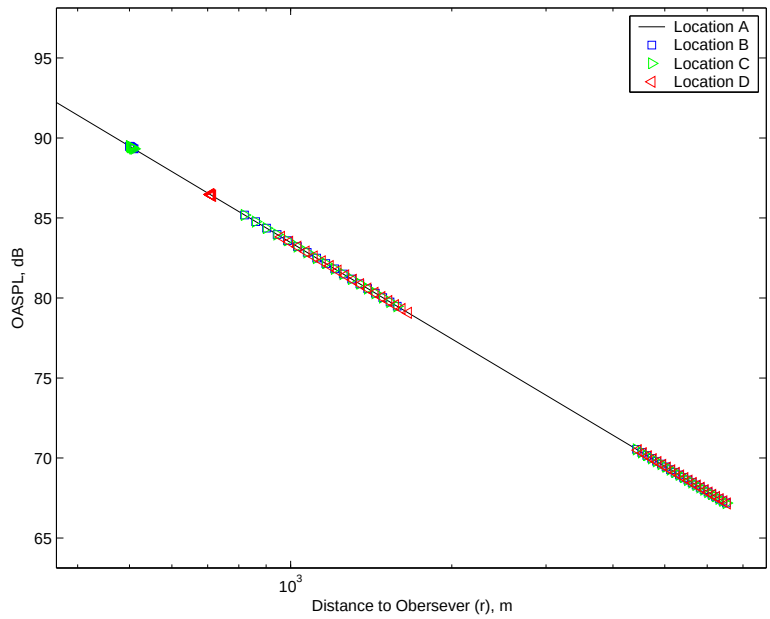

Figure 5-7: Variation of geometrically attenuated OASPL with height at all receiver locations

Atmospheric attenuation

As sound waves travel through the atmosphere, there are losses in energy due to molecular translation, molecular rotation, and internal vibrational relaxation of oxygen and nitrogen molecules. The acoustic energy is being dissipated as the molecules in the air translate and rotate. When molecular vibration relaxation occurs, the acoustic absorption depends on the maximum intensity loss per wavelength and the frequency at which this loss occurs. The maximum intensity loss is, in turn dependent on temperature and independent of pressure. The frequency at which this loss occurs is dependent on the amount of water vapour in the air. Thus, the amount of atmospheric attenuation is dependent on both the humidity and temperature of the air. In this analysis, the atmosphere was modelled as a single layer with a fixed temperature (298K) and humidity (70%).

Lateral attenuation

Evans et al. [15] define lateral attenuation as the difference between the one-third octave band under-the-flight-path and the sideline "free-field" sound pressure levels where the propagation distance, r, and source radiation angle associated with the two far-field sound pressure levels are the same ($\theta_s = \theta_u$ in Figure 5-5).

The difference in SPL is attributed to the absorption of sound energy by the ground as it propagates to the sideline receiver location. Compared to receiver locations along the projected flight path on the ground, more sound energy is absorbed by the ground as the sound wave travels towards receiver locations to the side of the projected flight path. Lateral attenuation depends on the location of the engines on the aircraft. Engines mounted at the end of the fuselage and under the wing were found to have different amounts of lateral attenuation. For this audit, it was assumed that the engines were mounted at the end of the fuselage.

The term "free field" sound pressure level is used to describe measured noise levels that have been corrected for the reflected wave from the ground surface. The magnitude of lateral attenuation increases with the distance and, at low elevation angles, increases with decreasing elevation angle. At larger distances (typically above $1200m$) the amount of lateral attenuation tends asymptotically to a value. This value depends on the frequency and elevation angle. These trends were observed in Figure 5-8 for locations B and D. Locations A and C had no change in OASPL, as per definition of lateral attenuation.

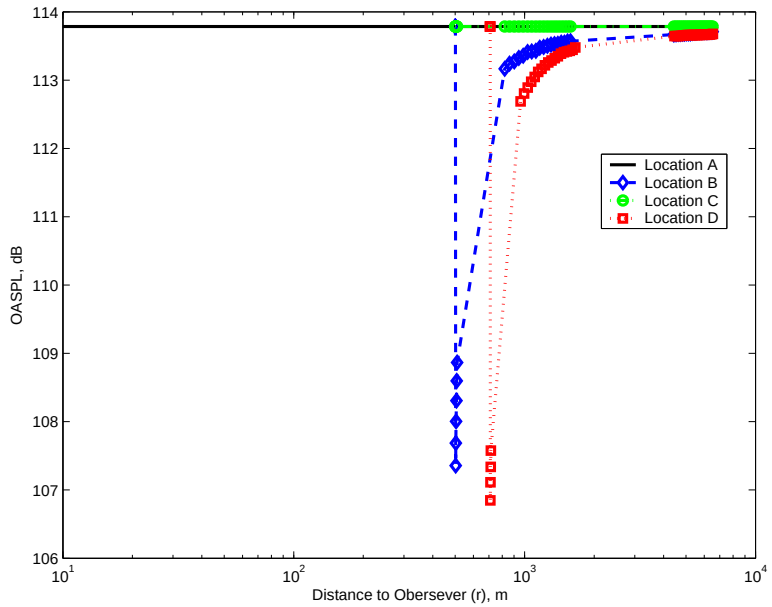

Figure 5-8: Variation of laterally attenuated OASPL with height at all receiver locations

Ground Reflection Corrections

Ground reflection corrections account for the difference between the measured and free-field spectra due to the reflection of sound propagating over a surface between a source and a receiver. For the audit, the surface was assumed to be grass (effective flow resistivity of 30 kNs/m^4), and inverse effective depth, 20 m^{-1}) and the atmosphere to be still (index of refraction 0). The ground reflection corrections either added to or reduced the SPL depending on the location of the source and receiver.

Figure 5-9 shows how the OASPL varied with height as each component of the propagation model was added. As expected, the atmospheric attenuation reduced the OASPL, increasing as the observer distance is increased. Adding lateral attenuation had no effect because the receiver location was directly below the noise source. Ground reflection corrections contributed significantly to increase the OASPL.

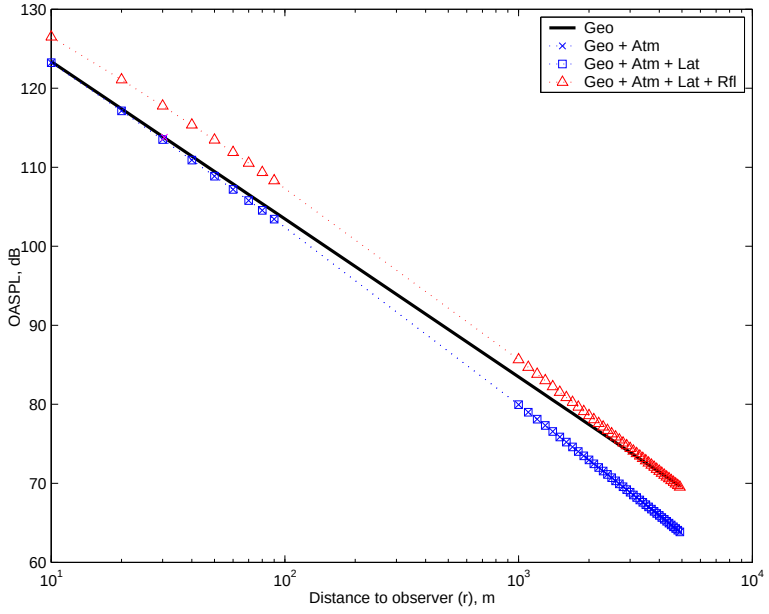

Figure 5-9: Variation of OASPL directly underneath source with height (all attenuation components)

5.5.3 Engine Noise Footprints and Results

Start of Climb Noise

It is expected that the loudest noise along the left and right boundaries of the airport that lie 450m to either side of the path of takeoff roll occurs at the start of climb condition. This location corresponds to a pre-cutback point with maximum throttle setting where the aircraft is still sufficiently close to the ground to have minimal attenuation due to propagation. The start of climb noise footprints for fan forward and rearward noise are shown in Figures 5-10 and 5-11, where fan rearward noise was overall more severe than the fan forward. The main reason for this was because of the shielding of the fan forward noise by the airframe. Note that the dashed lines represent the airport boundary. The loudest fan forward noise outside the airport boundary was only 55.8±5dBA whereas the fan rearward noise was at least 5dBA louder noisier.

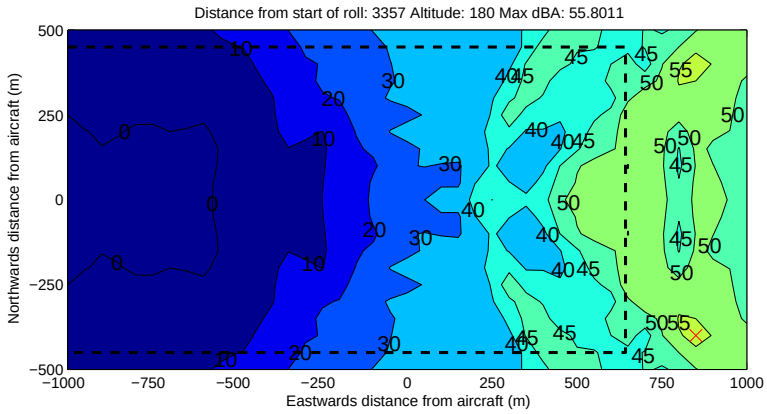

Figure 5-10: Fan forward noise (dBA) at start of climb condition

The core noise footprint, shown in Figure 5-12, was louder than both jet and turbine noise aft of the aircraft. Though the maximum point on the jet noise footprint, shown in Figure 5-13, was 3dBA quieter than the core noise, both their loudest points were within the airport boundary. Outside the airport boundary, the maximum noise of both components was the same.

The turbine noise footprint outside the footprint, shown in Figure 5-14, showed that it was generally about 5dBA quieter than jet and core noise.

All the engine noise sources were summed up using superposition (logarithmic sum of all SPLs) and the errors of all noise sources were accounted for. Based on the prediction

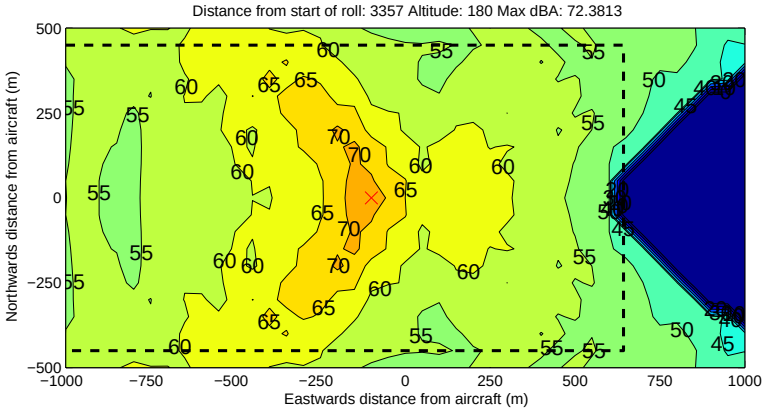

Figure 5-11: Fan rearward noise (dBA) at start of climb condition

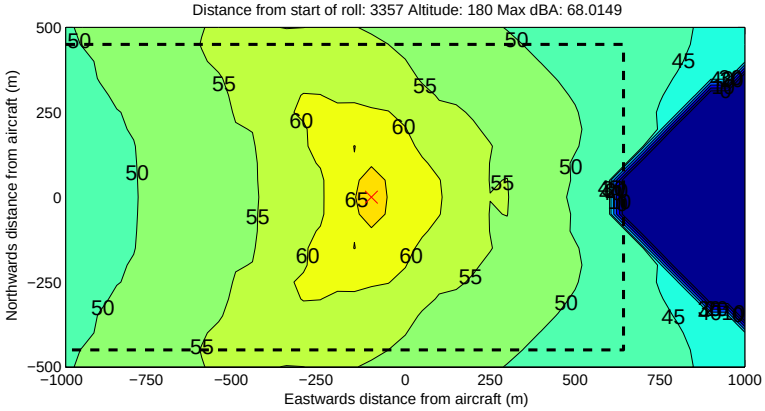

Figure 5-12: Core noise (dBA) at start of climb condition

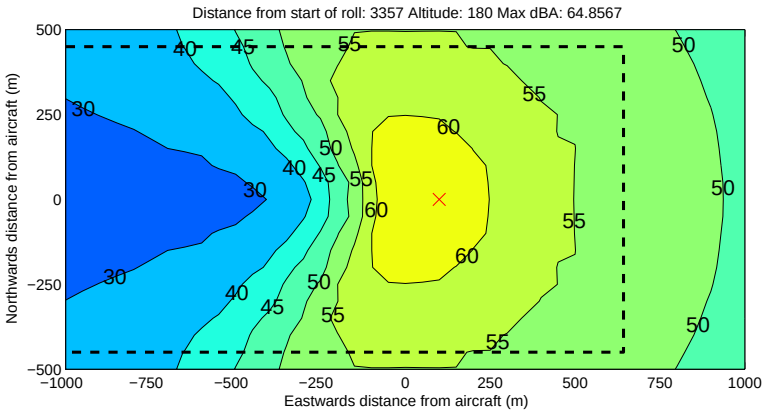

Figure 5-13: Jet noise (dBA) at start of climb condition

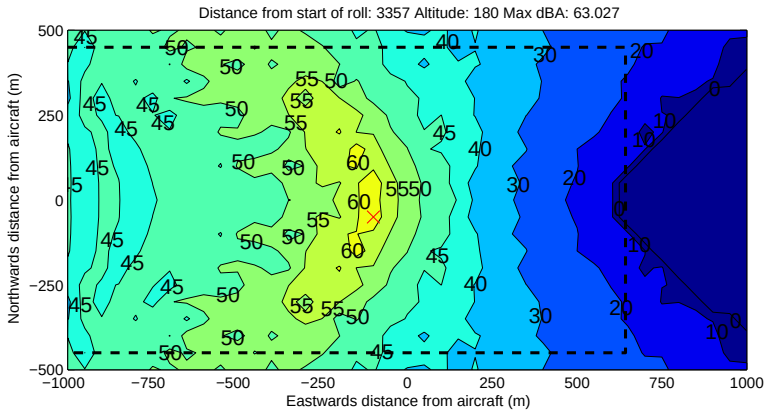

Figure 5-14: Turbine noise (dBA) at start of climb condition

method errors, the upper and lower bounds of engine noise footprints, shown in Figures 5-15 and 5-16 respectively, had about 10dBA difference in most locations on both footprints.

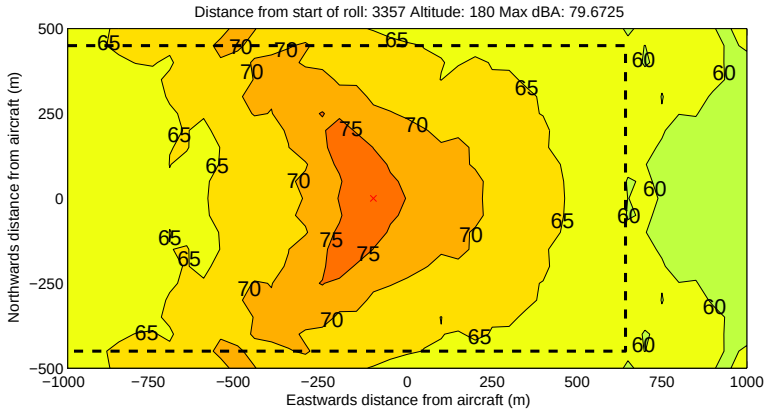

Figure 5-15: Estimated upper bound engine noise (dBA) at start of climb condition

The start of climb noise levels of all the components plotted in Figure 5-17, gives an overall view of the noise contributions of each component on the edge of the airport boundary. The thickest solid line represents total engine noise with its upper and lower bounds represented by the dashed lines. The peak of this solid line indicates that the loudest engine noise received at the edge of the airport boundary was about 66±5dBA. Fan rearward noise was the main contributor to total engine noise up till 800m in front of the aircraft, where fan forward noise became dominant.

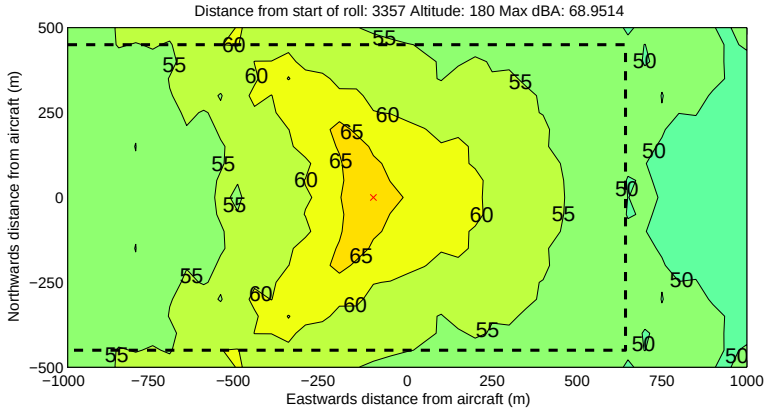

Figure 5-16: Estimated lower bound engine noise (dBA) at start of climb condition

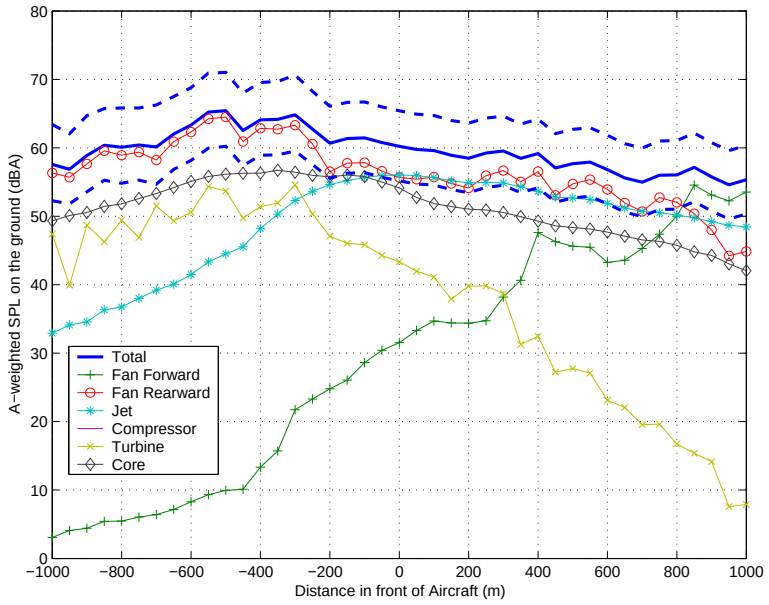

Figure 5-17: All engine noise components along airport sideline boundary at start of climb condition

Flyover Noise

At the flyover location, the aircraft has just passed the front airport boundary and is just about to perform a cutback. The altitude where cutback is performed is significantly lower than typical pilot procedures, which is about $1500ft$ [33]. This procedure is conducted to maintain low jet noise and is described in greater detail by Crichton et al. [11].

According to Figure 5-18, the maximum flyover noise was found to lie on the front boundary of the airport, directly below the flight path. Figure 5-19 indicates that the maximum noise source is 69±5dBA and was again caused by rearward fan noise. Turbine noise was the next significant contributor to noise aft of the aircraft. About $500m$ in front of the aircraft, the main contributor was jet noise.

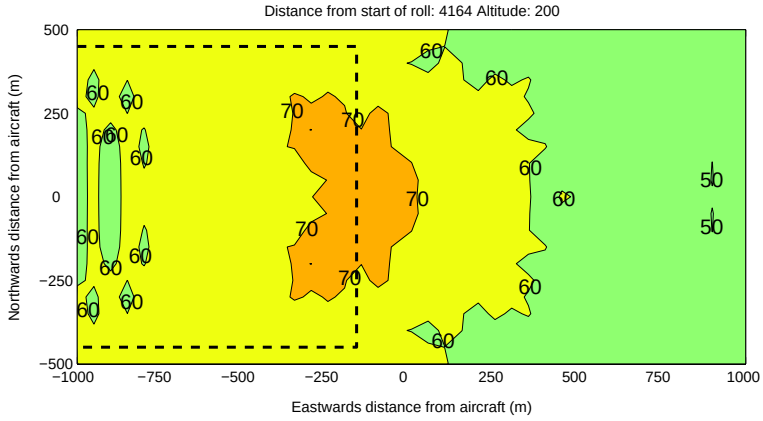

Figure 5-18: Estimated upper bound engine noise (dBA) at flyover condition

Approach Noise

For both the 3-degree and 6-degree glide slope approach, the engine was assumed to operate at the same idling condition with about $40kN$ of total thrust. The 3-degree approach, where the aircraft was closer to the ground, created louder noise. Figure 5-20 shows that the maximum noise occurred just outside the rear airport boundary. Figure 5-21 shows that the maximum noise outside the airport boundary for the approach was 78.5±5dBA, 9.5dBA louder than flyover, and 12.5dBA louder than start of climb.

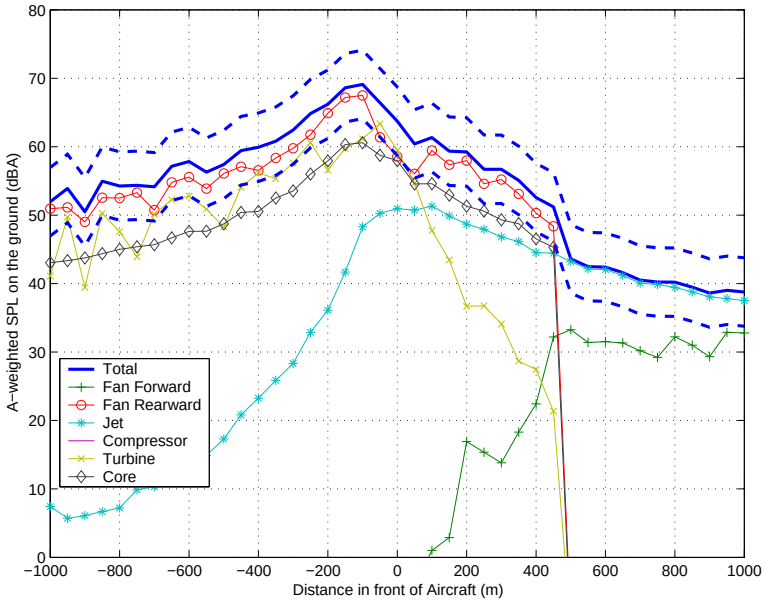

Figure 5-19: All engine noise components underneath aircraft at flyover condition

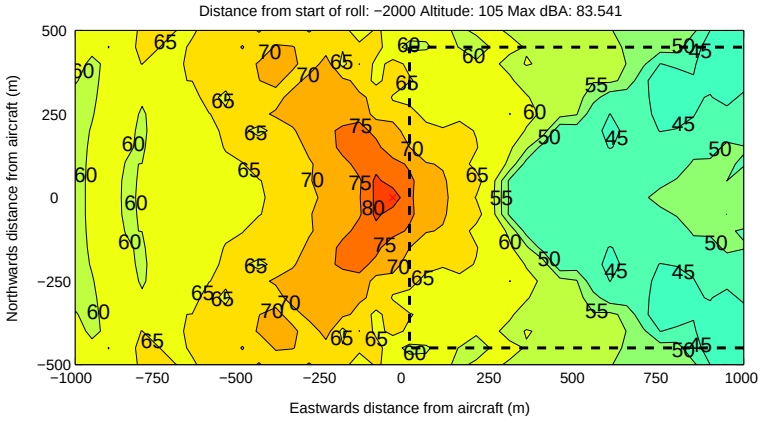

Figure 5-20: Estimated upper bound approach engine noise directly underneath aircraft

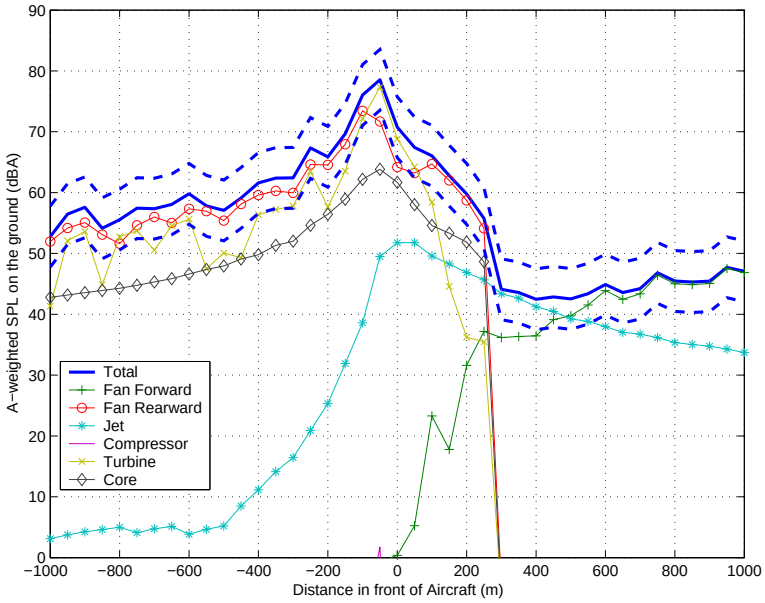

Figure 5-21: All engine noise components underneath aircraft at flyover condition

5.5.4 Airframe Noise Footprints and Results

Airframe noise for traditional aircraft designs is usually not a significant contributor to take-off noise. However, because of the reduced engine noise levels at takeoff, it was important to determine the airframe noise levels at all conditions.

For this audit, five components of airframe noise were considered: the airfoil, elevators, slats, drag rudders, and undercarriage. There were no conventional flaps on the SAX design, only elevators on the trailing edge of the airframe that deflect during takeoff.

Sideline Noise

During a conventional takeoff the undercarriage is stowed at around 20-60ft altitude [33]. For both locations at takeoff, the undercarriage was assumed to be stowed, and the only noise sources are the airfoil, elevators and slats, whose footprints are shown in Figures 5-22, 5-23, 5-24 respectively. The slat has the loudest noise levels, followed by elevators and airfoil.

All the airframe noise sources were summed up using superposition (logarithmic sum of all SPLs) and the upper and lower bounds of airframe noise footprints, shown in Figures 5-25 and 5-26 respectively, had about 10dBA difference in most locations on both footprints.

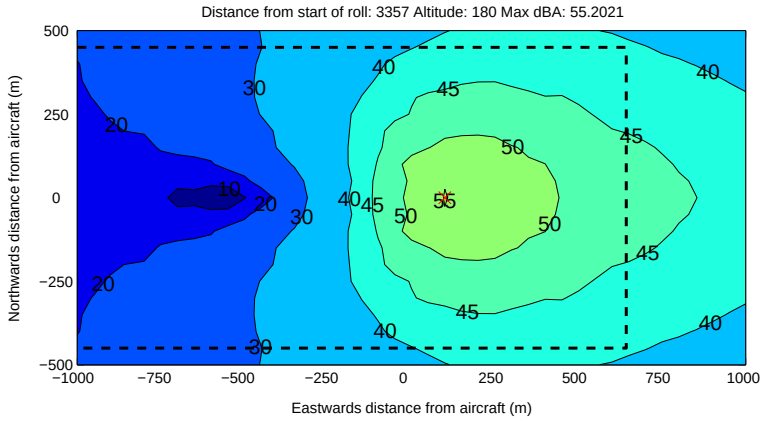

Figure 5-22: Airfoil noise (dBA) at start of climb condition

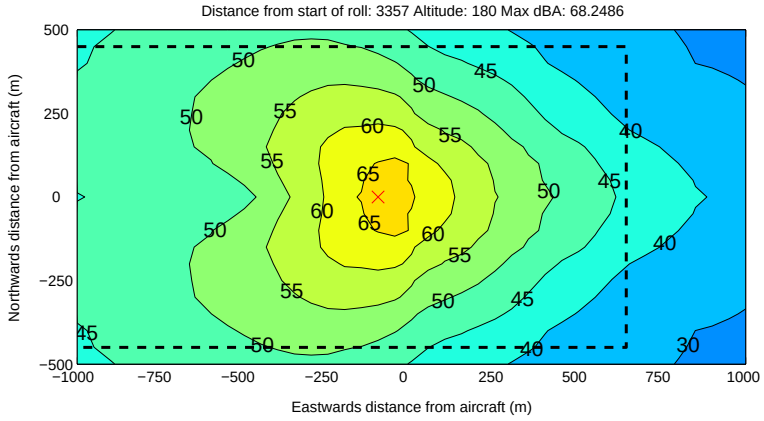

Figure 5-23: Elevator noise (dBA) at start of climb condition

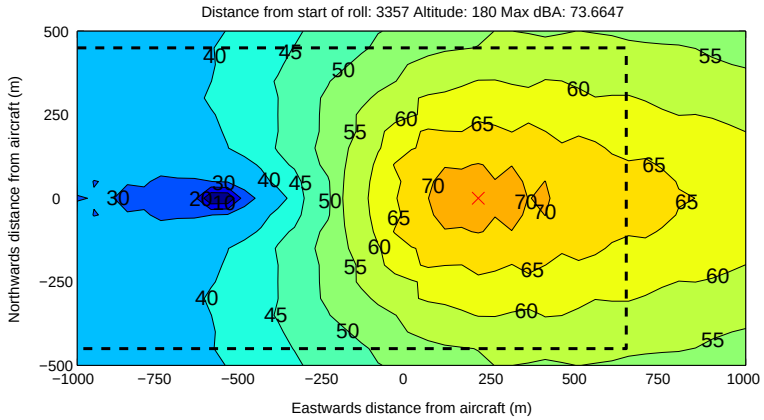

Figure 5-24: Slat noise (dBA) at start of climb condition

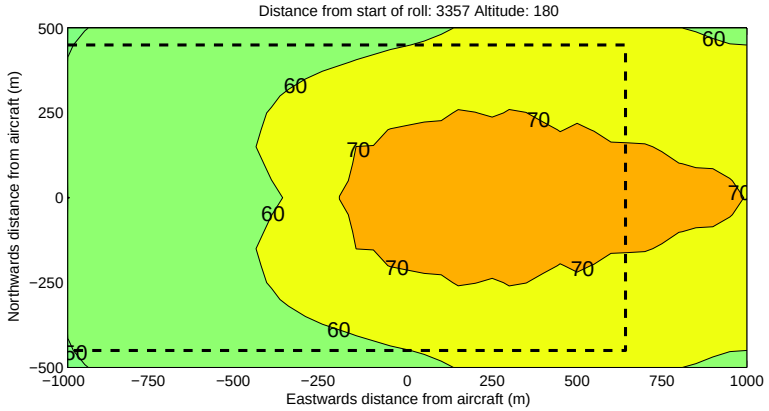

Figure 5-25: Estimated upper bound airframe noise (dBA) at start of climb condition

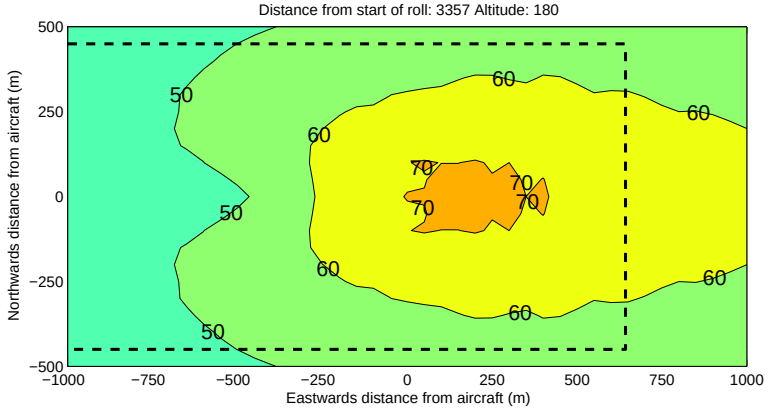

Figure 5-26: Estimated lower bound airframe noise (dBA) at start of climb condition

Figure 5-27 shows that the overall airframe noise was dominated by elevator noise aft of the aircraft, and slat noise in front of the aircraft. This made sense because the directivity of the noise coincided with the location of the high lift devices. The loudest noise received outside the airport is 57^{+6}_{-0}dBA, and is dominated by slat noise.

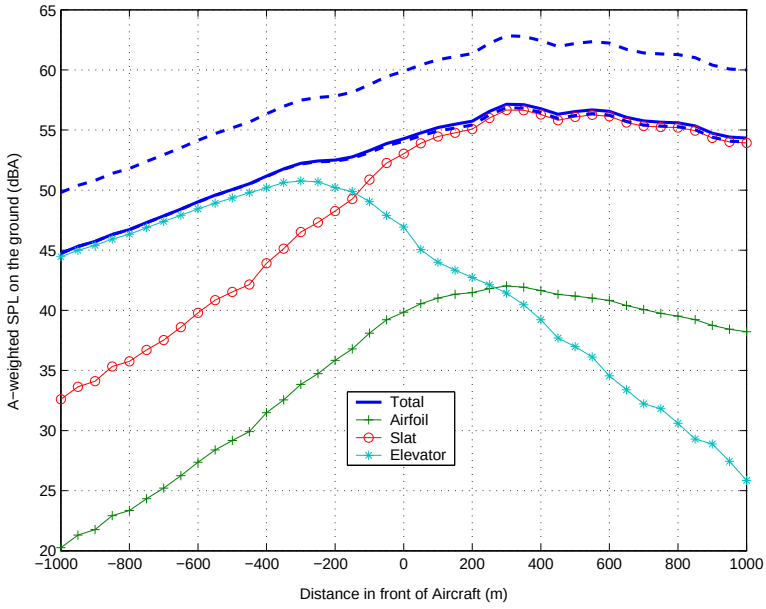

Figure 5-27: All airframe noise components along airport sideline boundary at start of climb condition

Flyover Noise

Figure 5-28 shows similar trends of component noise to those at the start of climb location except that the magnitude of noise levels are significantly different. The loudest noise received outside the airport is 73^{+6}_{-0}dBA, and is dominated by slat noise. The slat noise was louder because of the higher aircraft velocity at that point. Compared to the elevator noise on the start of climb location, the elevator noise underneath the aircraft dropped off faster as the distance away from the aircraft increased. This was due to the directivity function in the elevator noise prediction method. As the polar angle approaches 180, the elevator noise SPL falls at an increasing rate. Since the polar angle falls towards 180 faster along the flight path than the start of climb, the SPL also fell faster for in Figure 5-28 than Figure 5-27.

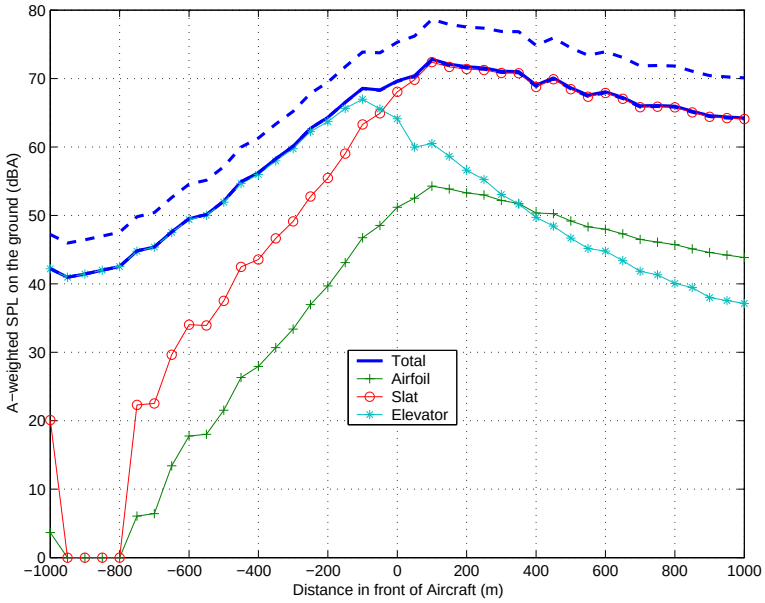

Figure 5-28: All airframe noise components underneath aircraft at flyover condition

Approach Noise

Because there was a finite amount idle thrust during approach, drag was needed to maintain the approach speed. Hence we assumed the deployment of a drag rudder for the approach condition. The undercarriage and drag rudder footprints in Figures 5-29 and 5-30 for a 3-degree approach show that they are significantly louder than other noise sources. The "zone of silence" around $600m$ behind the aircraft is due to the assumption that the undercarriage noise is shielded such that there is no undercarriage noise above the aircraft. This is a fair assumption for this analysis, but for a more accurate prediction, a study on how the shielding of the landing gear noise is affected by the airframe needs to be conducted.

Figure 5-31 shows us that when the drag rudder is deployed on approach, it is the single most dominant airframe noise source. The dashed line represents the total airframe noise when the drag rudder is not deployed. Without the drag rudder, the noise contributions come from elevator, undercarriage and slat noise, depending on the location of the receiver.

The total airframe noise footprints, shown in Figures 5-32 and 5-33, are significantly different with and without the drag rudder deployed. The maximum noise level outside the airport boundary is 84.8dBA with the drag rudder deployed, and 81.3dBA without.

Figure 5-35 shows all the noise components with the upper and lower bounds of the

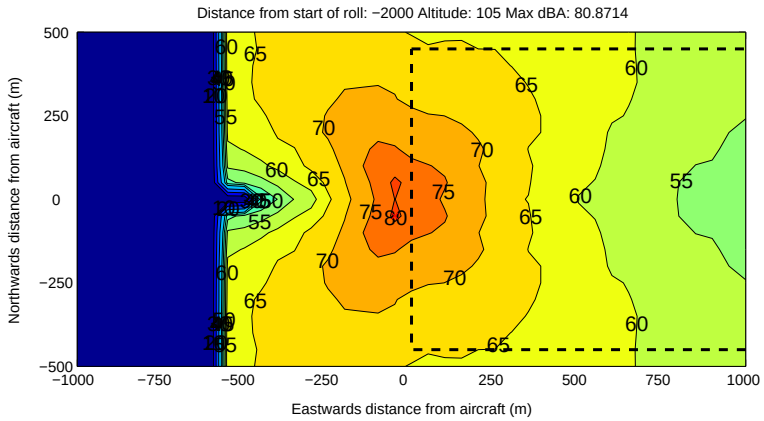

Figure 5-29: Undercarriage noise (dBA) at 3-degree approach condition

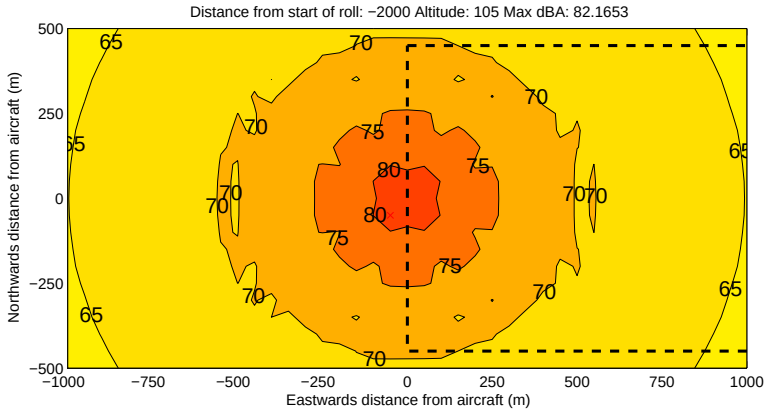

Figure 5-30: Drag rudder noise (dBA) at 3-degree approach condition

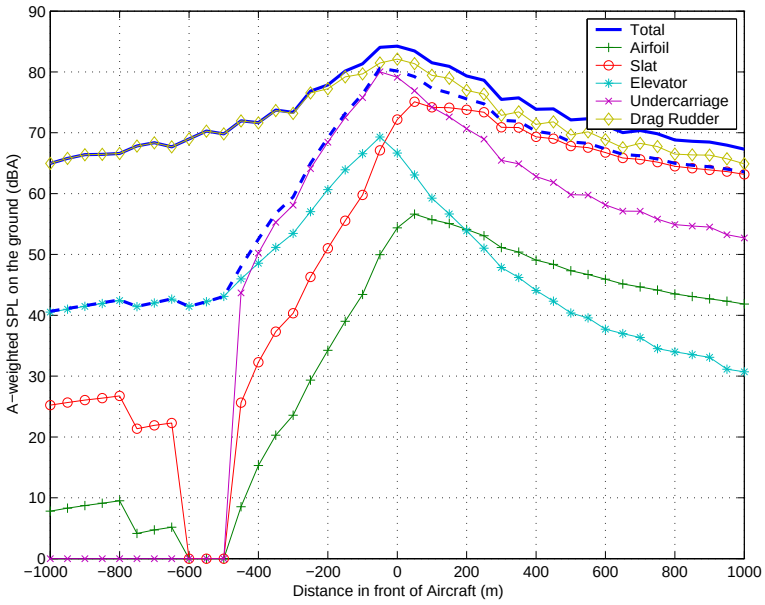

Figure 5-31: All airframe noise components underneath aircraft at 3-degree approach location (dashed line indicates total airframe noise when the drag rudder is not deployed)

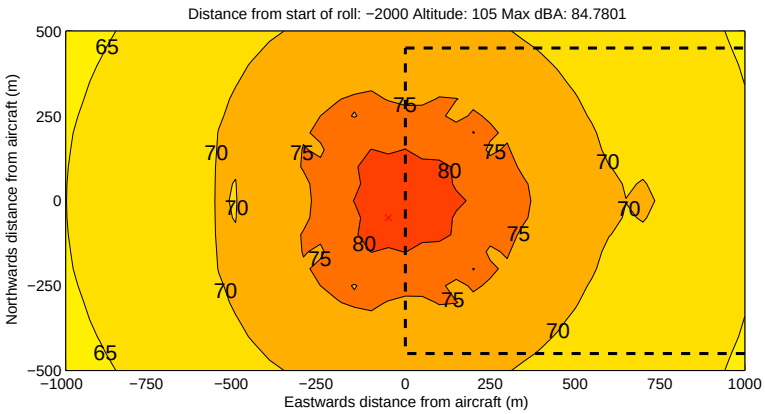

Figure 5-32: Airframe noise (including drag rudder) footprint for aircraft at 3-degree approach location

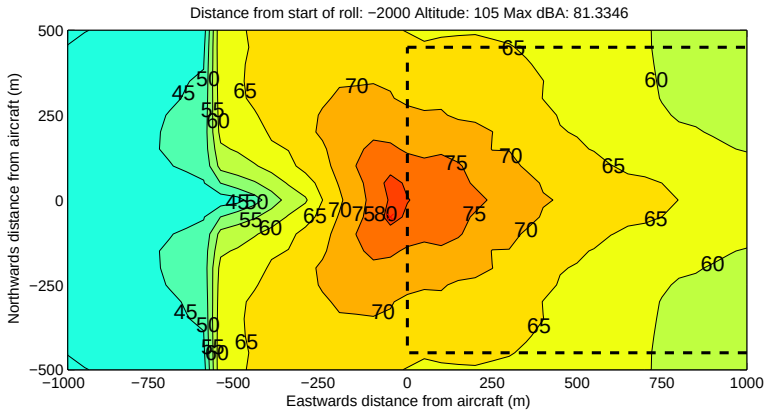

Figure 5-33: Airframe noise (without drag rudder) footprint for aircraft at 3-degree approach location

total airframe noise indicated by the thick dashed lines. This shows that the loudest airframe noise heard outside the airport boundary during approach is 83^{+5}_{-2}dBA. The airframe noise is mostly dominated by the drag rudder, but has significant contributions from the undercarriage and slats.

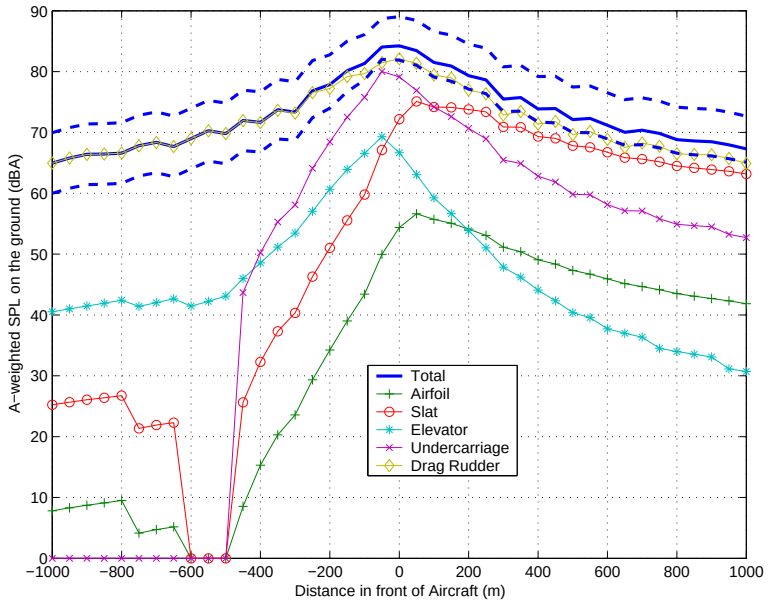

Figure 5-34: All airframe noise components underneath aircraft at 3-degree approach location (dashed lines indicate upper and lower bounds of total airframe noise)

For the 6-degree approach, the drag rudder noise is still dominant, as shown in Figure 5-35. But when it is not deployed, only the undercarriage and slat noise are the main

contributors to noise. This because the shielding of the undercarriage noise occurs further behind the aircraft on a 6-degree approach. The maximum noise level outside the airport boundary is 78.5dBA with the drag rudder deployed, and 75.5dBA without, both about 6dBA less than for the 3-degree approach.

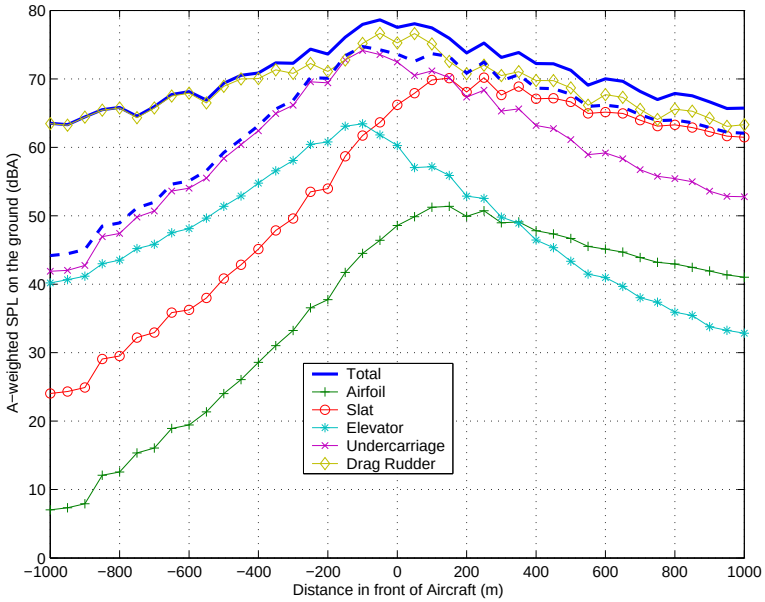

Figure 5-35: All airframe noise components underneath aircraft at 6-degree approach location

The maximum noise heard outside the airport for all three aircraft locations was plotted in Figure 5-36. This showed that the 3-degree approach was the most critical condition for noise, with the loudest noise source coming from the airframe. We also find that the loudest airframe noise heard outside the airport boundary during approach is almost 12dBA louder approach than the loudest noise during takeoff and about 9dBA for engine. The difference between the loudest airframe and engine noise is about 6dBA and occurs during the 3-degree approach.

5.6 Summary

In summary, we have discussed the concepts that contributed to the creation of the SAX design. We briefly examined the tools used predict airframe and engine noise levels, and the potential shielding effects. The noise was found to be most severe during approach, with the drag rudder and the undercarriage being the loudest airframe noise sources and the fan

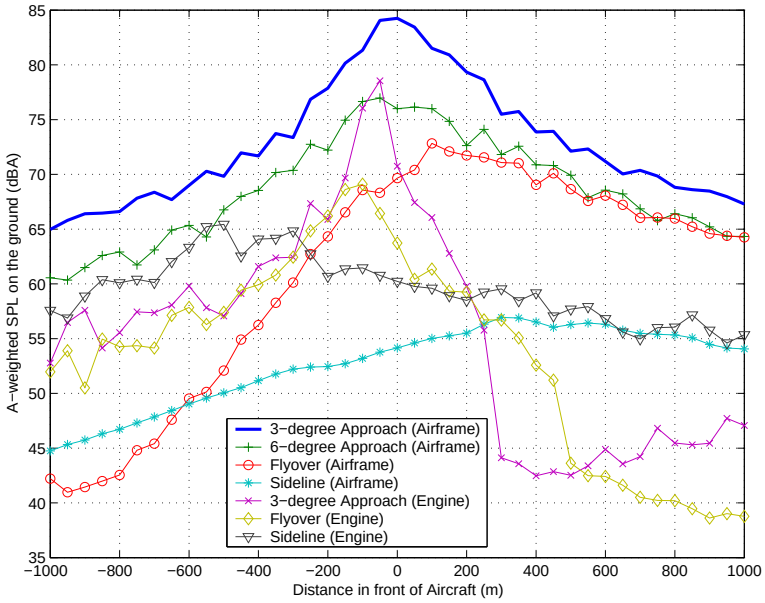

Figure 5-36: Maximum noise heard outside the airport boundary for all aircraft locations

rearward the dominant engine noise source. For all three aircraft locations, the maximum noise received outside the airport boundary was 84.8dBA and was due to drag rudder noise.

Chapter 6

Conclusion and Future Work

6.1 Summary and Conclusions

The ultimate goal of this project was to develop tools to identify the main drivers for aircraft noise so as to design an aircraft with noise as the main constraint. The first steps for this project involved the creation and use a framework to provide a qualitative assessment of the noise impacts of conventional and unconventional (blended-wing-body) designs. A detailed noise assessment was conducted on a SAX design that used a blended-wing-body airframe with embedded engine technologies. Based on these noise assessments, the main sources of noise from both airframe and engine were identified. Trade space studies were conducted on both tube-and-wing and SAX planforms to investigate the design space of these designs. The results of these studies can be summarized as follows:

- Range and takeoff field length are the main missions drivers of noise for both tube-and-wing and silent aircraft designs.
- Blended-wing-body designs with embedded propulsion systems have the potential to achieve a significant reduction in noise during takeoff and approach. Fan rearward noise is the most significant contributor to engine noise.
- The main source of noise for the SAX design comes from the drag rudder, which is deployed to offset the idle thrust during approach. The maximum noise level of the drag rudder is 6dBA louder than the next loudest source.
- The loudest airframe noise heard outside the airport boundary is during approach and

is almost 12dBA louder approach than the loudest airframe noise during takeoff.

- The loudest engine noise heard outside the airport boundary is during approach and is almost 9dBA louder approach than the loudest noise engine during takeoff.
- The difference between the loudest airframe and engine noise is about 6dBA and occurs during the 3-degree approach.
- The change in area of jet noise footprints for embedded engines on a blended-wing-body designs are less sensitive to changes in mission design parameters.

6.2 Recommendations for Future Work

Through this project, there were many lessons learnt about the design of aircraft primarily for noise reduction. The results from the trade space studies and noise assessments provide some guidelines for silent aircraft design and future work.

Noise prediction models based on ANOPP [48] were used extensively for this project. The validations on ANOPP done by Shivashankara et al. [40] have shown that there are potentially large errors (2-15dB for jet noise, and even more for other noise sources) in the current noise prediction methods used and the results have much uncertainty. As more accurate noise prediction tools are developed, the DIF framework needs to be updated and the noise audit done again to see if the principles of designing for low noise still hold.

The goal of the trade studies for silent aircraft designs was to identify the main drivers of noise among the high level design parameters. The methodology employed in this project showed how noise footprint changes can be used to identify these drivers. It must be noted that jet noise was the only noise source used for the silent aircraft trade study. Though this might be accurate for conventional tube-and-wing designs, where jet noise is the main contributor to takeoff noise, it did not capture the full noise effects of each design. It was noted in the trade study that jet noise is significantly reduced when a variable nozzle engine is employed. However, this means that other noise sources have become significant. For more accurate results, future trade studies should include all engine noise sources. This requires detailed engine data during the aircraft mission, which is not easy to predict.

Both trade studies conducted used the same trajectory for each design. In practice, the trajectory for each aircraft is different depending on the thrust available. Significant noise

reductions can result from noise abatement operations on approach, as shown by Clarke [9]. Antoine and Kroo [4] suggest that the noise reductions from thrust cutback procedures are minimal. As such, though it might be more realistic to vary the trajectory for future trade studies, it is not expected that the results will change much.

It would also be of interest to include shielding calculations for future trade studies. If simple scaling laws can be applied to shielding, trade studies can be used to investigate how shielding varies with high level design parameters.

The aircraft design tool (IDT) used in the trade study employed simple scaling laws to size a silent aircraft design for each set of design parameters. Using a design tool that can optimize each new planform in the trade study would yield weights, planform areas, and noise that will be more accurate. Wakayama and Kroo [46] have highlighted the potential use of the Wing Multidisciplinary Optimization Design (WingMOD) code as a design tool. Future work should involve setting noise as one of the objectives for WingMOD.

Based on the results of this project, we can make some recommendations for the design of a silent aircraft to meet the goal of being quieter than normal conversation levels, which is about 55dBA.

The main recommendation for high-level design parameters is that the design range should be kept minimal while still being economically feasible (currently $4000nm$). The cruise Mach number and altitude are flexible and can be varied to satisfy a quiet engine design.

The airframe noise needs to be reduced significantly on both takeoff and approach, with the situation being more severe during the latter. The main contributors of noise on approach are the drag rudder and the landing gear. Because of the large errors associated with drag rudder noise prediction, it is not clear whether the device should be employed. Another possible solution is to find an quieter method of creating drag. The landing gear noise needs to be shielded by as much as 25dB on a 3-degree approach. The slat and elevator noise also need be reduced by 20dB and 15dB respectively.

For the Granta-251 design, fan rearward noise is the main source of noise and needs to be reduced significantly during takeoff (13dB) and landing (18dB). On takeoff, the turbine and core noise need to be reduced by 8dB and 5dB respectively to meet the noise target. Turbine noise is actually more severe than fan rearward noise on approach and needs to be reduced by 13dB. Core noise needs to be reduced by 10dB.

Appendix A

Engine Cycle Parameters

	Static	Alt 200m, Mach 0.235
Net Thrust (lbs / kN)	55975/249	44691/199
TSFC ($lbs/lb-h$ / $g/kN-s$)	0.329/9.32	0.4186/11.86
Fuel Flow (lb/s / kg/s)	5.12/2.32	5.20/2.36
Bypass Ratio	5.05	5.05
OPR	30.4	30.4
Engine Inlet Area (in^2/ m^2)	6792/4.38	6792/4.38
Core Throat Area (in^2/ m^2)	871/0.562	871/0.562
Bypass Throat Area (in^2/ m^2)	2865/1.848	2865/1.848
Core Throat Mach Number	0.980	0.984
Bypass Throat Mach Number	0.818	0.855
Corrected Mass Flow at Inlet (lbs/s / kg/s)	1768/802	1768/802
Combustor Exit Static Temperature ($\circ R$ / K)	2841/1578	2842/1579
Combustor Exit Static Pressure ($psia$ / kPa)	420/2897	433/2989
Core Static Temperature ($\circ R$ / K)	1628/904	1629/899
Bypass Static Temperature ($\circ R$ / K)	545/303	550/306
Core Static Pressure ($psia$ / kPa)	26.7/184	26.7/184
Bypass Static Pressure ($psia$ / kPa)	22.8/157	23.5/162

Table A.1: CF6-80C2B8F Engine Cycle Values at Takeoff

Engine Inlet Area (m^2)	4.59
Fan Area (m^2)	4.59
T_{21}, Total Pressure aft of Fan (K)	401.10
W_{21}, Combustor Entrance Mass Flow (kg/s)	114.37
Fan Relative Tip Mach Number at Design Point	1.53 [26]
Rotor Stator Spacing, re Mean Rotor Blade Chord	2.60 [26]
Fan Rotational Speed (RPM)	3150 [26]
Number of Rotor Blades	32 [26]
Number of Stator Vanes	34 [26]

Table A.2: Fan Noise Prediction Module Input Values from Cycle Analysis of CF6-80C2B8F at Takeoff

Inputs	CF6-80C2B8F @ T/O	PW4056 @ T/O
Core Nozzle Total Pressure (kPa)	183	150
Bypass Nozzle Total Pressure (kPa)	160	168
Core Exhaust Jet Mach Number	0.9795	0.77
Bypass Exhaust Jet Mach Number	0.8555	0.88
Core Nozzle Total Temperature (K)	901.14	757.76
Bypass Nozzle Total Temperature (K)	304.60	340.48
Fully Expanded Core Jet Temperature (K)	756.05	677.78
Fully Expanded Bypass Jet Temperature (K)	255.56	304.54
Fully Expanded Core Jet Density (kg/m^3)	0.456	0.52
Fully Expanded Bypass Jet Density (kg/m^3)	1.349	1.16
Primary Stream Jet Velocity (m/s)	539.89	400.84
Secondary Stream Jet Velocity (m/s)	274.14	308.57
Fully Expanded Core Jet Area (m^2)	2.534	0.80
Fully Expanded Bypass Jet Area (m^2)	0	2.15

Table A.3: Comparison of Engine Noise Prediction Module Input Values from Cycle Analysis of CF6-80C2B8F and PW4056

	Static	Alt 200m, Mach 0.235
Net Thrust (lbs / kN)	91084/405	69700/310
TSFC ($lbs/lb-h$ / $g/kN-s$)	0.2832/8.02	0.4324/12.25
Fuel Flow (lb/s / kg/s)	7.17/3.25	8.37/3.80
Bypass Ratio	8.4	8.4
OPR	39.7	39.7
Engine Inlet Area (in^2/ m^2)	11873/7.66	11873/7.66
Core Throat Area (in^2/ m^2)	1804/1.164	1804/1.164
Bypass Throat Area (in^2/ m^2)	6059/3.909	6059/3.909
Core Throat Mach Number	0.578	0.587
Bypass Throat Mach Number	0.793	0.831
Corrected Mass Flow at Inlet (lbs/s / kg/s)	3228/1464	3232/1466
Combustor Exit Static Temperature ($\circ R$ / K)	3306/1837	3356/1864
Combustor Exit Static Pressure ($psia$ / kPa)	554/3823	563/3880
Core Static Temperature ($\circ R$ / K)	1572/873	1586/881
Bypass Static Temperature ($\circ R$ / K)	597/332	601/334
Core Static Pressure ($psia$ / kPa)	18.3/126	18.0/124
Bypass Static Pressure ($psia$ / kPa)	22.2/153	22.6/156

Table A.4: GE90-90B Engine Cycle Values at Takeoff

Bibliography

[1] Agarwal, A., Dowling, A.P., Nov 2003, "Acoustic shielding of engine noise by the Silent Aircraft airframe," *Paper 2pNS3, 148thASA Meeting*, San Diego.

[2] Ahuja, K.K., 1973, "Correlation and Prediction of Jet Noise," *Journal of Sound Vibration*, vol 29(2), pp. 155-168.

[3] Antoine, N.E., Kroo, I.M., Sept. 2002, "Aircraft Optimization for Minimal Environmental Impact, " *AIAA 2002-5667, 9th AIAA/ISSMO Symposium on Multidisciplinary Analysis and Optimization*, Atlanta, Georgia.

[4] Antoine, N., Kroo, I., Oct 2002, "Optimizing Aircraft and Operations for Minimum Noise," *AIAA-2002-5868, AIAA's Aircraft Technology, Integration, and Operations (ATIO) 2002 Technical*, Los Angeles, California.

[5] Antoine, N., Kroo, I., Willcox, K., Barter, G.., Sept 2004, "A Framework for Aircraft Conceptual Design and Environmental Performance Studies," *AIAA-2004-4314, 10th AIAA/ISSMO Multidisciplinary Analysis and Optimization Conference*, Albany, New York.

[6] "Boeing 767-300ER/767-200ER Technical Data", *http://www.boeing.com/commercial/767family/technical.html*, Jun 2004.

[7] "Boeing 747-400/747-400ER Technical Data", *http://www.boeing.com/commercial/747family/technical.html*, Jun 2004.

[8] Brooks, T.F., Pope, D.S., Marcolini, M.A., Jul 1989, "Airfoil Self-Noise and Prediction," *NASA-RP-1218*.

[9] Clarke, J.B., Jan 1997, "A System Analysis Methodology for Developing Single Events Noise Abatement Procedures," *Ph.D. thesis, Massachusetts Institute of Technology.*

[10] Cottington, R.V., et al., "Air Travel - Greener by Design, The Technology Challenge," *Report of the Technology Sub-Group*, Society of British Aerospace, London, UK.

[11] Crichton, D., Tan, D., Hall, C., Nov 2004, "Required Jet Area for Silent Aircraft at Take-off," *CEAS 8th Aeroacoustics Workshop*, Budapest, Hungary.

[12] Diedrich, A., Feb. 2005, "The multidisciplinary design and optimization of an unconventional, extremely quiet aircraft," *Masters of Science Thesis, Massachusetts Institute of Technology.*

[13] Elmer, L., et al., Jun 2002, "A Study of Noise Abatement Procedures using Ames B747-400 Flight Simulator," *AIAA-2002-2540, 8th AIAA/CEAS Aeroacoustics Conference*, Breckenridge, Colorado.

[14] Emmerling, J.J, Kozin, S.B., Matta, R.K. , Mar 1976, "Core Engine Noise Control Program. Volume III, Supplement I - Prediction Methods," *FAA-RD-74-125, III-I.*

[15] Evans, P., Nov 1981, "An Introduction to Aircraft Noise Lateral Attenuation," *Engineering Sciences Data Unit (ESDU) Lateral Attenuation Manual*, Item 81035, ESDU International, London, England.

[16] Federal Aviation Administration, Advisory Circular 36-3H, "Estimated Airplane Noise Levels in A-Weighted Decibels.".

[17] Federal Aviation Regulations, Nov 2002, $http://www.airweb.faa.gov/Regulatory_and_Guidance_Library/rgFAR.nsf, Dec2004.$

[18] Fink, M.R., Mar. 1977, "Airframe Noise Prediction Method," *FAA-RD-77-29.*

[19] Hall, C., Crichton, D., Nov 2004, "Integration of the Silent Aircraft Propulsion System," *CEAS 8th Aeroacoustics Workshop*, Budapest, Hungary.

[20] Hall, C., Crichton, D., Law, T., Madani, V., Agarwal, A., Dec 2004, "Personal Communication," *Dec 2004.*

[21] Heidmann, M.F. , 1975, "Interim Prediction Method for Fan and Compressor Source Noise," *NASA Report TM X-71763.*

[22] Holbeche, T.A., et al., 2003, "Aiframe Noise Prediction," *Engineering Sciences Data Unit (ESDU) Airfram Noise Prediction Manual*, Item 90023, ESDU International, London, England.

[23] Howe, M.S.,"A review of the theory of trailing edge noise," *J. Sound Vib., Vol. 61, no. 3, pp. 437-465, 1978.*

[24] Huber, J., 2003, "Noise Propagation Model for the Design of Weather Specific Noise Abatement Procedures," *Master of Science Thesis, Massachusetts Institute of Technology.*

[25] Kontos, K.B., Janardan, B.A., Gliebe, P.R., Aug. 1996, "Imporved NASA-ANOPP Noise Prediction Computer Code for Advanced Subsonic Propulsion Systems, Volume I: ANOPP Evaluation and Fan Noise Model Improvement," *NASA Contractor Report 195480.*

[26] Kontos, K.B., Janardan, B.A., Gliebe, P.R., Aug. 1996, "Imporved NASA-ANOPP Noise Prediction Computer Code for Advanced Subsonic Propulsion Systems, Volume I: ANOPP Evaluation and Fan Noise Model Improvement," *NASA Contractor Report 195480* pp. 46-49.

[27] Kurzke, J., 2001, "A Program to Calculate Design and Off-Design Performance of Gas Turbines," *GasTurb 9 User's Manual*, Concepts NREC, White River Jct., Vermont.

[28] Liebeck, R.H., Jan 2004, "Deisng of Blended Wing Body Subsonic Transport," *Journal of Aircraft*, Vol. 41, No.1.

[29] Liebeck, R.H., Page, M.A., Rawdon, B.K., Jan 1998, "Blended-Wing-Body Subsonic Commercial Transport," *AIAA-1998-438, 36th Aerospace Sciences Meeting and Exhibit*, Reno, Nevada.

[30] Lockard, D.P. and Lilley, G.M., "The Airframe Noise Reduction Challenge," *NASA TM-2004-213013, 2004.*

[31] Manneville, A., June 2004, "Propulsion System Concepts for Silent Aircraft," *Masters of Science Thesis, Massachusetts Institute of Technology.*

[32] Matta, R.K., Sandusky, G.T., Doyle, V.L. , Feb 1977, "GE Core Engine Noise Investigation - Low Emission Engines," *FAA-RD-77-4.*

[33] Midkiff, A., "Personal Communication," *Jun 2004.*

[34] Kroo, I., Jan 2003, "Noise Sources of Aircraft", *http://adg.stanford.edu/aa241/AircraftDesign.html*, Dec 2004.

[35] FAA Noise Division (AEE-100), Sept. 2004, "CFR Part 36, Noise Standards: Aircraft Type and Airworthiness Certification,", *http://www.aee.faa.gov/noise/index.htm*, Jan 2005.

[36] Pilczer, D., June 2003, "Noise Reduction Assessments and Preliminary Implications for a Functionally Silent Aircraft," *Masters of Science Thesis, Massachusetts Institute of Technology.*

[37] Rackl, R., Miller, G., Guo, Y. and Yamamoto, K., Feb. 2001, "Airframe Noise Studies - Review and Future Direction," *NASA Informal Contractor Report, Contract NAS1-97040 Task 12.*

[38] Sakaliyski, K., "Personal Communication," *Dec 2004.*

[39] Shevell R. S. , "Fundamentals of Flight," Prentice Hall Inc.

[40] Shivashankara, B.N., 1980, "Aircraft Noise Prediction Program Validation," *NASA Report CR-159333*, Figures 16a and b.

[41] Silent Aircraft Initiative, Nov 2003, *http://silentaircraft.org/news/*, Jan 2005.

[42] Stone, J.R. , 1974, "Interim Prediction Method for Jet Noise," *NASA Report TM X-81470.*

[43] Stone, J.R., Groesbeck, D.E., Zola, C.L., 1981, "An Improved Prediction Model for Noise Generated by Conventional Profile Coaxial Jets," *NASA Report 82712.*

[44] Tam, C.K.W., Gelebiowski, M., Senier, J.M., 1996, "On the Comparison of Turbulent Mixing Noise from Supersonic Jets," *AIAA Paper 96-1716*.

[45] Tam, C.K.W., Zaman, K.B.M.Q., 1999, "Flow and Noise Field of Subsonic Jets from Asymmetric Nozzles," *AIAA 99-3583*.

[46] Wakayama, S., Kroo, I., 1998, "The Challenge and Promise of Blended-Wing-Body Optimization," *AIAA Paper A98-39726*.

[47] Williams, J.E., Dowling, A.P., Nov 1983, "Sounds and Sources of Sounds," John Wiley and Sons.

[48] Zorumski W.E. , Feb. 1982, "Aircraft Noise Prediction Program Theoretical Manual, " *NASA Report TM-83199, Part 2*.